Design, Synthesis And Characterization Of Acyclic Bola-Amphiphiles That Form Ion Channels

By
Paul Kahu Eggers
B.Sc., Okanagan University College, 2000

A Thesis Submitted in Partial Fulfillment of the
requirements for the Degree of

MASTER OF SCIENCE

In the Department of Chemistry

We accept this thesis as conforming
to the required standard

[redacted]
Dr. T.M. Fyles, Supervisor (Department of Chemistry)

[redacted]
Dr. D.J. Berg, Departmental Member (Department of Chemistry)

[redacted]
Dr. N.J. Livingston, Outside Member (Department of Biology)

[redacted]
Dr. G.A. Poulton, External Examiner (Department of Chemistry)

University of Victoria

Supervisor: Dr. Thomas M. Fyles

Abstract

A demacrocyclization design strategy for the creation of ion channel-forming compounds was explored. Beginning with an active bis-macrocyclic bola-amphiphile, two and four tailed acyclic bola-amphiphiles were identified. These target compounds were prepared by a modular synthetic approach based on ester and amide linking reactions resulting in an increased overall yield from previous macrocyclic compounds. Transport activity was measured by pH-stat titration methods. All three compounds exhibited significantly high activity. The compound containing central esters was clearly less active than the compounds containing central amides. All compounds are apparently strongly partitioned to a vesicle bilayer membrane.

Examiners

[redacted]

Dr. T.M. Fyles, Supervisor (Department of Chemistry)

[redacted]

Dr. D.J. Berg, Departmental Member (Department of Chemistry)

[redacted]

Dr. N.J. Livingston, Outside Member (Department of Biology)

[redacted]

Dr. G.A. Poulton, External Examiner (Department of Chemistry)

Table of Contents

List of Tables

List of Figures

List of Schemes

Acknowledgements

I would like to express my gratitude to my supervisor Dr. T.M. Fyles for his patience, support and guidance. Thanks are extended to my co-workers, especially Chi-wei Hu for his help and Todd Sutherland for letting me use his bilayer clamp data. I would also like to thank the chemistry department staff and faculty, in particular Dr. David McGillivray for his work on the mass spectra.

Chapter 1: Introduction

1.1 Biological Channels:

Cells have an exterior membrane in order to maintain a different environment inside the cell than outside the cell. The membranes are composed of two layers of lipids, oriented with non-polar alkyl tails pointing towards each other and the polar head groups pointing towards the aqueous solution. This bilayer is a mixture of several different lipids and various proteins within and associating with the lipid. The current model for describing the mechanics behind this system is the fluid mosaic model. The name describes the system: the lipids and proteins are constantly shifting laterally within the membrane[1]. Figure 1.1 sketches a cell membrane according to the fluid mosaic model.

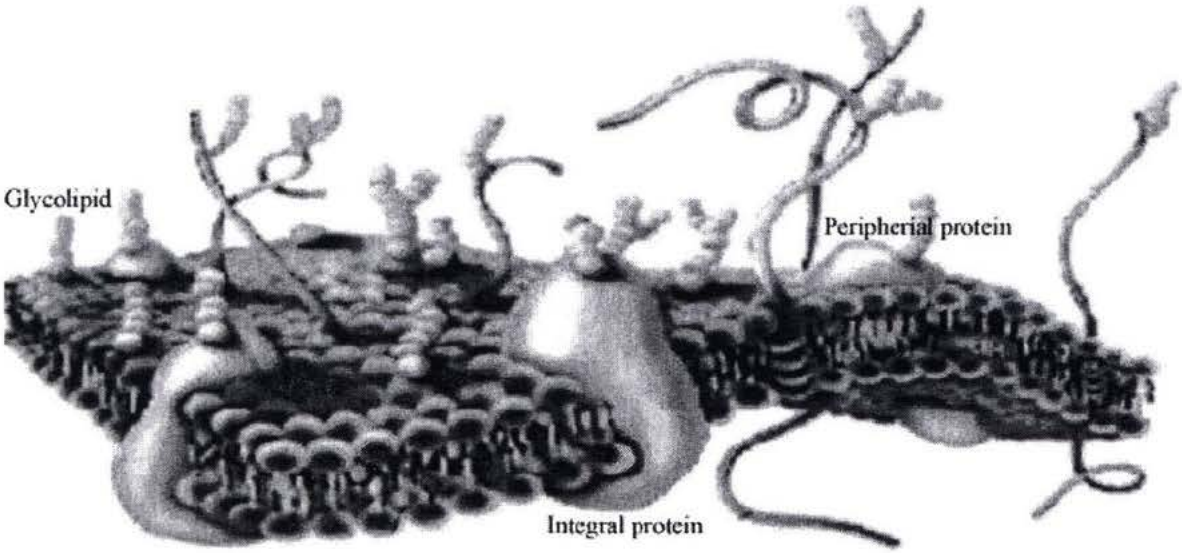

Figure 1.1: Representation of a cell membrane

In order for a complex multicellular organism to function, material and information must be able to transverse the membrane. Diffusion allows lipophilic compounds and small molecules to move through the membrane. However, ions and other hydrophilic compounds, such as amino acids and sugars, diffuse through the

membrane at very slow rates. The rapid transport of these compounds is accomplished by membrane spanning proteins that can selectively transport both ions and neutral compounds[1].

The nervous system provides an excellent example of a key role for ion channels. The nervous system functions via minuet electrical impulses that move through out the organism. These electrical signals are developed by ion concentration gradients across the membrane. When ion channels open, ions move through the ion channels and down their concentration gradients. The net movement across the membrane changes the membrane potential and generates an electrical signal as a membrane potential drain[2]. External control and ionic specificity are very important in this action since they allow different ions to move across the membrane independently of each other. For example the independent flow of K^+ and Na^+ is what makes the initiation of a nerve impulse possible[2].

Little is known on the molecular level of the structure and control of large ion channels. However, recently protein structures have begun to appear, which describe the protein structure. However, it is still unclear in some cases where and how the transport occurs[3,4]. Natural protein aggregates tend to have molecular weights around 250,000 Da and are composed of multiple subunits.

The active conformation of these structures is highly dependent on the external environment. Thus, a complete picture of what these structures look like in the membrane and how they function on the molecular level would be very difficult to obtain. However, smaller natural products such as gramicidin A and amphotericin B have been thoroughly studied and have provided a lot of information which has gone into the synthetic channels being developed today.

Gramicidin (**1**) is a linear peptide produced by *Bacillus brevis*. It consists of 15 alternating L- and D-amino acid residues[5]. In the membrane it forms a head to head single helix dimer with the N-termini at the mid plane of the bilayer. The internal diameter of the helix is 0.4 nm. Carbonyl groups line the interior of the helix and the hydrophobic chains are on the periphery[6]. This forms an aqueous pore with a metal cation selectivity order of $Cs^+ > Rb^+ > K^+ > Na^+ > Li^+$ [7]. The divalent cations Ca^{2+} and Ba^{2+} can block the gramicidin channel activity[8].

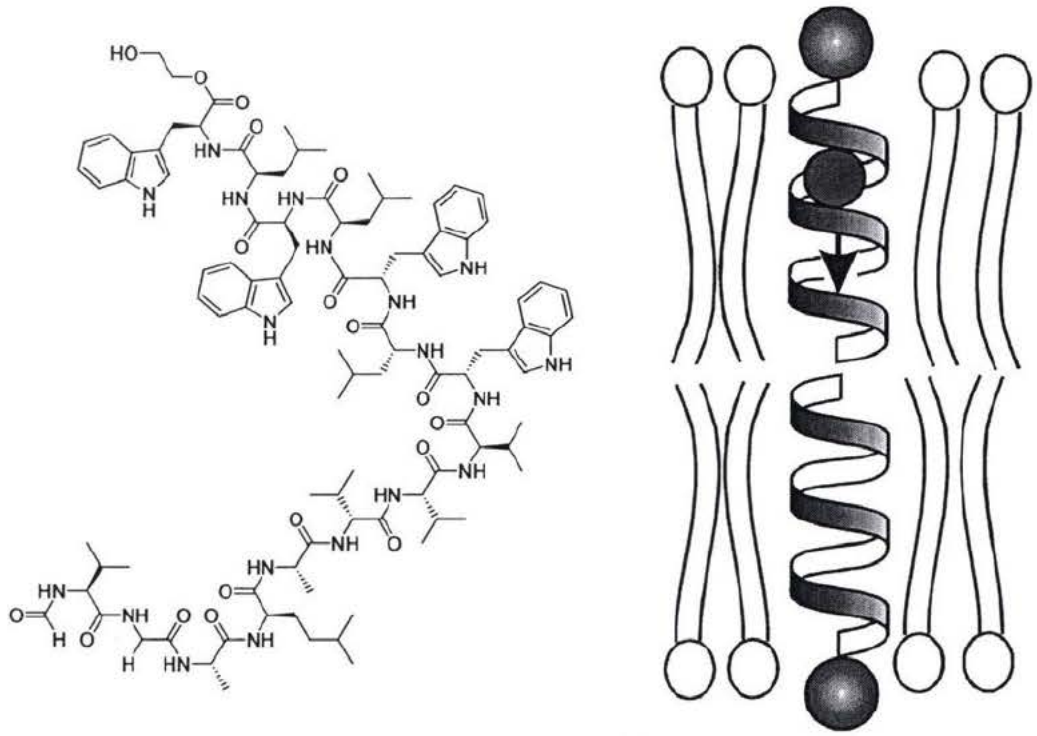

a) **1** b)

Figure 1.2: a) Structure of gramicidin and b) schematic representation of the gramicidin mechanism

Amphotericin (**3**) on the other hand is one of greater than two hundred non-peptide, polyene macrolide antibiotics produced by *Streptomyces sp.* It has been suggested that Amphotericin self-assembles within the bilayer to a barrel stave configuration. It is thought that between 12 to 20 molecules aggregate with the

hydrocarbon face towards the lipids and the alcohols lining a water filled pore. The length of the compound is around 2.5 nm, which is about half the thickness of a bilayer[9,10].

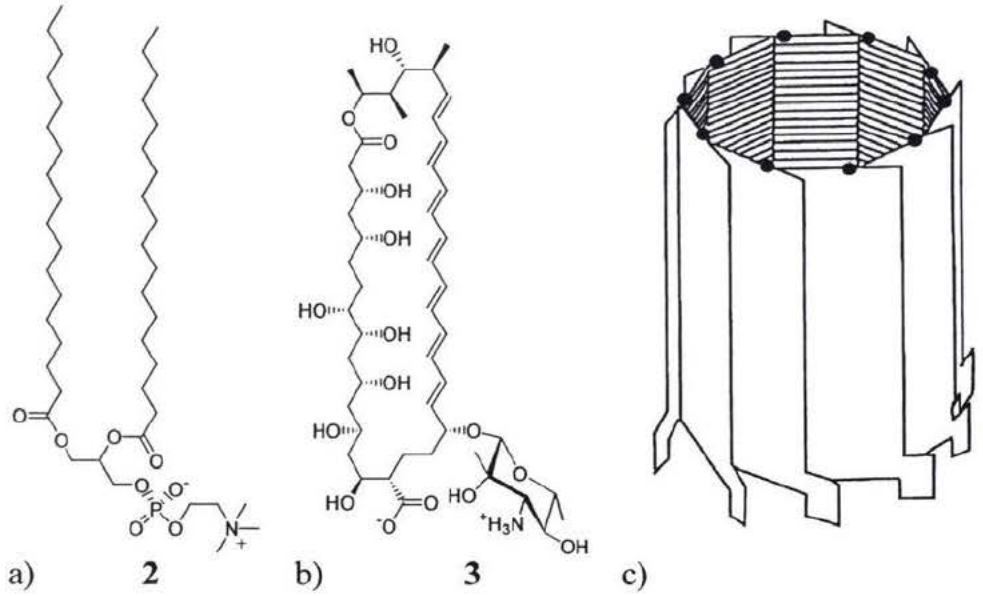

Figure 1.3: a) Structure of phosphatidylcholine, b) structure of amphotericin and c) proposed aggregated half channel of Amphotericin

As shown in Figure 1.3 the macrocyclic structure of Amphotericin mirrors a lipid's structure (**2**). Amphotericin is the model membrane ion channel for those thought to be formed from a barrel stave macrocylic aggregate[11].

1.2 Synthetic Channels:

As mentioned previously, the large biological channels are complex and difficult to study. Although synthetic ion channels generally do not look anything like their protein counterparts, they provide invaluable information. Unlike the natural systems, synthetic channels can be tailor-made to elicit how a specific molecular component influences the compound's activity. It has been determined that there are three main mechanisms for a channel to transport an ion across the bilayer: a defined tunnel, of which gramicidin is an

example, an aggregate pore, of which amphotericin is an example and a disrupting agent. The schematic mechanisms for these are shown in Figure 1.4.

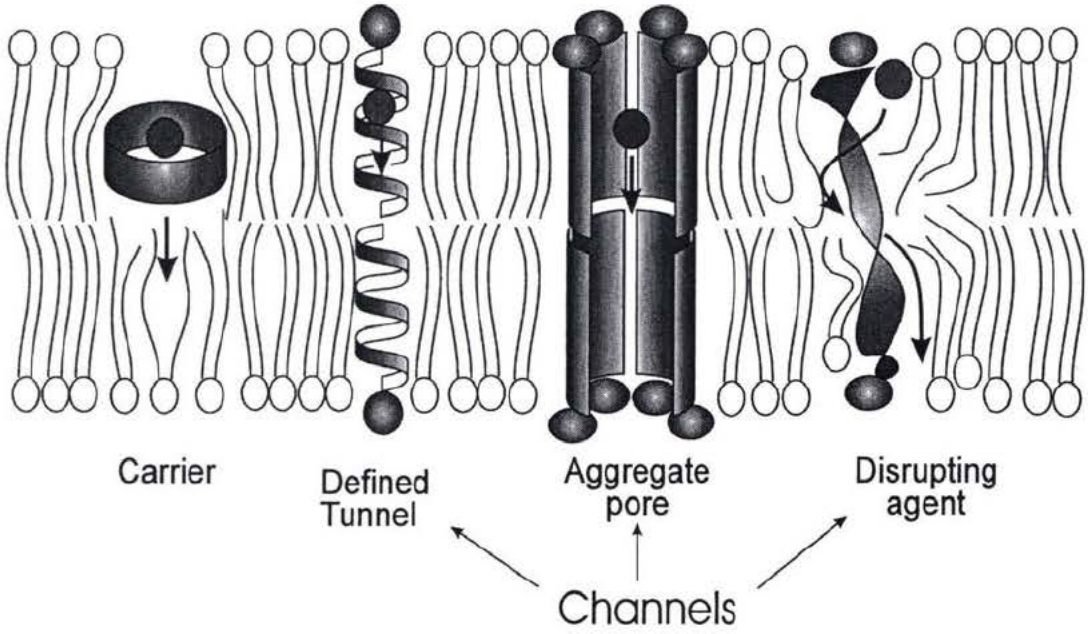

Figure 1.4: Schematic representation of a transporter's mechanism

Figure 1.4 also shows a carrier mechanism. The carrier is not classified as a channel since it does not physically span the bilayer. The carrier is a lipophilic ion complexing agent. Carriers have to diffuse through the membrane and thus typically have ion translocation rates on the order of 10^3 ions s^{-1}. This is quite sluggish compared to the gramicidin rate of 10^7 ion s^{-1} [12].

Four main criteria have been developed in the design of synthetic ion channels; 1) they should span the 4 nm thickness of the bilayer, 2) they should be able to surround an ion of at least 0.3 nm in diameter, 3) they should have polar head groups at the membrane-water interface to orient the channel within the membrane and 4) they should have a complementary balance between polar and non-polar groups through the membrane. If 1 through 4 are met to the appropriate degree then the compound should

insert into the bilayer and adopt a transmembrane orientation. In addition, for practical reasons, the channel forming compounds must be prepared by a feasible and efficient synthesis[13,14]. As the understanding of ion channels has increased, the design has placed a greater emphasis on synthetic issues.

1.3 Survey Of Macrocycle Components Of Synthetic Channels:

Macrocycles have emerged as a key unit to ion channel design because they were believed to be a useful building block to facilitate synthesis[15], provide portals for cation entry and transfer through the bilayer[16] and provide rigidity to limit the conformations available to the channel[17].

In 1982 Tabushi and coworkers reported the first synthetic transporter, **4**. The structure used a β-cyclodextrin that was tetra-substituted on the primary face with alkyl groups to insert into the bilayer and had 14 hydroxyl groups on the secondary face to provide a polar head group. It was hypothesized that two compounds would aggregate, one on either side of the bilayer, and the β-cyclodextrin would give the structure a 0.7 nm pore opening. The total length of this dimer was estimated to be 3.8nm. This channel supported a transport rate constant of $4.5*10^{-4}$ s^{-1} for Co^{2+} transfer[18].

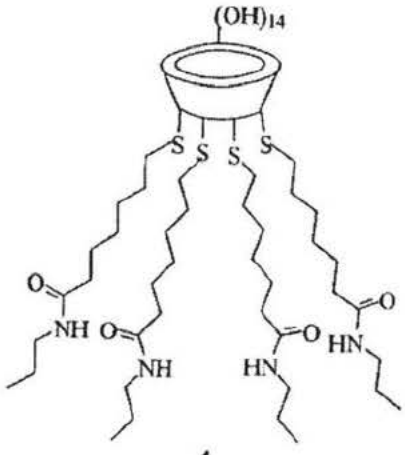

4

Kobuke later tried to expand on this principle with compound **5** that provides a cavity made from four resorcinol rings extended with (C_{17}) alkyl chains. This compound was selective to potassium ions over sodium ions with a permeability ratio (P_{K^+}/P_{Na^+}) of roughly 3. It should be noted that shorter (C_{11}) alkyl chains were tried but the activity was significantly reduced. It was necessary to apply this compound to both sides of the bilayer as its flip-flop within the bilayer was relatively slow. However, it had a specific conductance in KCl of 6.1 pS[19].

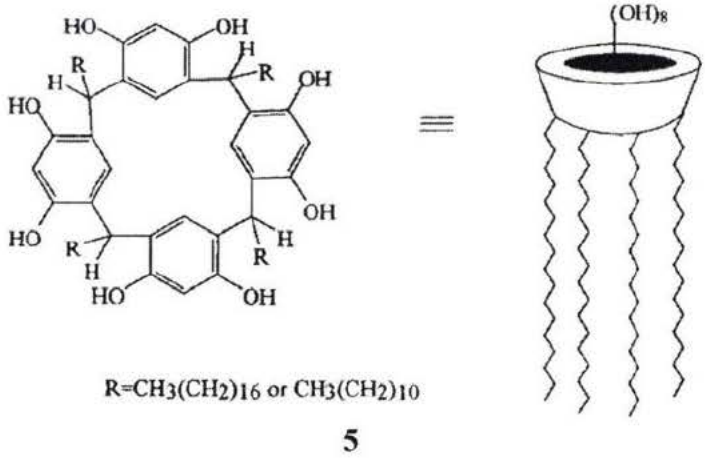

R=$CH_3(CH_2)_{16}$ or $CH_3(CH_2)_{10}$

5

Lehn has described a channel that has several poly(oxyethylene) or polymethylene chains with polar head groups grafted onto a central crown ether or cyclodextrin. Structure **6** is one of the various iterations on this structure. In principle, once inserted into the bilayer it should form a bound cylindrical dimer with an estimated length of 5 nm. This channel was able to support an anti-port mechanism for opposing sodium and potassium ion gradients. The ions exchanged in a one to one ratio, thus there was no evidence for any selectivity between them. All transport rates for the variations on this design were on the order of 10^{-3} min^{-1} [20,21,22,23].

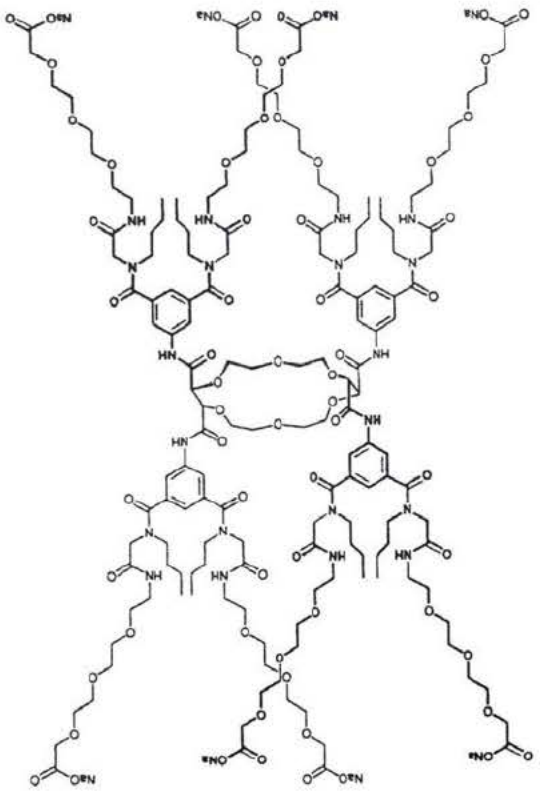

6

Gokel et al have studied a tris crown ether system **7**. They report that the central crown ether can be reduced in size from diaza-18-crown-6 to diaza-15-crown-5 without any reduction in activity. The compounds showed the highest activity when the alkyl chains linking the crown ethers were between 12 and 14 carbons long. If the linkers are two carbons longer or shorter, the activity is decreased two fold. The specific conductance for these compounds is about 14 pS for a range of R groups in NaCl[24,25,26].

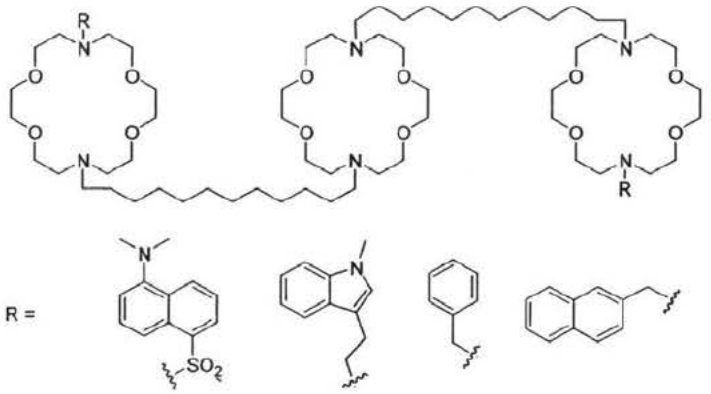

7

Nolte prepared an isocyanide polymer which was substituted at each residue with a crown ether (**8**). The polymer adopts a helical structure that completes one full turn every four residues. This provided a structure which could potentially have four functioning channels. An oligomer with 40 repeating units was approximately 4 nm in length and the distance between staked macrocycles was 0.4 nm. It had a relatively slow cobalt transport rate on the order of 10^{-4} s^{-1} [27,28].

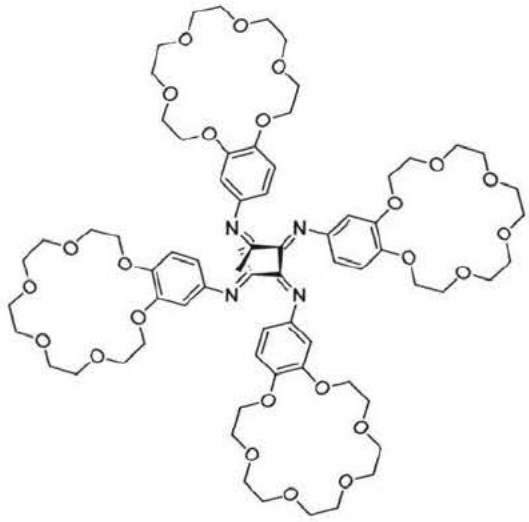

8

Voyer followed a similar design structure. However, instead of using the isocyanide polymer, he used the helical structure of oligo L-Leucine. The structure was t-BOC-N(Leu-Phe-Crown-Leu-Leu-Leu-Phe-Crown-Leu)$_3$OMe, **9**. The location of the crown ethers with in the primary sequence allows the crown ethers to stack one on top of another when in the α-helical form[29].

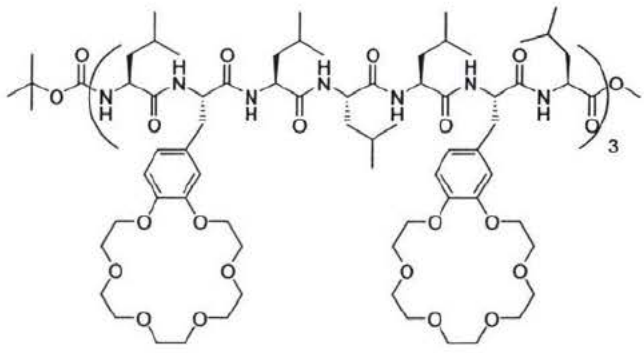

9

Ghadiri developed a self-assembling cyclic β^3 peptide structure. Three structures were tried, cyclo[(-β^3–HTrp)$_4$-], cyclo[(-β^3–HTrp-β-HLeu)$_2$-] (**10**) and cyclo[(-β^3–HLeu)$_4$-]. Of the three, the last structure did not show activity in the survey that was done. The other two show specific conductance of 56 pS in KCl. It was shown that the cyclic peptides stack one on top of another via hydrogen bonding to form a nanotube structure (Figure 1.5a) with a pore diameter of 0.27 nm. However, it is plausible that several of these tubes aggregate to form a larger channel[30]. Ghadiri has recently published a paper describing the antibacterial properties of this particular channel system[31].

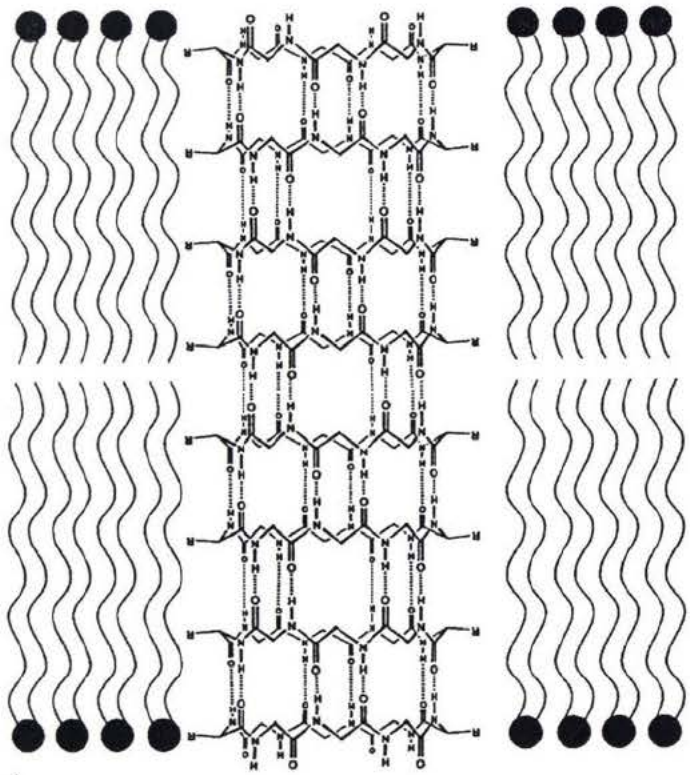

a)

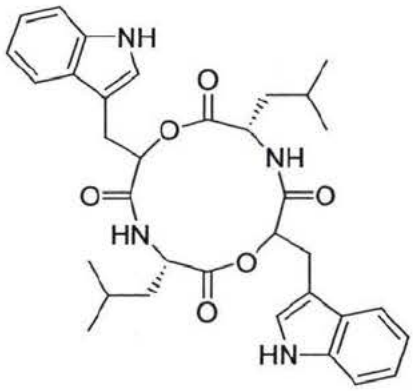

b) **10**

Figure 1.5: a) Proposed aggregate of **10** designed by Ghadiri b) the structure of one of the channel forming cyclic peptides

Fuhrhop's group designed the first macrocyclic bola-amphiphiles (**11**). The term bola-amphiphile is given to compounds with polar head groups at both ends of a hydrophobic core. The actual compounds designed were a synthetic membrane monolayer. These 2 nm thick monolayers were normally impermeable to lithium. However, it was found that monensin pyromellitate (**12**) could perforate the synthetic membrane and make it permeable to Li^{+} [32,33].

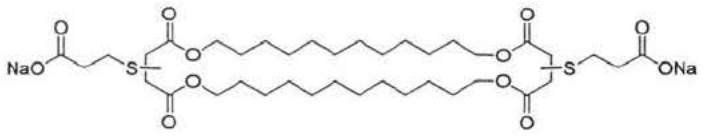

11

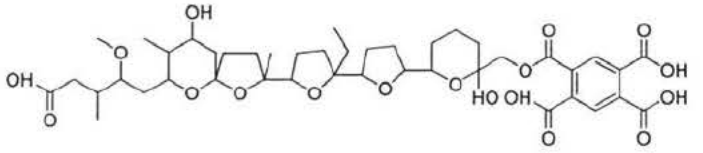

12

It was the synthetic membrane designed by the Fuhrhop's group for which the Fyles group attempted to design the first macrocyclic bola-amphiphile channel. However, it was quickly found that vesicles formed by synthetic membranes suffered from excessive leakage. The solution to the vesicle leakage was to switch to a bilayer formed from egg phosphatidylcholine. Thus it was necessary to increase the channel length from 2 nm to 4 nm. This was achieved by linking two macrocycles end to end[34].

Tony James, a former student of the Fyles group, completed the first suite of compounds under this format.

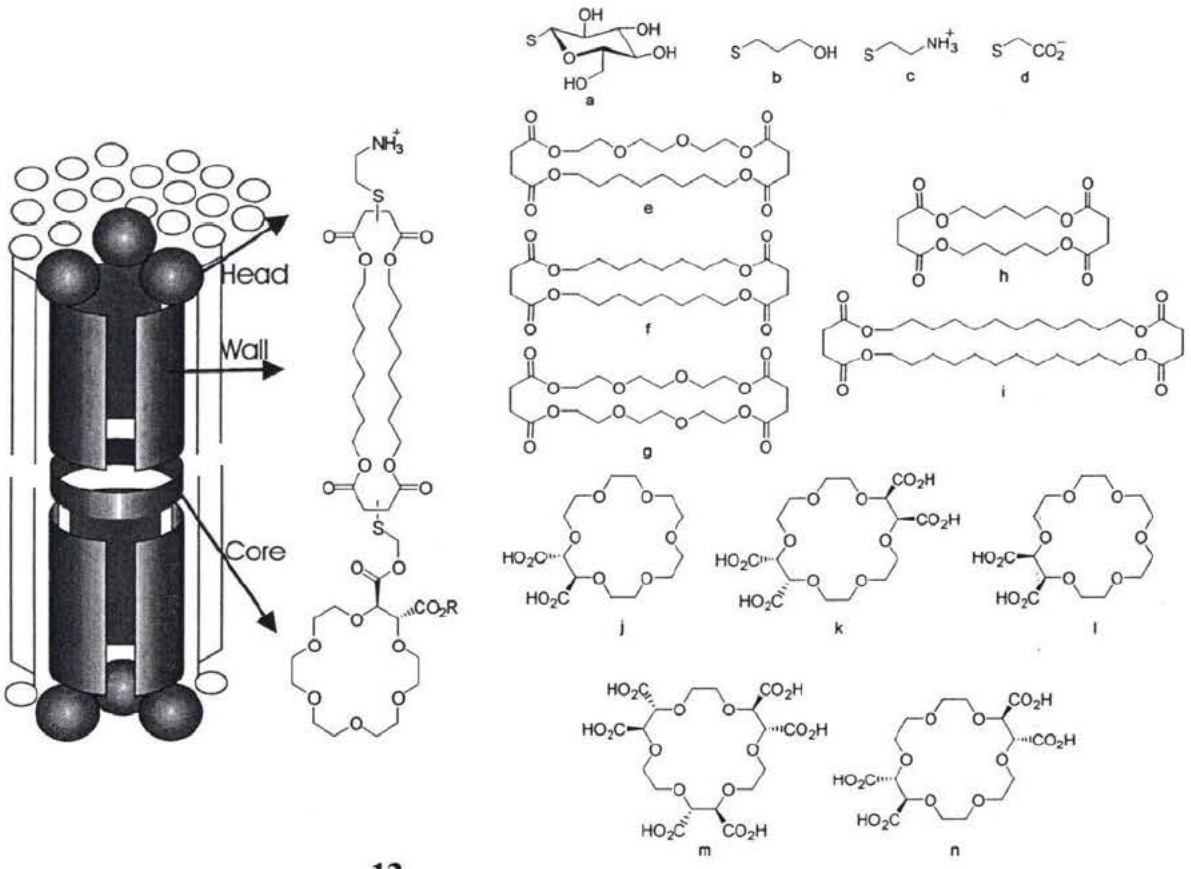

13

Figure 1.6: Suite of compounds synthesized by James

As shown in figure 1.6 the channel was envisioned as a defined tunnel. Out of a possible 100 compounds from the set of building blocks, James synthesized and tested 21. Crown ethers were used to provide a rigid conformation for the core units. The cores were made from hexa-, tetra, or di substituted 18-crown-6 ethers. It was found that only **m** and **n**, or the hexa and tetra substituted crown ethers acted like ion channels. The cores, such as **k**, which had all the wall units pointing in one direction acted like carriers. This suggested that it was necessary for at least two pairs of wall macrocycles, which span the bilayer, to form a channel. The wall units, **i** and **g** provided no activity. James thought that **i** was too long and **g** was too hydrophilic. The wall units **f** and **e** provided the most activity. No activity was found in any of the compounds with the head group **b**[35,36].

The synthetic route designed by James to create unimolecular channels results in a tedious synthesis with low yields. Another student, Mohammad Zojaji, synthesized a suite of macrocyclic bola-amphiphiles that were thought to aggregate within the bilayer to form channels, shown in Figure 1.7. This suite included the same types of building blocks used by James.

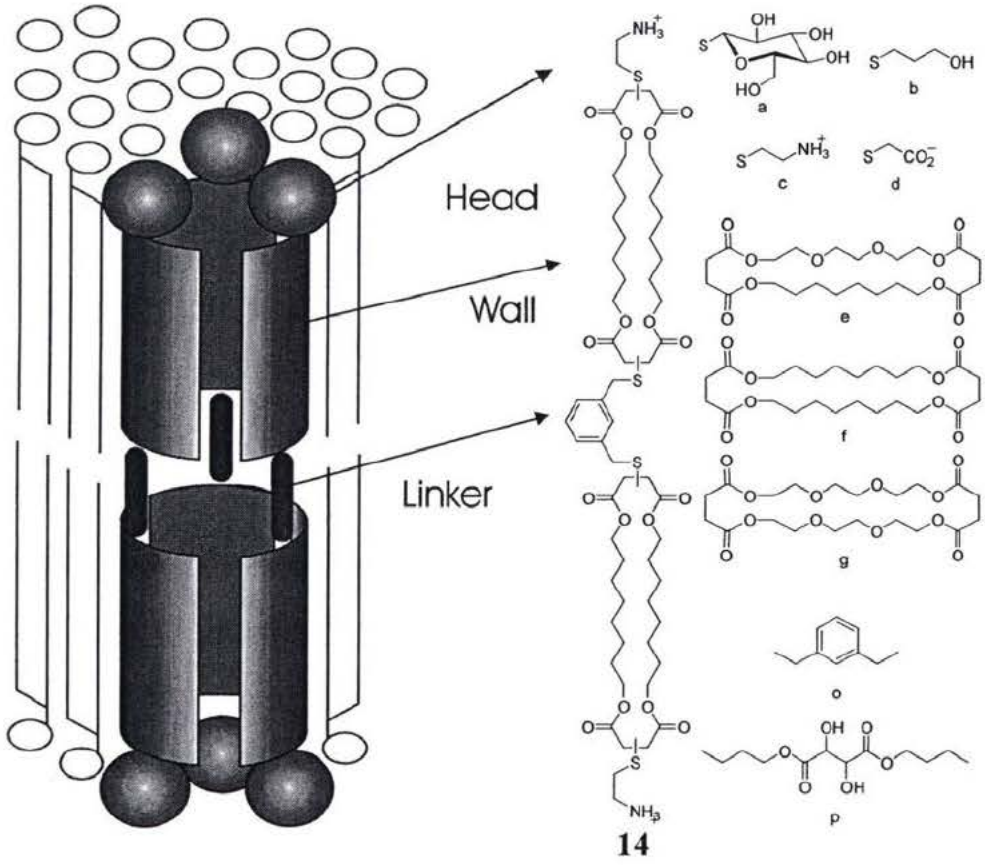

Figure 1.7: Suite of compounds synthesized by Zojaji

In this study 14 compounds were synthesized. Three of the 14 compounds had similar or higher activity than Amphotericin. Those compounds were, in decreasing order of activity, composed of **c-e-o-e-c**, **a-g-p-g-a** and **a-e-p-e-a**. It should be noted that the combination of linker **c-e-p-e-c** was not tried. The linker **p** produced higher activity than the linker **o** when they were used in compounds with the same head group. This was

probably due to the hydrogen bonding ability of linker **p.** Hydrogen bonding would allow for stronger intermolecular interactions within an aggregate. The order of activity in the wall units was **e** ≈ **f** > **g**. Once again, the reason given was **g** was too hydrophilic. All of the compounds with the linker **o** and either **a** or **b** as the head groups were inactive[37].

A third suite of aggregate pore formers, synthesized by Xin Zhou, focused on developing channels that switched on and off depending on the transmembrane potential. The response to membrane potential requires different charged groups at either end of the channel. The channel structure was similar to Zojaji**,** the difference was in the polar head groups and linkers used[38,39].

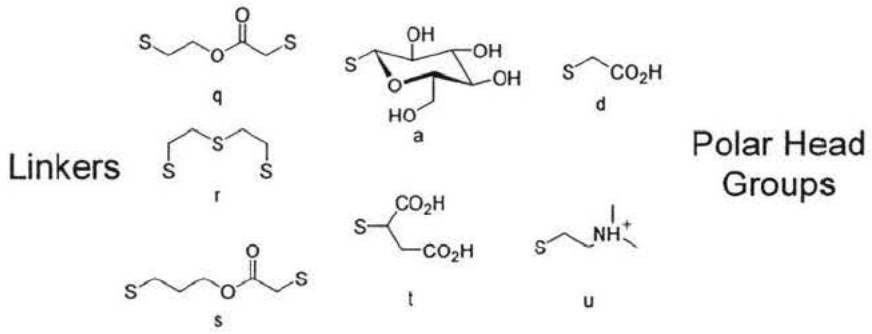

Figure 1.8: Linker and head groups that Zhou used with the wall units that James and Zojaji used

It was found that the combination **t-e-s-e-d** gave the most efficient voltage gated system. Zhou found that compounds with the **e-s-e** wall linker wall combination had an apparent kinetic order of about 2. This suggested that they formed active dimers. The one exception to this was the voltage gated **t-e-s-e-d** that had a kinetic order greater than 2, which suggested that it formed a higher order oligomer[38,39].

In order to synthesize compounds with different head groups the synthetic efficiency was decreased significantly. Although aggregated pore formers (Zojaji, Zhou) result in a higher yielding and a shorter synthesis than the defined tunnels (James), the

overall synthesis still has some problems. The first is the low overall yield; the cyclization step alone had a yield of 6.5%. The ends of the initial macrocycle are not differentiated yet this is required. This results in poor yields in the linking steps due to statistical mixtures. Also, using the Michael addition on the ends of the macrocycles to both link the macocycles and add head groups results in a large number of regio isomers.

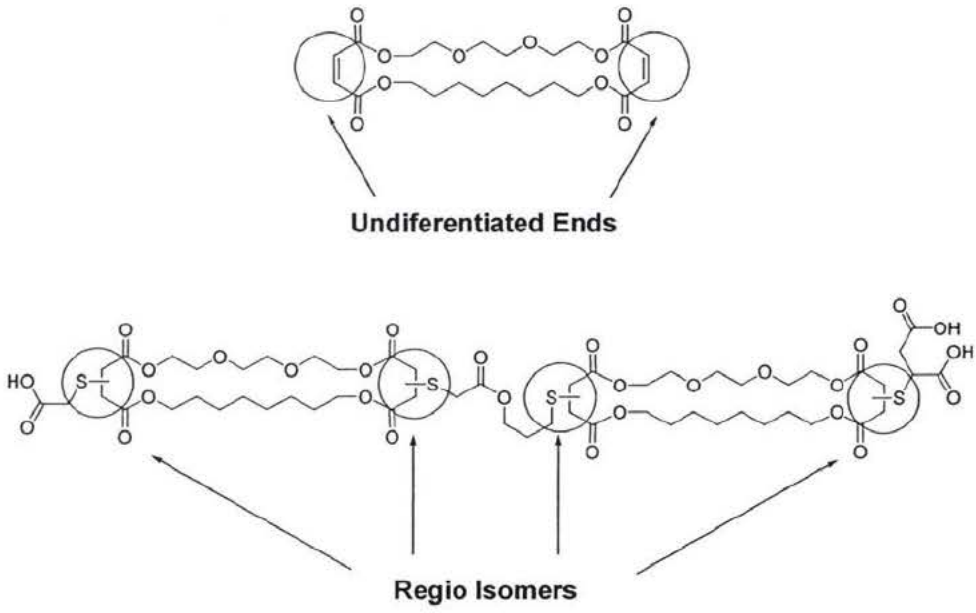

Figure 1.9: Problems with macrocyclic bola-amphiphile synthesis

These deficiencies in the tetraester macrocycle synthesis resulted in the design and synthesis of **15** by former student Lynn Cameron.

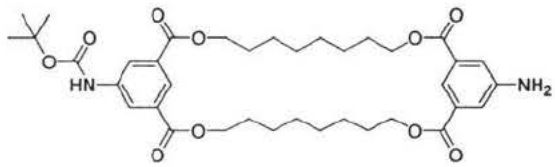

15

Her target had a cylization yield of 16%, had differentiated ends and was axially symmetric, which eliminated the regio isomer problem. This meant that the linking reaction had greatly increased yields. The new macrocycle, **15**, is similar in length to the

previous macrocycles and it had the same proportion of hydrophilic components as macrocycle **f**[40].

In the subsequent synthesis by Chi-Wei Hu two of these macrocycles were linked as a terephthalamide and then deprotected to form **16**. Compound **16** is very difficult to work with as it is soluble only in hot DMSO. It is however an active channel transporter. The specific conductance of single channel opening events was 13.7±1.7 pS with peak specific conductivities of 620 pS. The most interesting property of this compound was the variation in behavior with variation of the method of application to the bilayer. When the compound was applied with a brush, discrete openings were observed as described by the single channel opening events. However, if the compound was applied directly to the bilayer via DMSO, a general increase in bilayer conductance occurred for hours, with current voltage characteristic changing on a scale of minutes. The peak conductance measure from this compound was 620 pS, which makes this compound the most active ion channel ever constructed. The low solubility was believed to be in part responsible for the novel activity of this compound.[40].

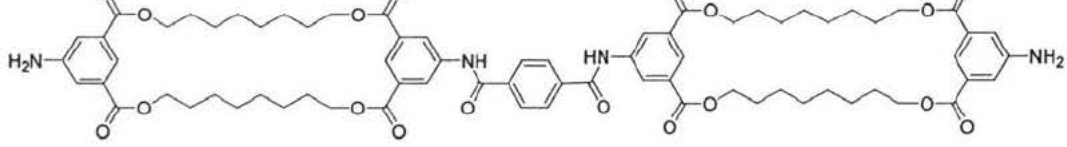

16

The trend in the last five years in the Fyles group has been toward simpler compounds with shorter synthesis. This is clearly shown by the progression from unimolecular channels to the bismacrocyclic bola-amphiphiles. In the last year the process of simplification has gone even further. Chi-Wei Hu showed that a macrocycle can be removed and the resulting compound still retains ion channel activity[41].

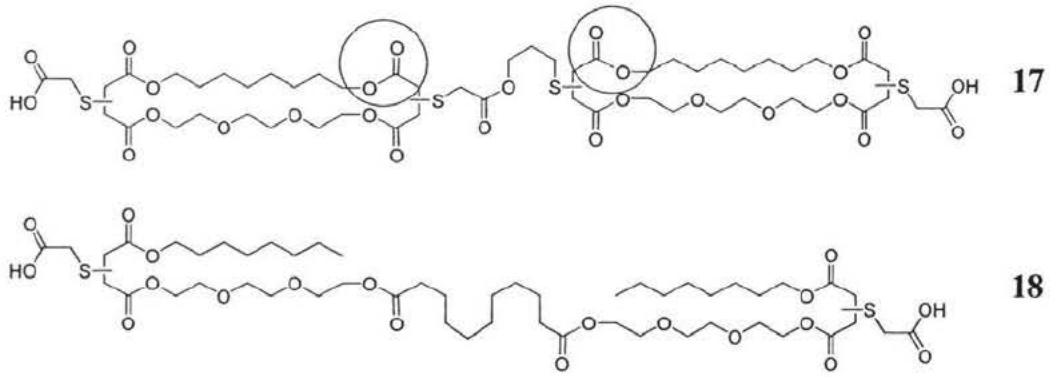

Figure 1.10: Design of the Fyles group's first non-macrocyclic channel

Figure 1.10 shows that the difference between **17** and **18** is the deletion of the circled esters in **17** to open up the macrocyclic ring and the replacement of the thioether and ester in the linker unit with methylenes. The resulting change in the specific conductance was from 15 pS in **17** to 14 pS in **18**[41]. The macrocycles were apparently not necessary for the function of **17**.

1.4 Design:

Macrocycles have a low yielding synthesis. If macrocycles can be completely eliminated and the resulting compounds still maintain their channel activity then this is both a step forward for the synthetic efficiency and it will also give insights into the functioning of the channels themselves. The design of the compounds for this thesis was intended to explore if the demacrocyclization strategy that gave **18** from **17** without less activity is generally true for other bis macrocycle bola-amphiphiles. The high activity of **16**, its tedious synthesis and its very poor solubility made it a perfect candidate for answering this question. Furthermore, this thesis will begin to explore the role of the volume taken up by the wall units and the significance of hydrogen bonding groups in the linker. The effect of the length on the compounds overall activity will most likely be

explored in a later synthesis, once the activity of the compounds designed in this thesis is established.

Using a molecular mechanics modeling system it was found that the estimated through space distances between the polar head groups of **17** and **18** are shorter than the average bilayer thickness. The fluidity of the bilayer is such that in some places in it will be thinner than others[39]. If the length estimate is correct, the compounds must have inserted in such away that their solvated head groups initially formed divots in the bilayer. This would suggest that the solvated polar groups of **18** were being pulled towards the aqueous layer producing a tension that gave **18** an element of rigidity, eliminating the need for rigidity from the macrocyclics of **17**. The terminal alkyl chains are not subject to the bilayer induced tension and may reduce activity by spinning around and disrupting the channel. However, as shown by the difference in activity between the wall units **g** and **e**, the lipophilicy of the alkyl chain was probably necessary for the insertion of **18** into the bilayer.

Compound **16** and compounds with the macrocylic wall **f** showed as good or better activity with an axially symmetrical structure than compounds with the asymmetric macrocylic wall unit **e**. Therefore, to preserve the both the axial symmetry and the rigidity induced by solvated head groups, the demacrocyclization of **16** was carried out at either end by adding a second head group, creating **19** (refer to figure 1.11).

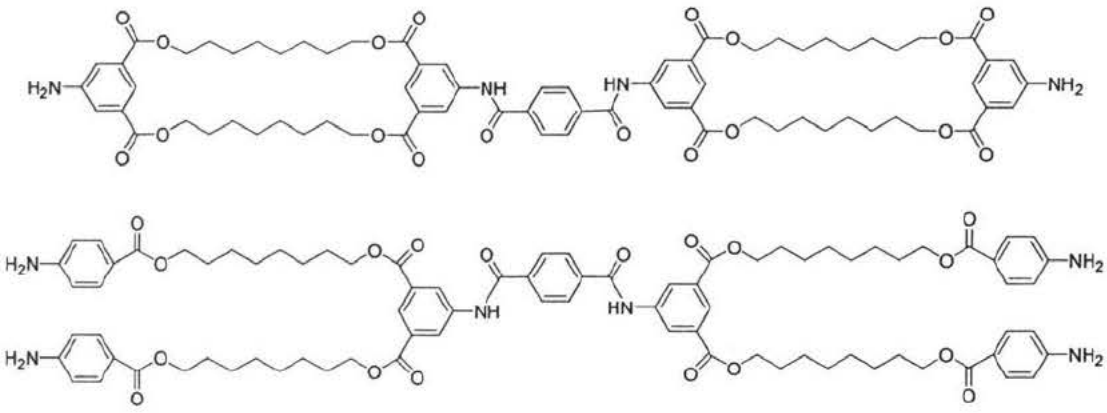

Figure 1.11: Design and structure of the compound **19**

Figure 1.12 shows a computer generated model of **19** within a lipid membrane represented by four phosphatidylcholine lipid pairs. Crystal structures have shown the phosphatidylcholine has a chain tilt of 41° with respect to the layer normal[42]. Thus the angle of the lipid dimers in Figure 1.12 has been approximated to 41° with respect to the layer normal. The rotation of the carbon-amide, amide-carbonyl and carbonyl-carbon bonds in the linker section produced three conformations of **19**, (a), (b) and (c). The conformations were arranged such that they are approximately central with respect to the lipid dimer. All three of the conformations show approximately the same energies with respect to the gas phase estimates given by MM2 calculations. None of the conformations have been optimized for the self-orientating structure of the membrane, since this would be a project in itself.

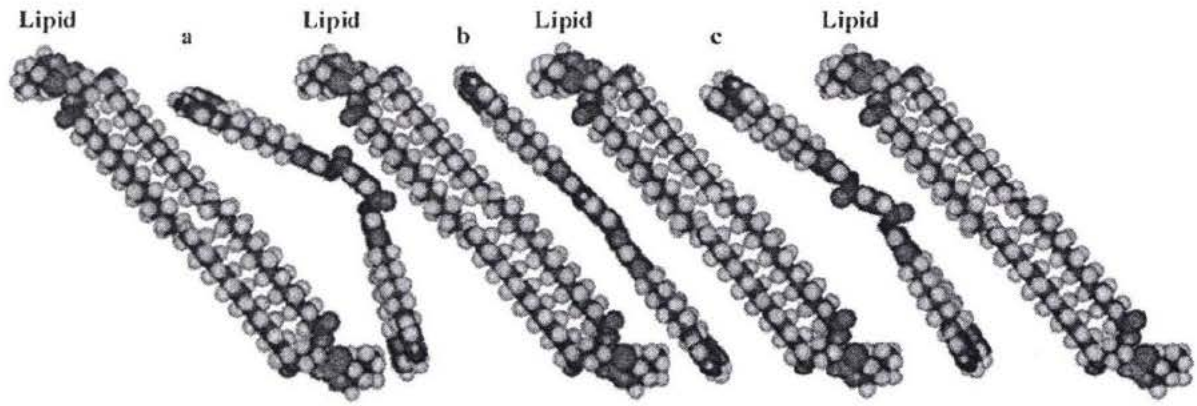

Figure 1.12: Molecular model sketch of the effects of three different conformations of the linker section of **19** on the overall length relative to phosphatidylcholine dimers tail-to-tail

The bilayer can be viewed as being composed of three regions; the central region containing hydrophobic tails, the exterior layer, containing charged polar head groups and, between these two regions, a polar region where hydrogen bonding between the carbonyl and hydroxyl groups of the lipids is a dominant force[42]. All three of the conformations of **19** resulted in the through space distance between the amine head groups that was shorter than the bilayer thickness. The distance was 4.4 nm for conformations (b) and (c) and 3.9 nm for conformation (a) compared to 5.2 nm, which is the through space distance between the quaternary ammonium groups of phosphatidylcholine. This suggests the solvated head groups will still add tension to any of the conformations of the linker section. Initially it would appear, due to the span of (a) that the alkyl tails of (a) would adjust to span the bilayer, and/or the linker section would twist such that conformation (a) would not exist in the bilayer. However, conformation (a) may span the bilayer vertically. The through space distance between the quaternary ammonium groups of phosphatidylcholine is 4.0 nm with respect to the layer normal. The other force which may play a role in the stability of this structure within the bilayer is the

hydrogen bonding region. In the lipid mix which will be used to test these compounds, phosphatidic acid is used to increase the packing density[14]. Thus this additive might play a role in the stability and conformation of the compounds within the membrane. The estimated through space distance between the terminal ester carbonyls of conformations (b) and (c) is 3.9 nm. This compares to the estimated 4 nm through space distance between the ester carbonyls of phosphatidylcholine. The approximate distance between the carbonyl groups of phosphatidylcholine with respect to the normal layer is 3.1 nm; this compares to the 3.2 nm estimate for of the terminal ester separation for conformation (a). Thus, in this series of compounds the esters at the end of the tails should sit in the hydrogen bonding region of the bilayer and the charged aminobenzene groups should sit in the polar head group region.

Ever since Dr. T. James and Dr. M. Zojaji's work, it has been believed in the Fyles group that the channels form as dimers. The vesicle studies and bilayer clamp experiments on compounds synthesized by Zhou confirmed that the majority of the macrocyclic aggregates were dimers. If this were to be true for **19**, then the flexibility of the four tails should allow them to move into positions that form a cylindrical pore. However, if two of the tails were removed the resulting compound **20** would occupy less volume than either **16** or **19**. Compound **20** should have greater potential for aggregation, since its simple structure may allow it to pack with a higher stability than an aggregate of **19**. Thus, it might form channels from several molecules stacked into a barrel stave conformation. The through space distance between the carbonyls at the ends of the tails of **20**, assuming it adopts either conformation (b) or (c), is 4 nm. This is identical to the estimate for the bilayer thickness. The estimated through space distance between the

amine groups of **20** in conformation (b) or (c) is 5.4 nm, which is slightly longer than the phophatitylcholine dimer separation of the quaternary ammonium group, at 5.2 nm.

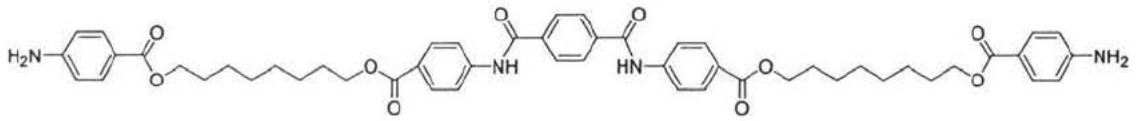

20

The linker of **16, 19** and **20** has the possibility of self-hydrogen bonding. Figure 1.13 displays the optimum stacking conformation of the linker section, which would result in the strongest intermolecular forces. This conformation includes two amide-carbonyl hydrogen bonds and three places where pi-stacking may occur. This is reminiscent of the intermolecular forces between the base pairs adenine and thymine, which have a hydrogen bond length of 0.28 nm. Thus 0.28 nm was used as the hydrogen bond distance in the model shown in figure 1.13. This produced an aromatic spacing of 0.55 nm.

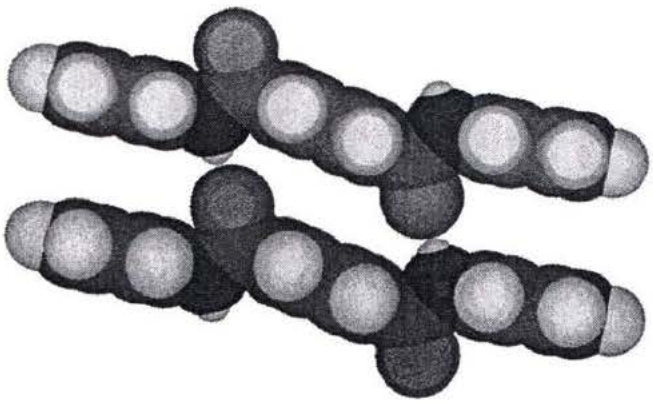

Figure 1.13: Representation of the orientation for the linker sections to hydrogen bond in compounds **16, 19** or **20**

The intermolecular forces in the linker, combined with the rigidity of the macrocycles in **16** probably played a significant role in the high insolubility of the compound. Thus, if hydrogen bonding plays a significant role in this series of compounds

it should be shown by **20**, still having low solubility. However, due to the flexibility of the tails outside the bilayer, it should have a higher degree of entropy and thus a higher solubility than **16**. Compound **19**, having twice the number of tails, should have a higher solubility than **20**.

In this thesis whether the compounds hydrogen bond or not will play a significant role in determining how the compounds span the bilayer. If hydrogen bonding plays significant role in the intermolecular forces between compounds, it is likely that **16**, **19** and **20** would orient the linker as shown in Figure 1.14 and conformation (c). In order to assess the role hydrogen bonding played in this series, compound **21** was created. In **21** the amides in the linker section were replaced with oxygens, thereby eliminating the possibility of a carbonyl-amide hydrogen bond between linkers.

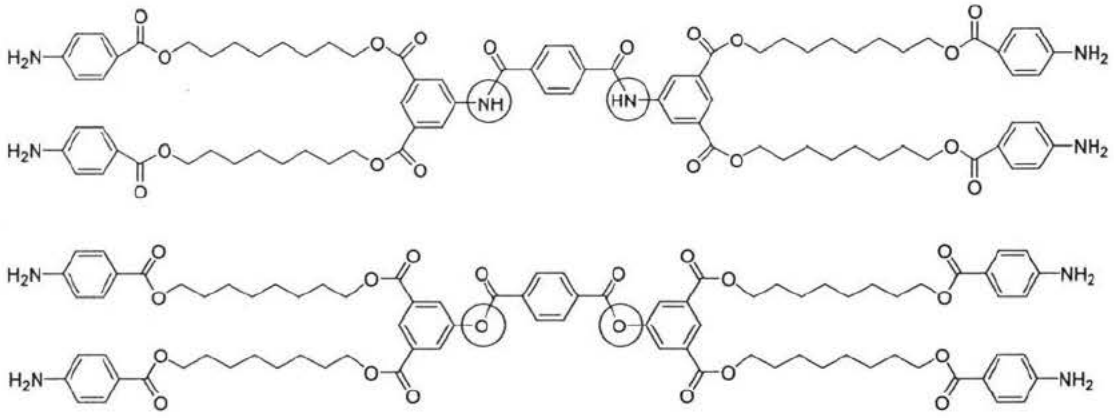

Figure 1.14: Design and structure of the compound **21**

In summary the bismacrocyclic bola-amphiphile, **16**, was split forming the two tails of **19**. To show if the volume occupied by the macrocycle in **16** or the four tails in **19** played a role, **20** was formulated by removing two of the tails. Finally, in order to show if a possibility of hydrogen bonding in the linker segment amplified the activity of the channel, **21** was devised by replacing the two amide groups in the linker with oxygens.

Chapter 2: Synthesis Of Channel Forming Compounds

2.1 Overview:

A convergent synthesis using modular subunits was used to construct the channel forming compounds in this thesis.

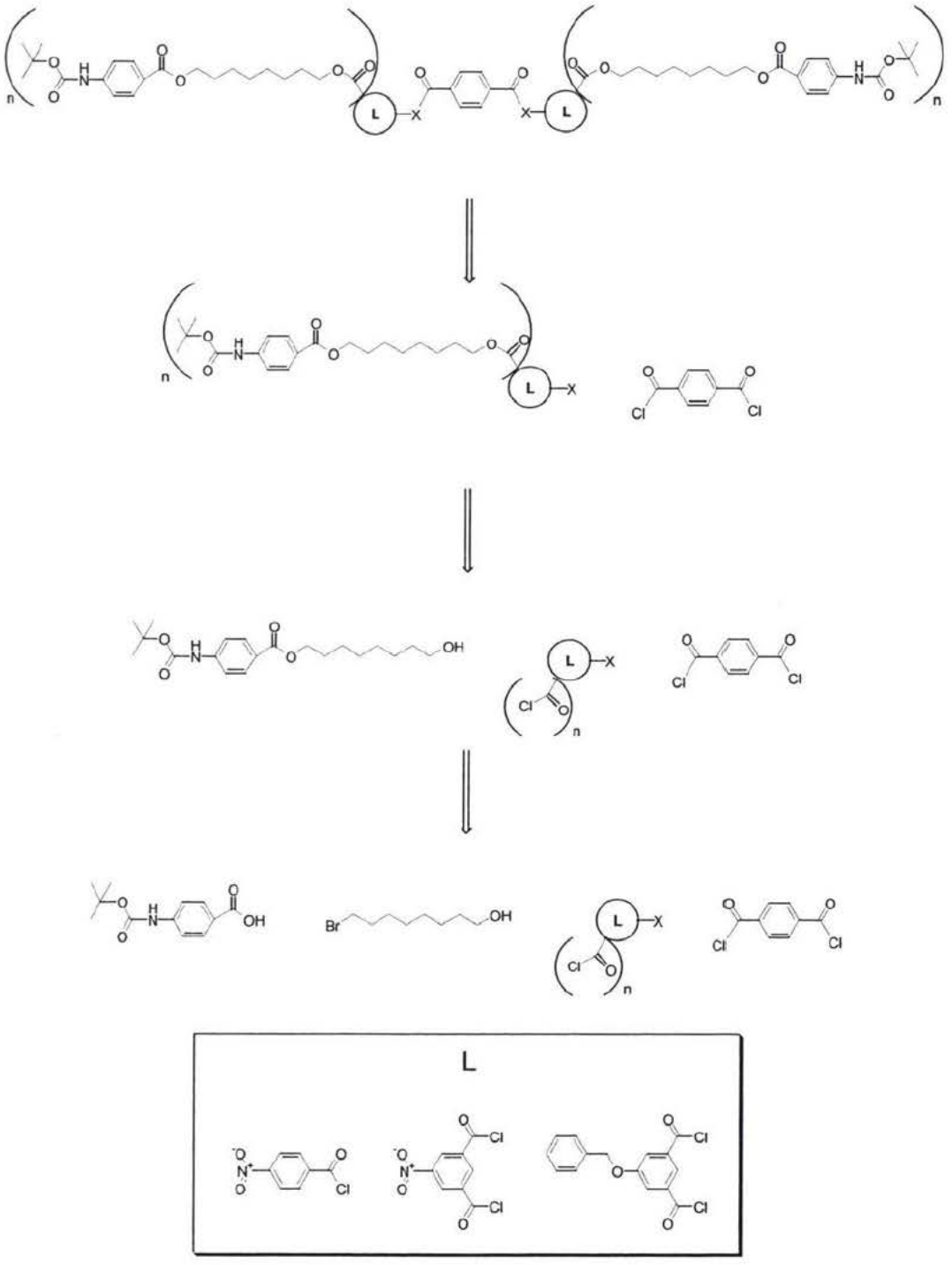

Figure 2.1 Retroanalysis of the synthesis of compounds **19**, **20** and **21**

As show in Figure 2.1, all three compounds could be made by varying only one component, the L subunit. This allowed for the three compounds to be made under very similar procedures. In order to simplify the synthesis further, commercial reagents were used wherever possible.

It will be helpful when discussing the synthesis to have a common reference label for each carbon or proton for each compound. Thus the proton NMR spectra were labeled via α and the carbon NMR spectra were label via β.

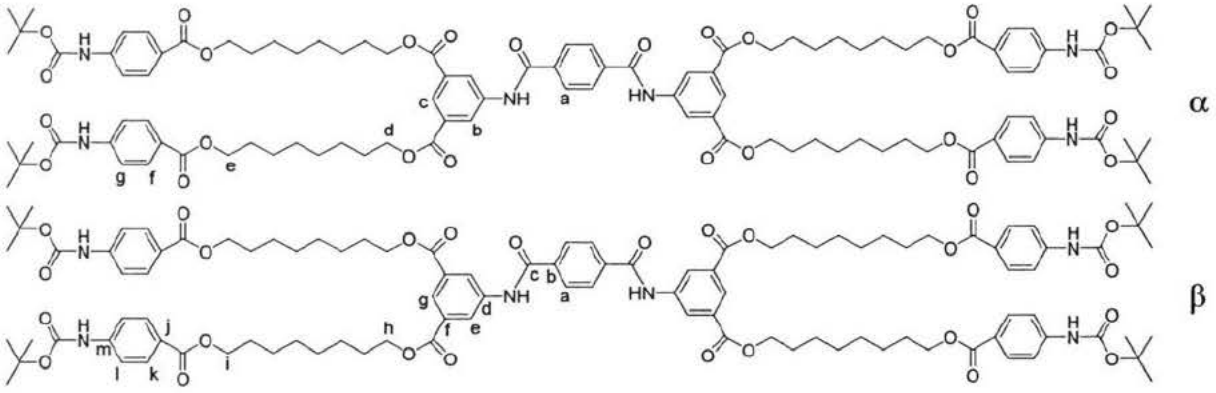

2.2 Synthesis of 27:

Compound **27** was the common piece for all three compounds and was readily made as shown Scheme 1

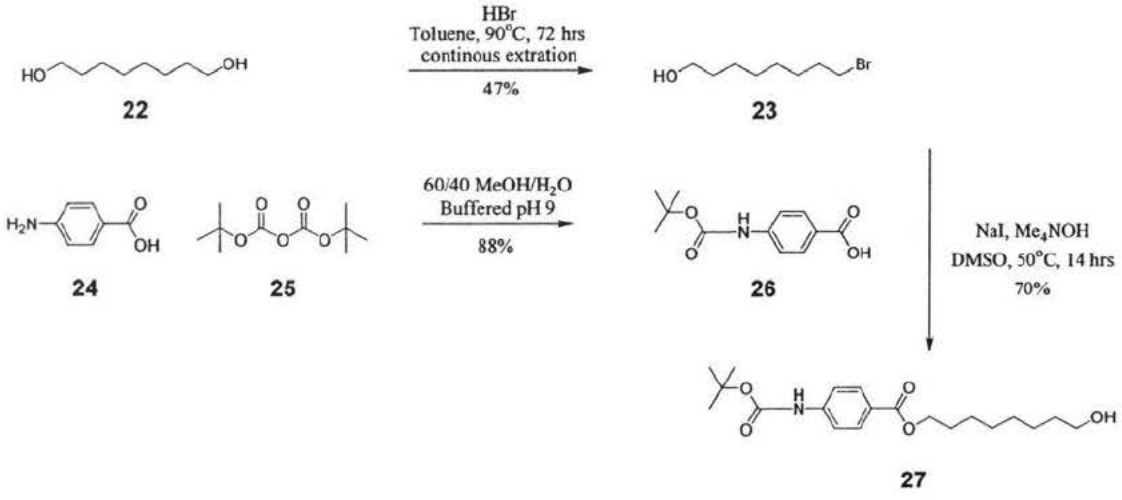

Scheme 1: Synthesis of **27**

Compound **23** was formed by a substitution reaction with HBr. The appearance of the 3.36 ppm peak in the proton NMR spectrum and the addition of four peaks in the carbon NMR spectrum showed the completion of the reaction. The carbon NMR spectrum and proton NMR spectrum chemical shifts were in accordance with structural calculation and literature values[43].

The protection of the amine in **24** was necessary to prevent side reactions in the following steps. Boc was chosen due to its robust nature and its acid catalyzed removal. Compound **26** was obtained by mixing **24** and **25** at pH 9. The proton NMR spectrum was consistent with the structure, showing the chemical shifts of the aromatic amine protons at 8.78 ppm, the two peaks for the aromatic protons at 7.98 and 7.68 ppm and the Boc protecting group protons at 1.42 ppm Both the carbon and proton NMR spectra were similar to the estimated values given by structural calculations.

The esterification to form **27** was done via a substitution reaction using tetramethylammonium hydroxide to form the carboxylate salt of **26**, followed by the addition of **23** sodium iodide was added to convert the bromide to an iodide in situ. The purification was done by silica chromatography. The proton NMR spectrum of the product showed the formation of **27** by the chemical shift of the CH_2 protons next to the Br in **23** shifting from 3.36 ppm to 4.25 ppm when **27** had formed. The carbon NMR spectrum mirrored this by a peak consistent with ester formation appearing at 65.2 ppm. All of the compound peaks in both the proton NMR spectrum and carbon NMR spectrum were consistent with the estimated values by structural calculations.

2.3 Synthesis of 19:

The overall synthesis for **19** is shown in scheme 2.

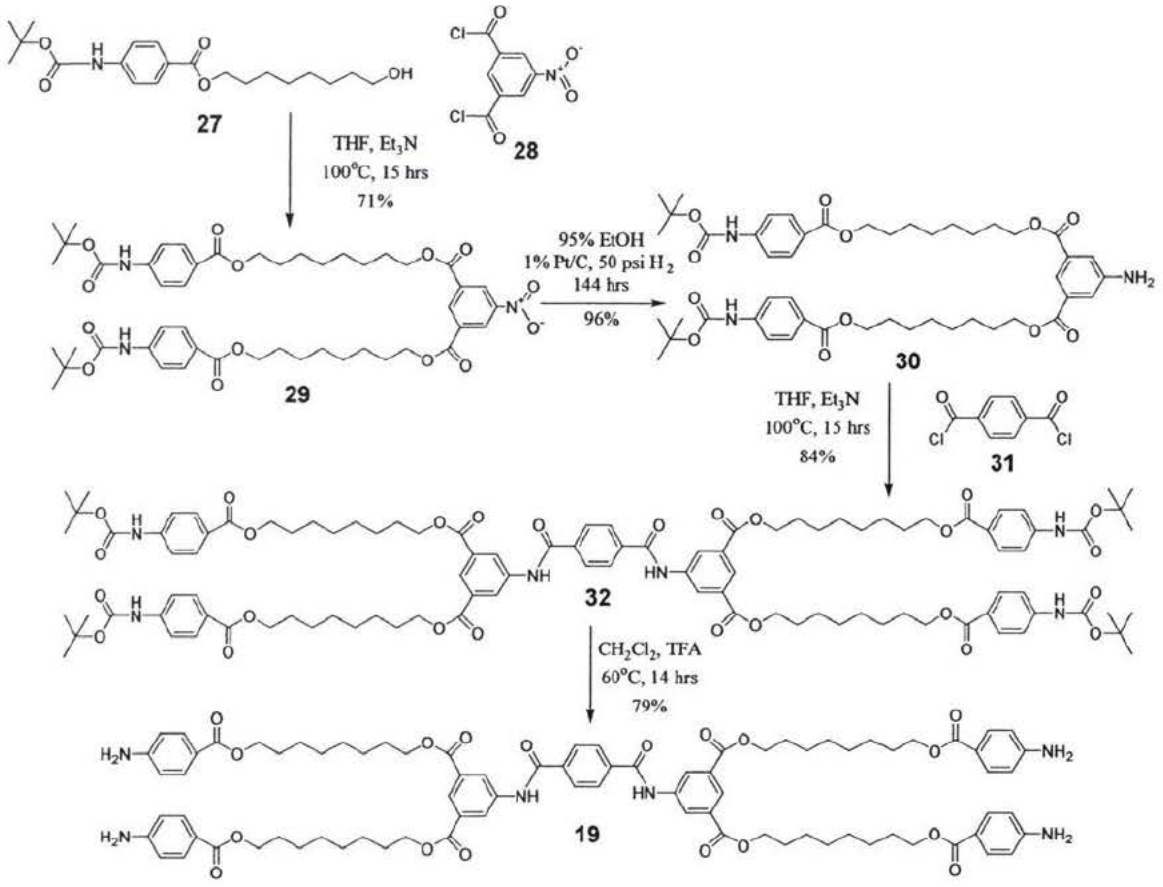

Scheme 2: Synthesis of **19**

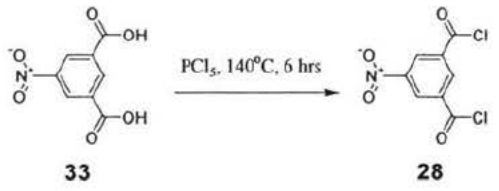

Scheme 3: Synthesis of **28**

The acid chloride **28** was shown to have formed by the downfield shift of the aromatic proton and carbon chemical shift from **33** and the upfield shift of the carboxylic acid carbon chemical shift to 165.6 ppm. The carbon and proton NMR spectra of **28** are consistent with chemical shift calculations of the assigned structure.

The esterification to form **29** was done via an acid chloride reaction with the alcohol **27**, followed by purification by silica chromatography. The proton NMR spectrum of the product (Figure 2.2) is consistent with the structure of **29.** Notably, the signal for the **d** protons appears at 4.38 ppm in **29,** downfield from 3.50 ppm for the same methylene group in **27**. Similarly the carbon NMR spectrum (Figure 2.3) shows the **h** carbon at 66.4 ppm in **29** compared to at 62.4 ppm in **27**. The integration of the proton NMR is consistent with a 2:1 ratio of components derived from the two reactive pairs (protons **d**, **e**, **f** or **g** : protons **b**). All of the compound peaks in both the proton NMR spectrum and carbon NMR spectrum were consistent with chemical shift calculations of the assigned structure.

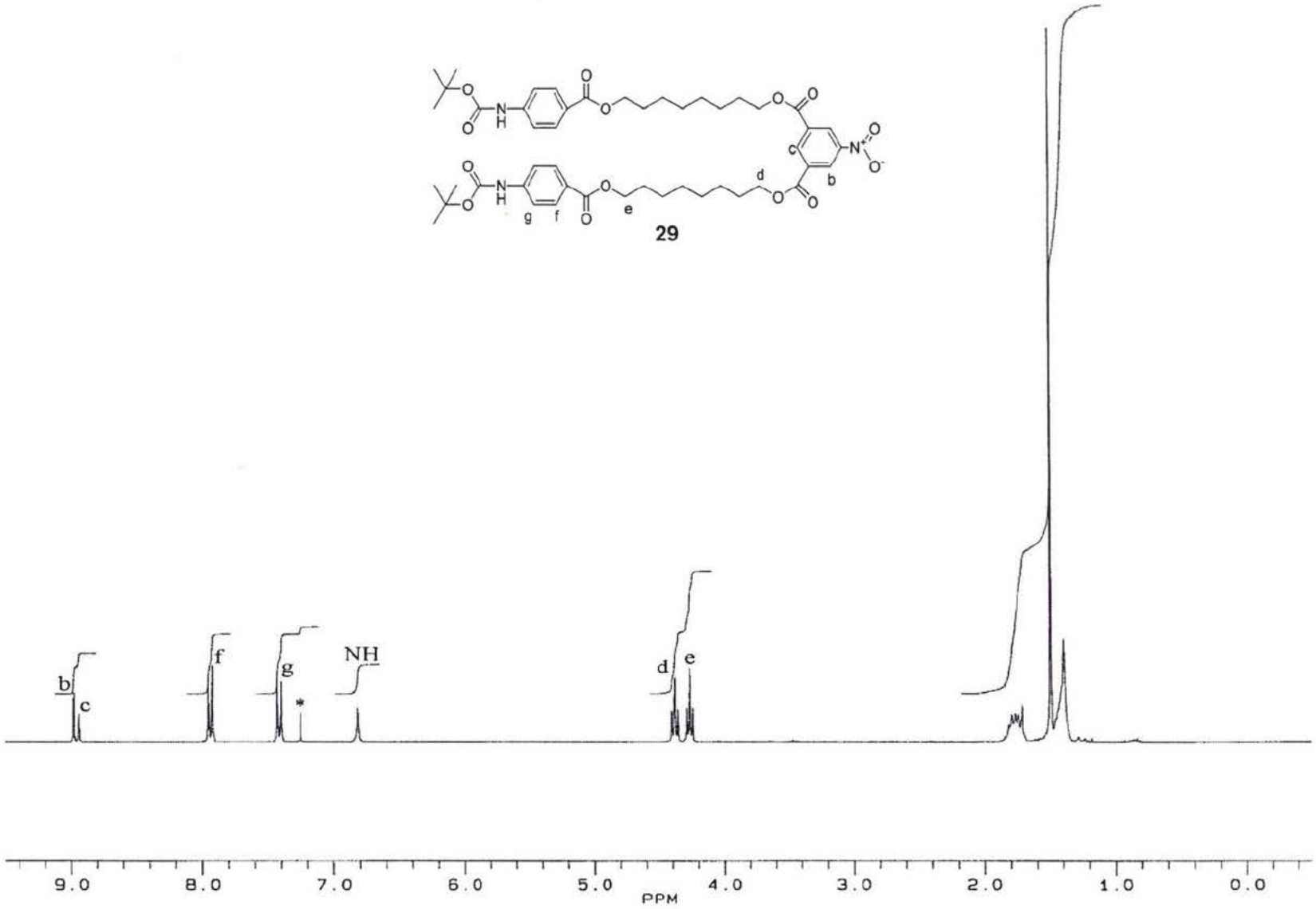

Figure 2.2: Proton NMR spectrum of compound **29**

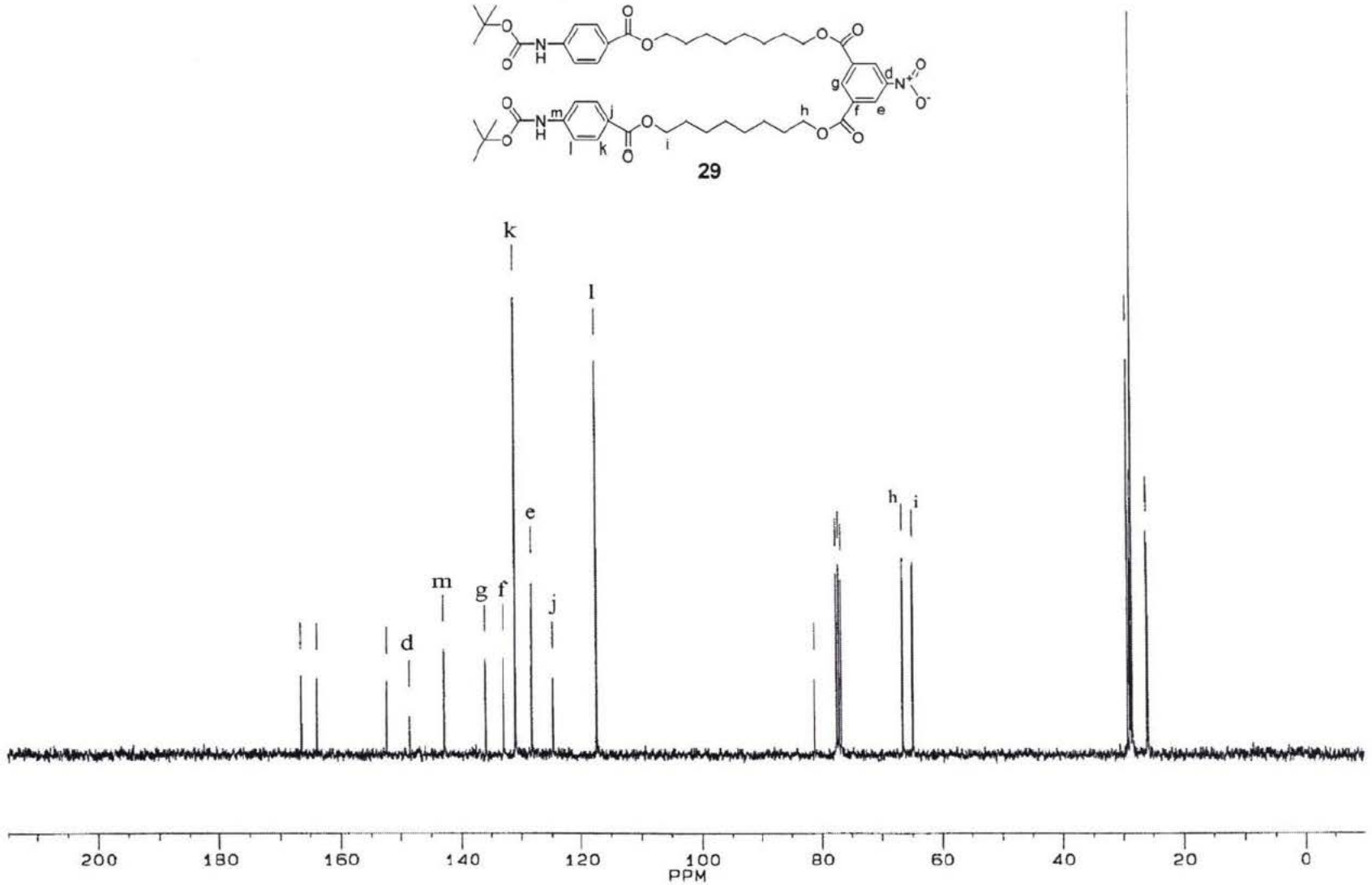

Figure 2.3: Carbon NMR spectrum of compound **29**

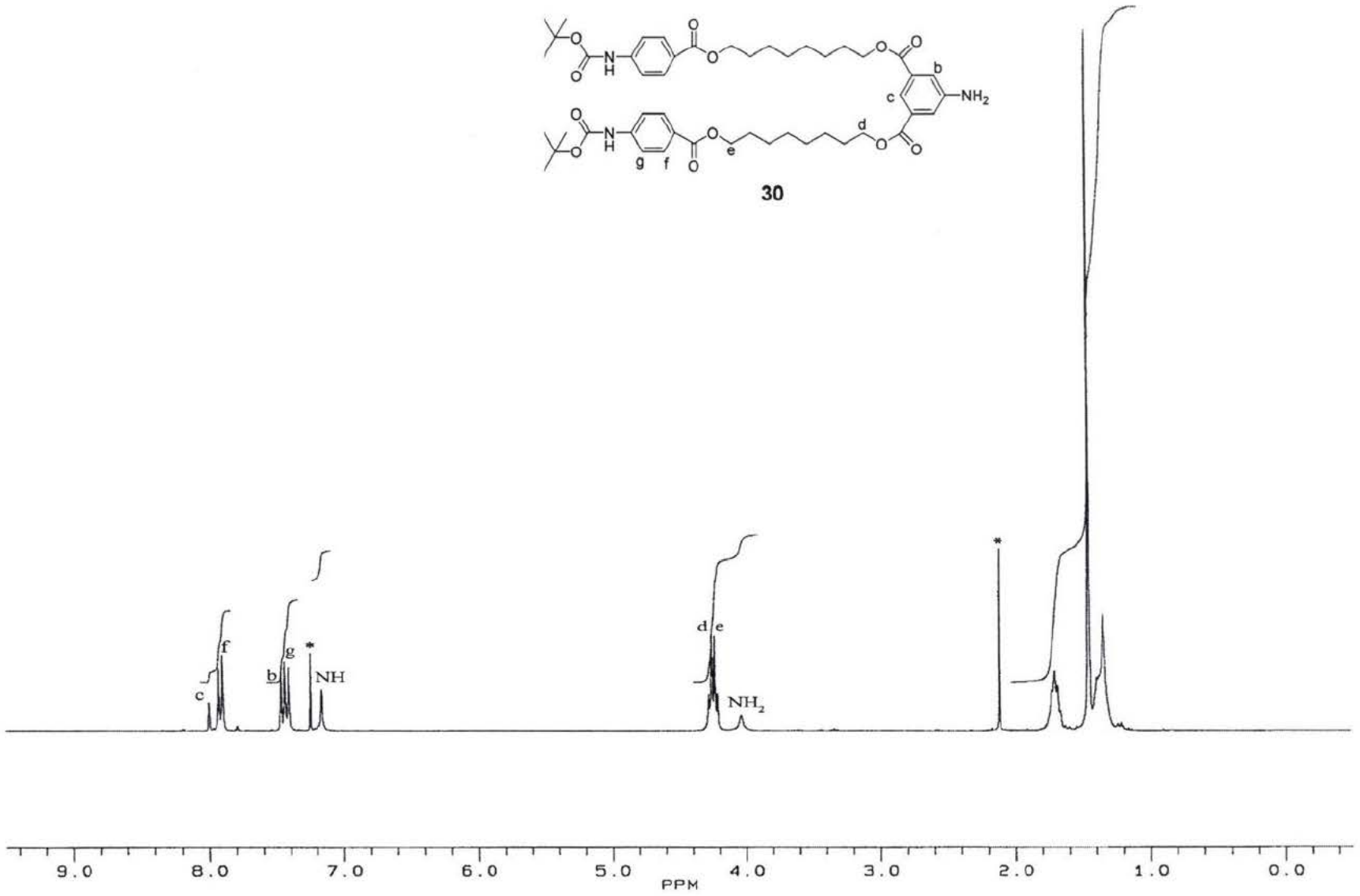

Figure 2.4: Proton NMR spectrum of compound **30**

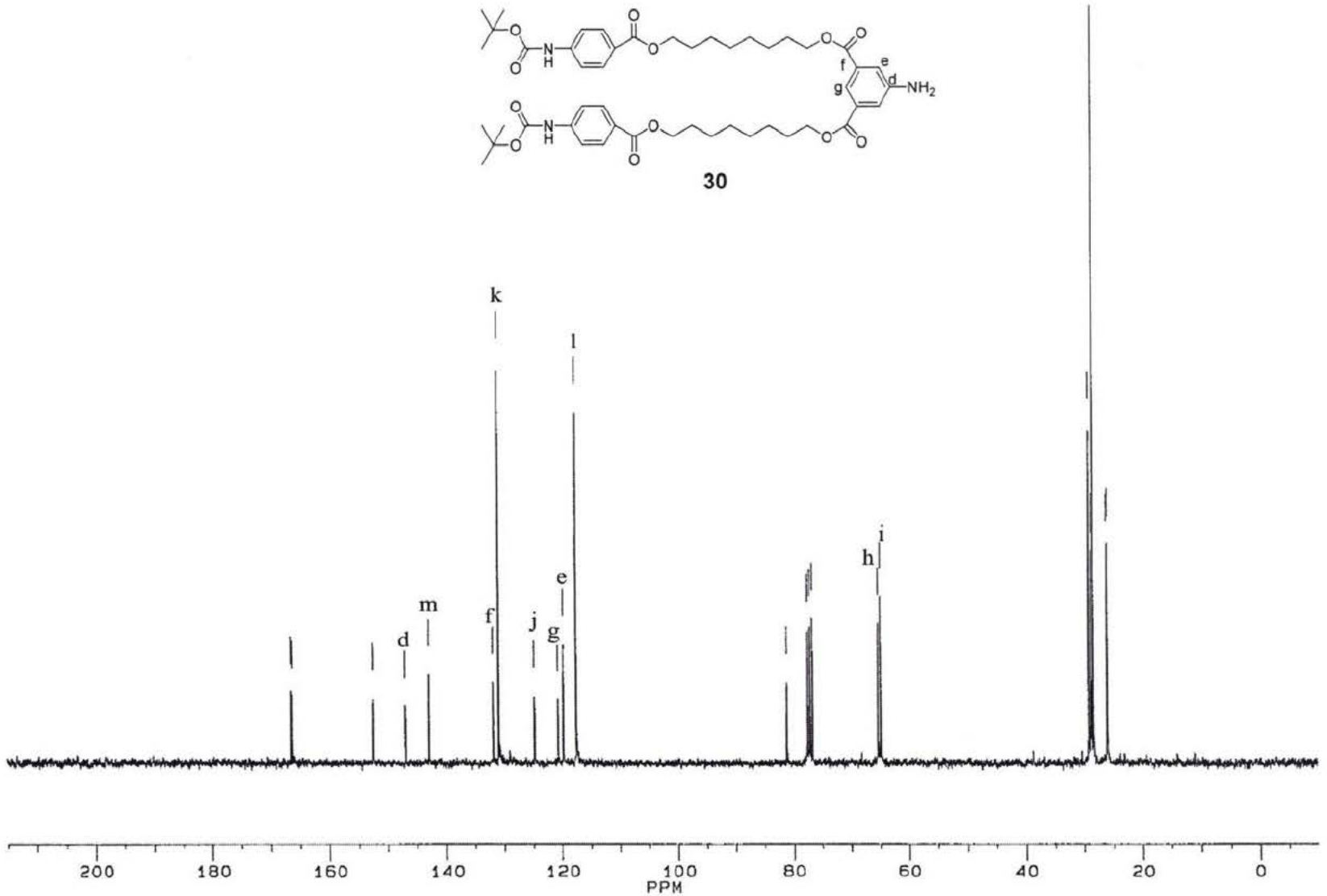

Figure 2.5: Carbon NMR spectrum of compound **30**

Two molecules of **30** were linked via reaction with terephthaloyl dichloride to form **32** and the mixture was purified by silica chromatography. The integration of the proton NMR spectrum (Figure 2.6) is consistent with a 2:1 ratio of components derived from the two reactive pairs. The proton NMR spectrum of **32** shows the inclusion of terephthalamide with a peak at 7.90 ppm (**a**). Similarly the carbon NMR spectrum of **32** (Figure 2.7) shows the three expected peaks from terephthalamide at 165.4(**c**), 137.5(**b**) and 127.7 ppm (**a**). The changes in chemical shifts of the **b** and **c** protons between **36** and **37** were consistent with a decrease in electron donating capability of an aromatic primary amine changing to a secondary amide. Upon reaction, the **b** protons underwent a downfield shift from 7.47 ppm in **30** to 8.57 ppm in **32.** A smaller downfield shift for the **c** protons from 8.01 to 8.42 ppm, is also observed. The chemical shift of the carbons **d**, **e** and **g** changed: **d** shifted from 146.8 to 138.6 ppm, **e** changed from 119.6 to 126.6 ppm and **g** changed from 120.5 to 125.6 ppm in **32**. These shifts are also consistent with a decrease in the electron donating capability of an aromatic primary amine changing to a secondary amide. All of the respective peaks in both carbon and proton NMR spectra matched the structural calculation estimates.

An exact mass spectrum was not possible. The mass spectrometer conditions deprotected **32** to varying degrees providing an ion with a measured exact mass 1481.7164, which corresponds to the calculated exact mass of compound **19** (1481.7172).

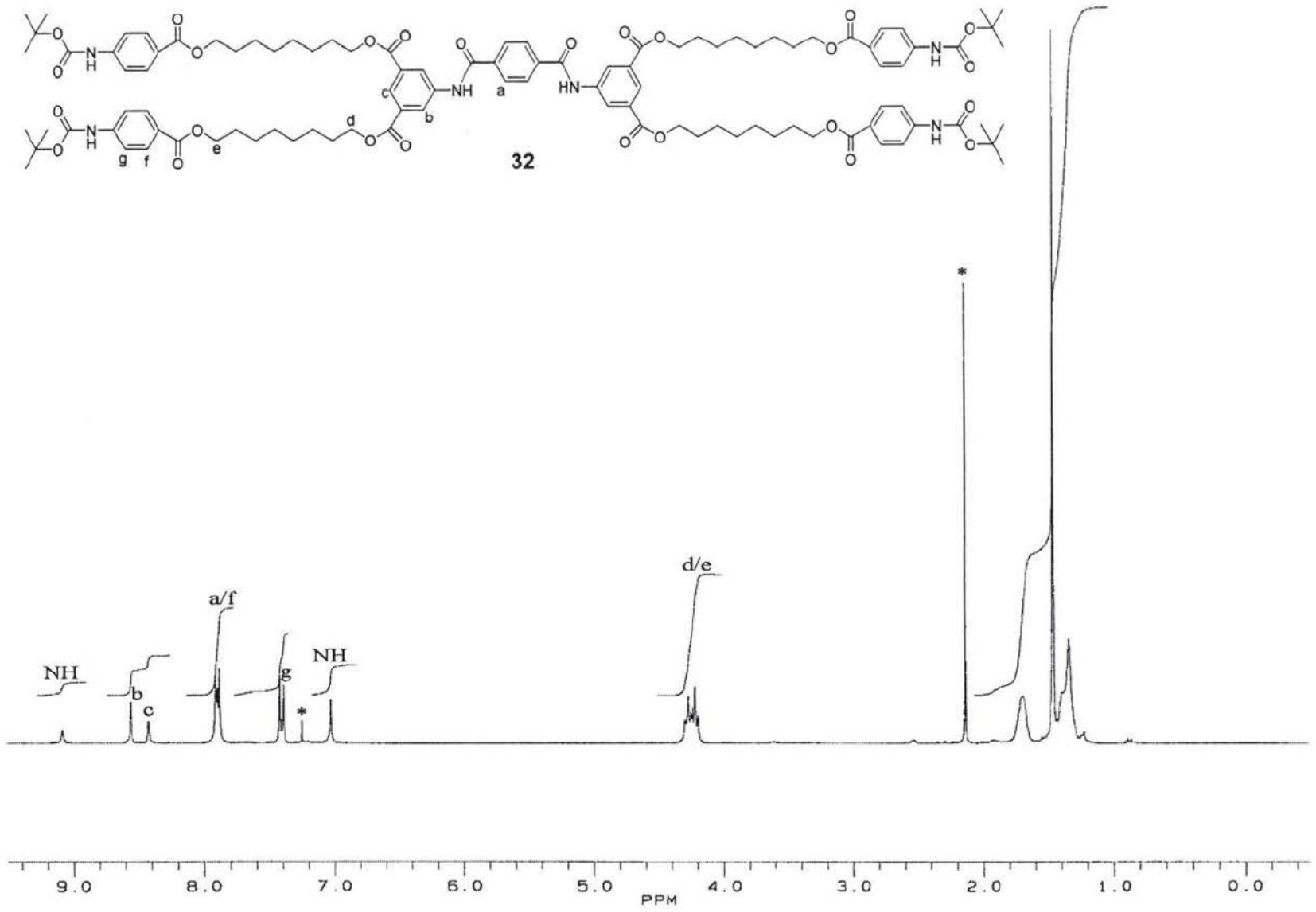

Figure 2.6: Proton NMR spectrum of compound **32**

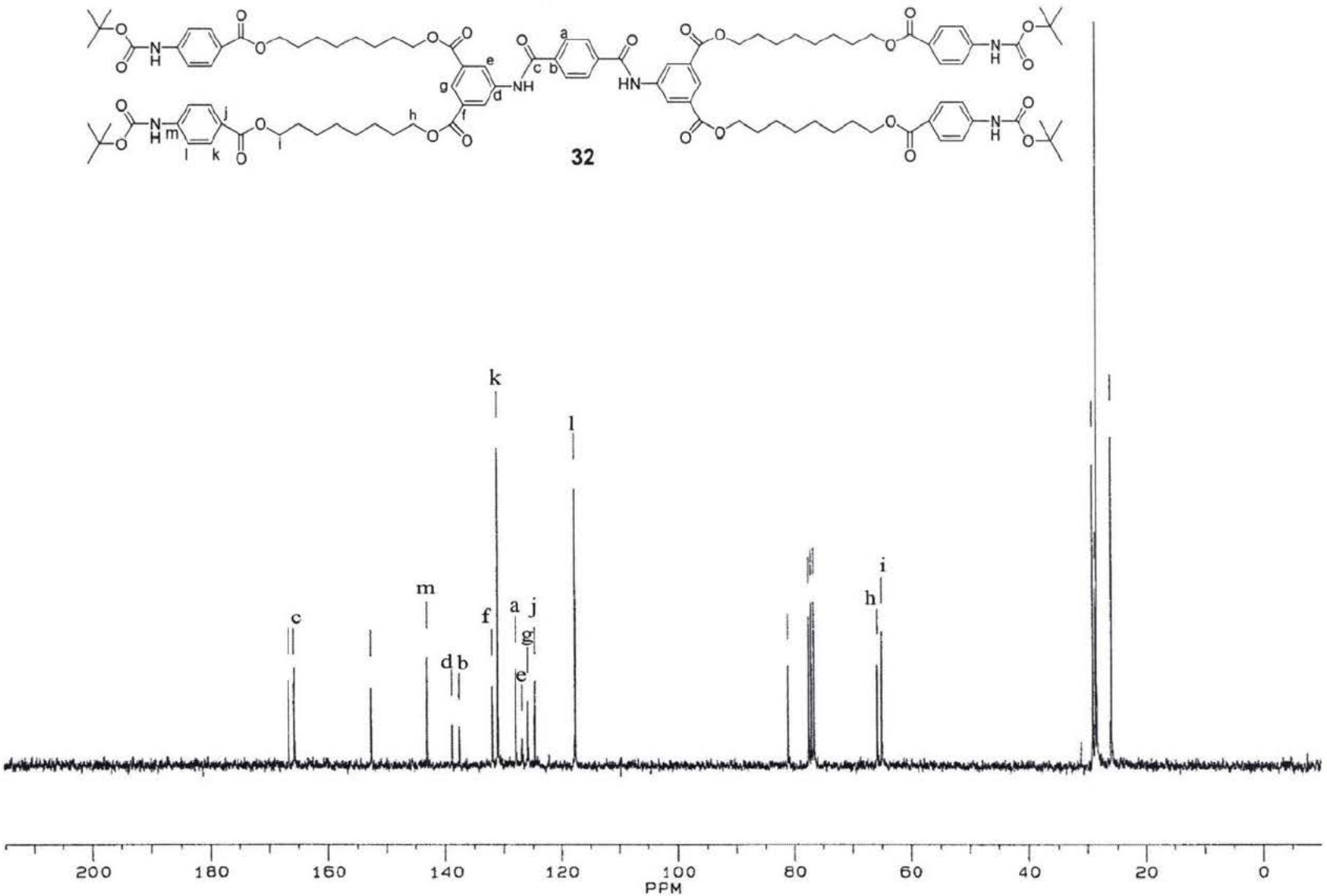

Figure 2.7: Carbon NMR spectrum of compound **32**

The deprotection of **32** forming **19** was done with TFA in dichloromethane and the product was washed with dichloromethane to eliminate residual TFA and other impurities. There was no evidence of the 1.40 ppm peak of the Boc protecting group in the proton NMR spectrum (Figure 2.8) or the 81.0, 29.1 and 152.4 ppm peaks of the Boc protecting group in the carbon NMR spectrum (Figure 2.9). The chemical shift of the newly formed amine protons varied depending on the solution of **19**. Both the carbon and proton NMR spectra are consistent with the removal of a Boc protecting group from an aniline aromatic system. This is shown by the chemical shift of aromatic protons **f** and **g** shifting upfield from 7.90 and 7.41 ppm in **32** to 7.72 and 6.79 ppm in **19** respectively. Also, this was shown in the carbon NMR spectra by the chemical shift of carbon **m** shifting from 142.9 to 153.4 ppm, **l** shifting from 117.4 to 112.6 ppm and **j** shifting from 124.5 to 116.0 ppm. All these shifts are consistent with chemical shift calculations of the assigned structure.

Compound **19** was a white crystalline material that dissolved in DMSO with heat, but stayed dissolved thereafter. There was no evidence of residual TFA in the carbon NMR spectrum, low resolution mass spectrum or the IR spectrum. Also, the compound was basic compared to pH 5 when dissolved in DMSO.

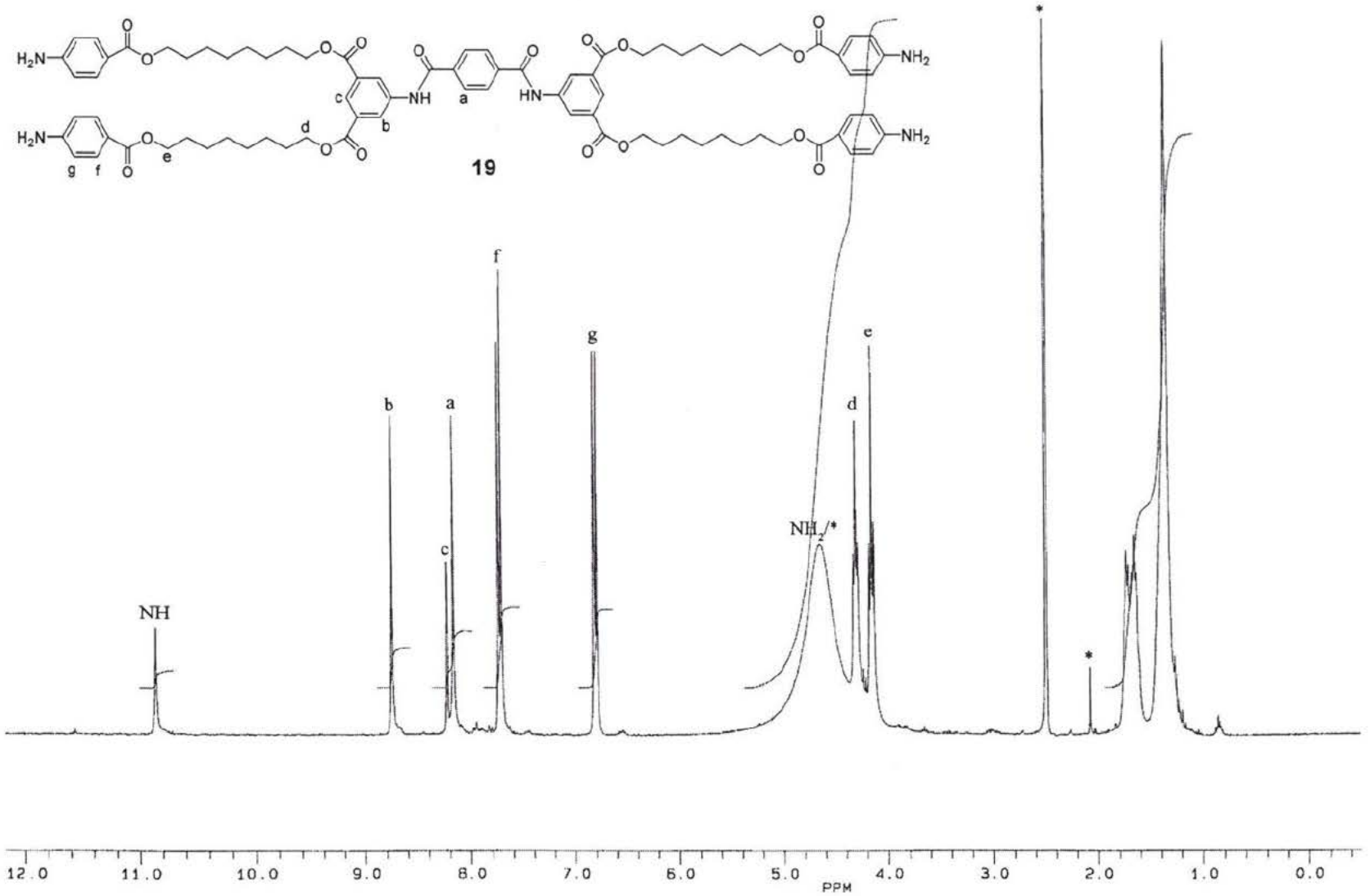

Figure 2.8: Proton NMR spectrum of compound **19**

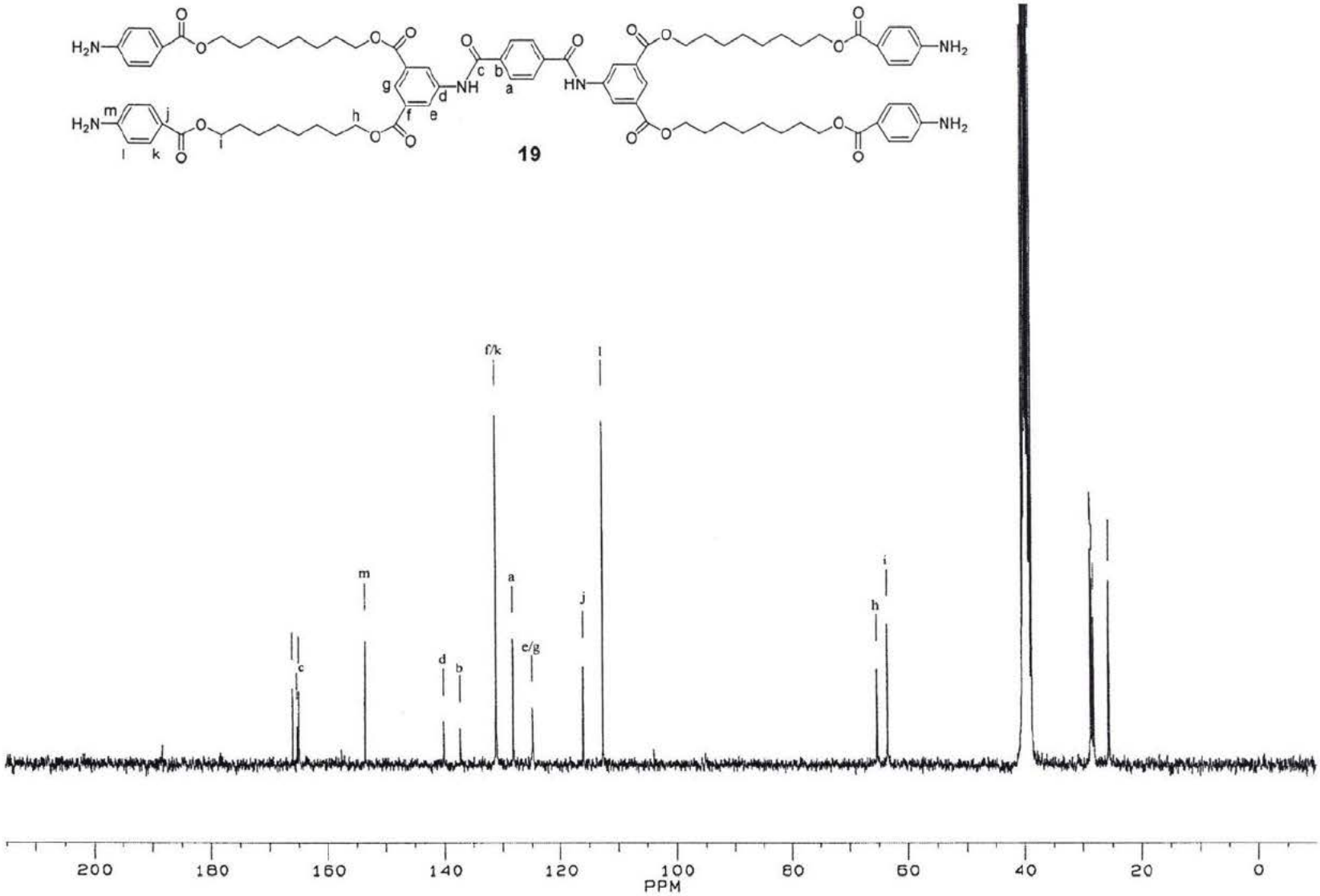

Figure 2.9: Carbon NMR spectrum of compound **19**

2.4 Synthesis of 20:

The synthesis of compound **20** is shown in scheme 4

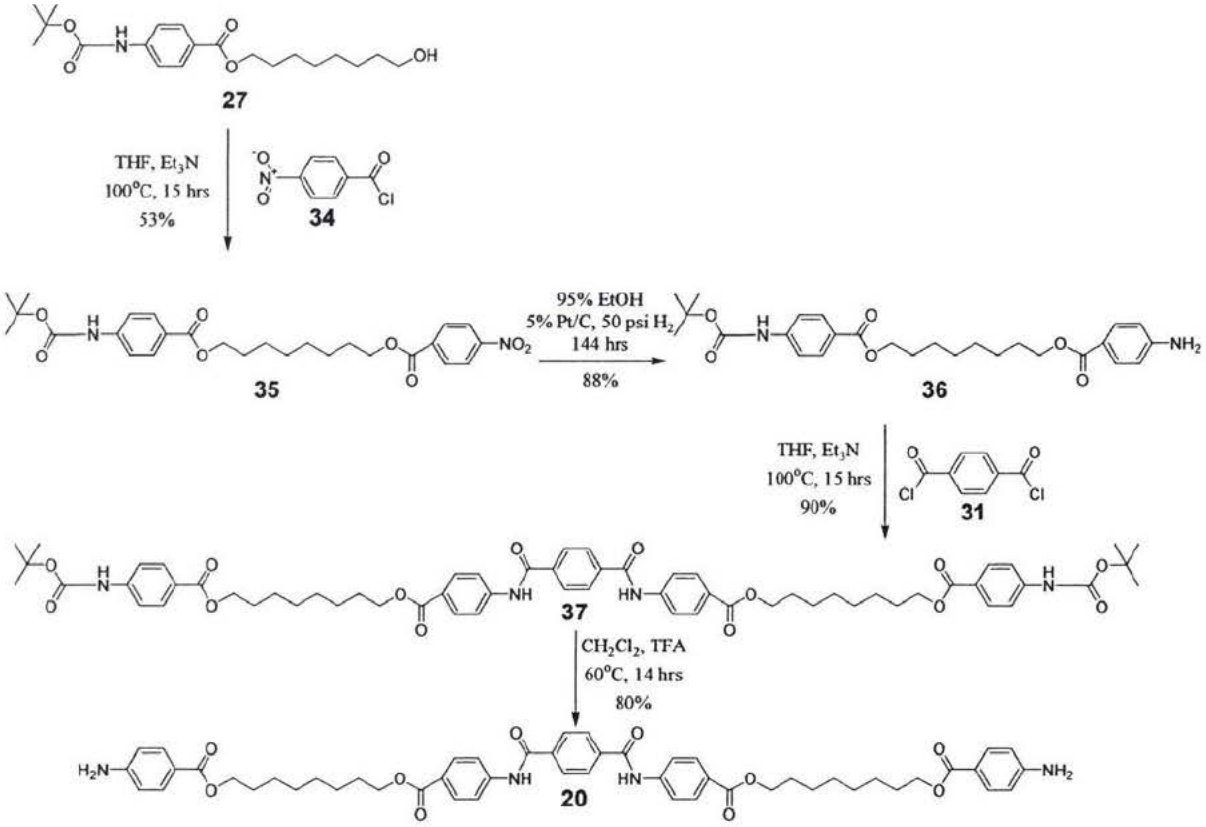

Scheme 4: Synthesis of compound **20**

The esterification to form **35** was done via an acid chloride reaction with the alcohol **27**, followed by purification by silica chromatography. The proton NMR spectrum of the product (Figure 2.10) is consistent with the structure of **35.** Notably, signal for the **d** protons appears at 4.32 ppm in **35,** downfield from 3.50 ppm for the same methylene group in **27**. Similarly the carbon NMR spectrum (Figure 2.11) shows the **h** carbon at 64.8 ppm in **35** compared to at 62.4 ppm in **27**. The integration of the proton NMR is consistent with a 1:1 ratio of components derived from the two reactive pairs. All of the compound peaks in both the proton NMR spectrum and carbon NMR spectrum were consistent with chemical shift calculations of the assigned structure.

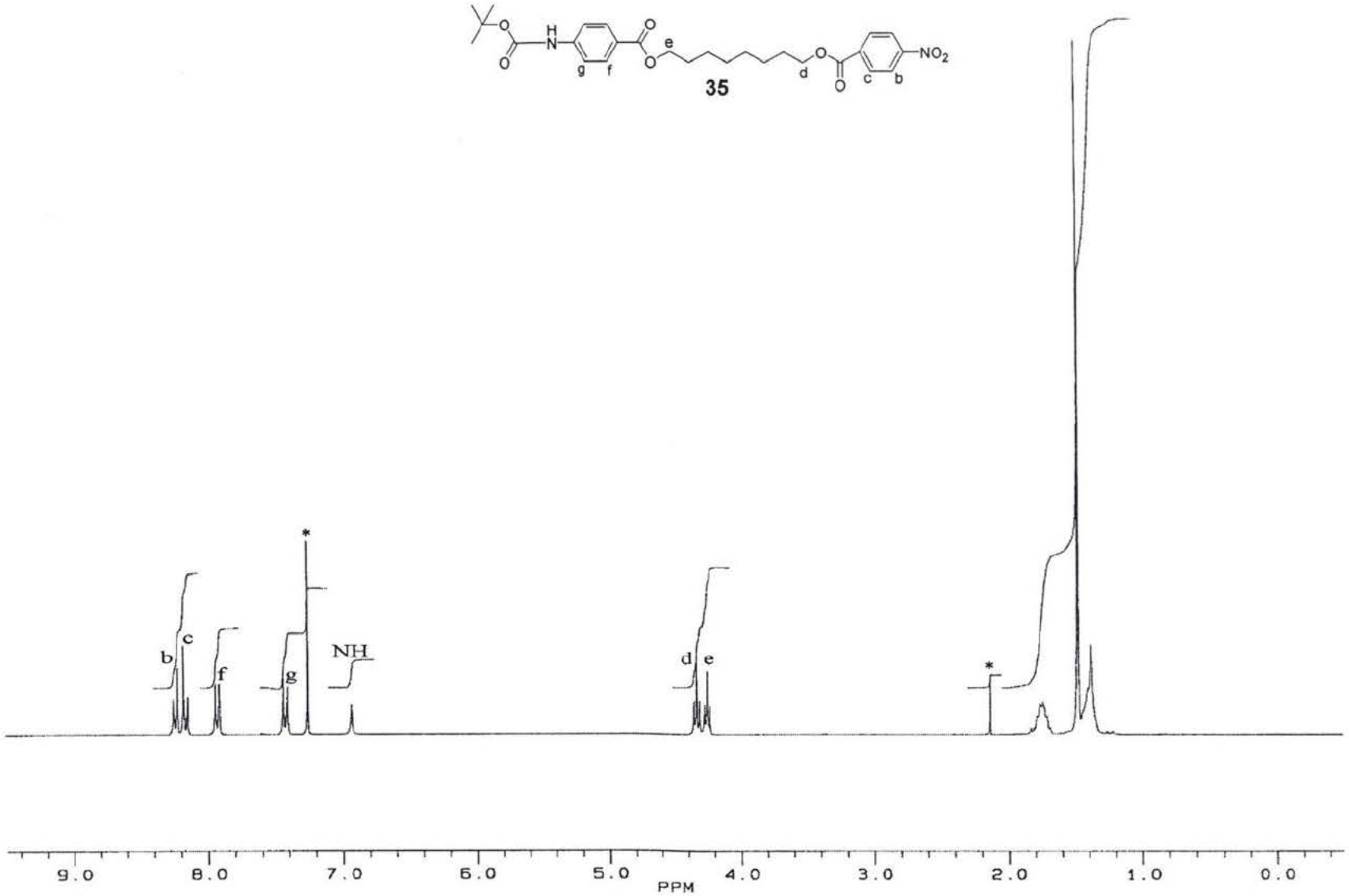

Figure 2.10: Proton NMR spectrum of compound **35**

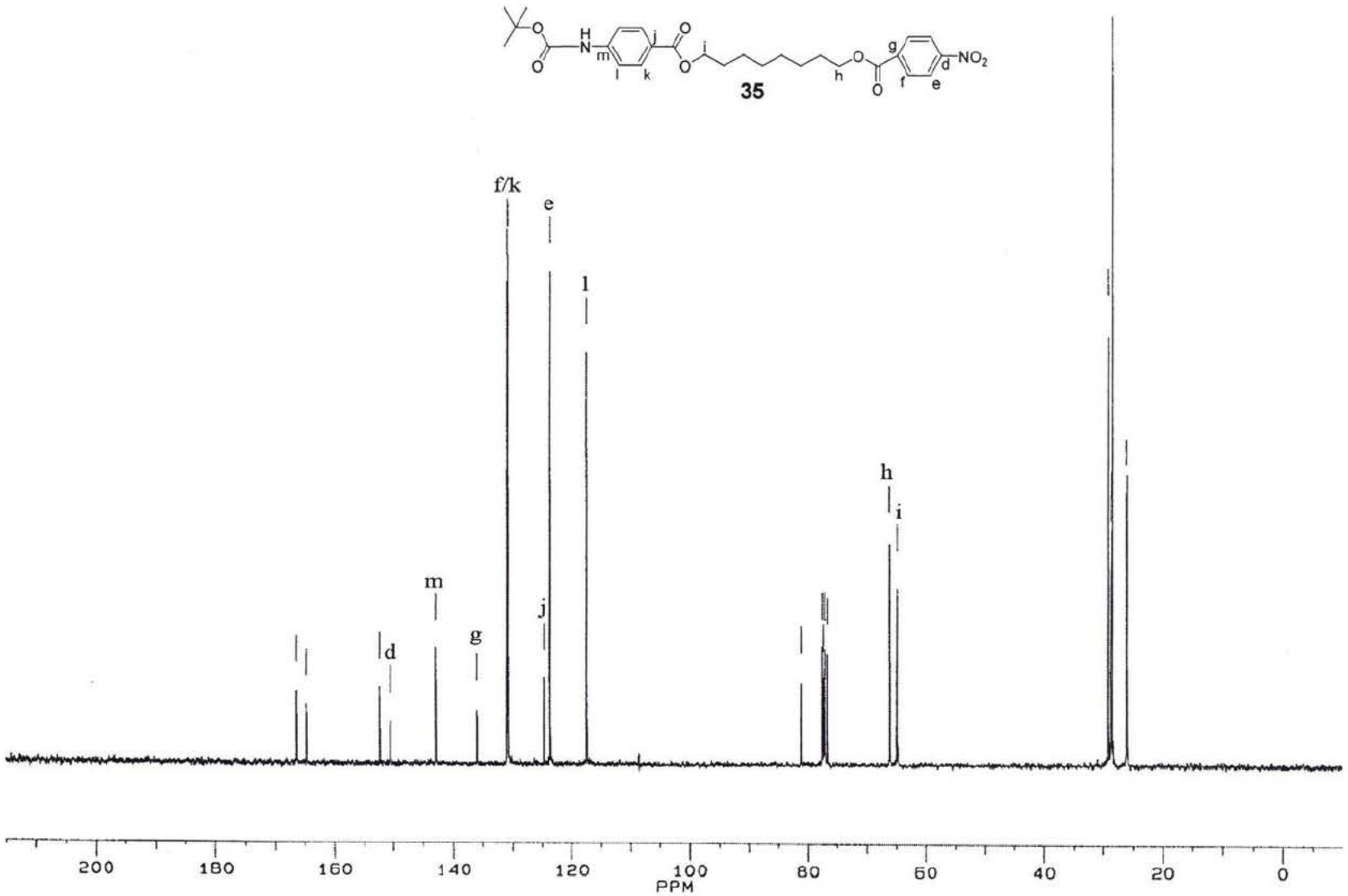

Figure 2.11: Carbon NMR spectrum of compound **35**

Compound **35** was reduced to compound **36** via H_2 under pressure with 5% Pt/C. The reaction was monitored via the chemical shifts of the **b** and **c** protons. Upon reaction the **b** protons undergo an upfield shift from 8.23 in **35** to 6.61 ppm in **36** (Figure 2.12) A smaller upfield shift for the **c** protons, 8.18 to 7.84 ppm, is also observed. Other spectroscopic changes in the proton NMR spectra are smaller, including the shift of the **d** protons from 4.32 in **35** to 4.25 ppm in **36**, but consistent with the reduction of the nitro group to the amino group. The carbon NMR spectrum (Figure 2.13) shows significant changes in the aromatic region: notably, the chemical shifts from **35** to **36** of carbon **e** from 123.5 to 113.8 ppm and **g** shifted from 135.9 to 120.2 ppm This is consistent with the increase in electron density of the ortha-para positions when an aromatic nitro group is reduced to an amino group. All of the peaks in the carbon and proton NMR spectra were consistent with chemical shift calculations of the assigned structure.

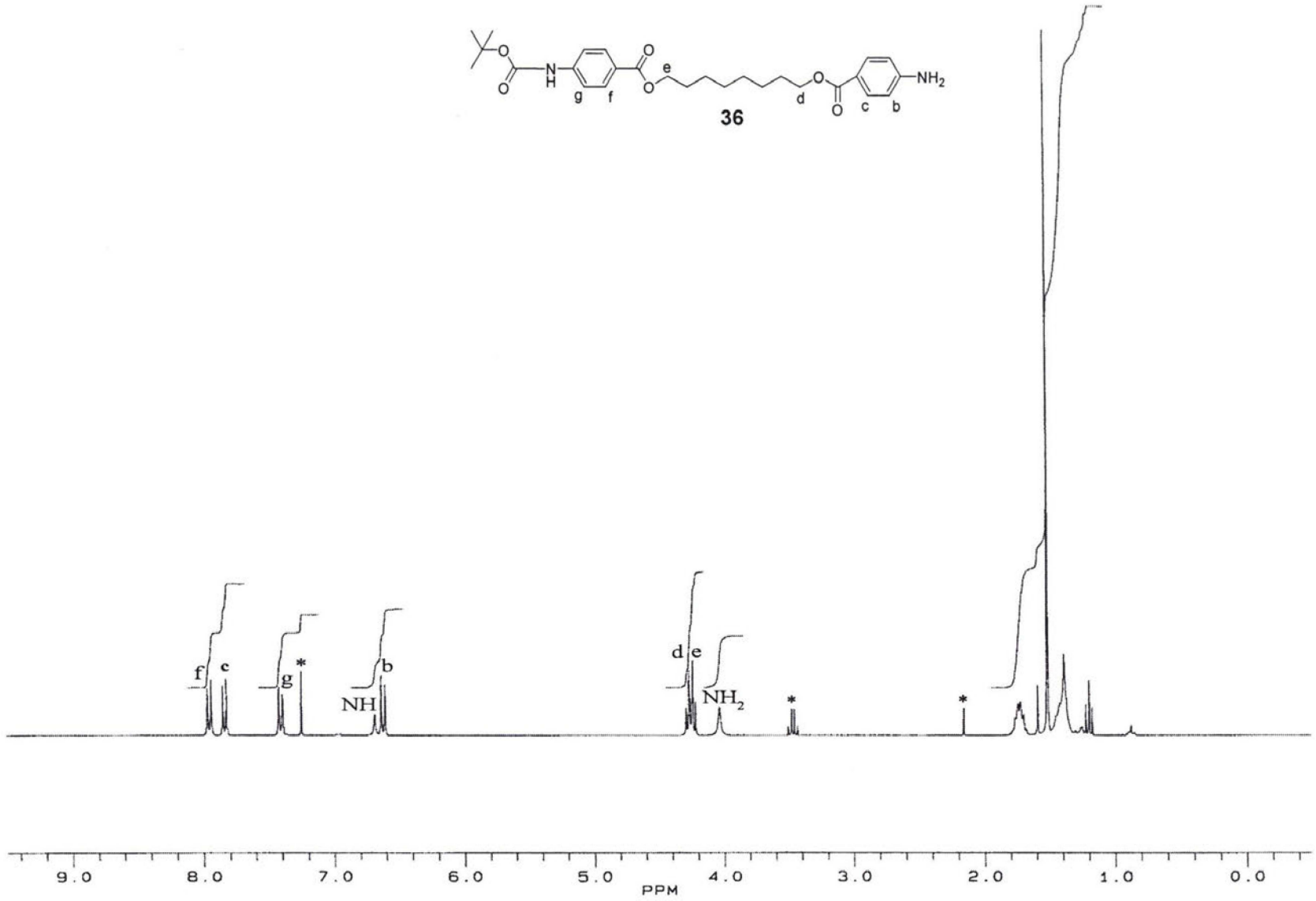

Figure 2.12: Proton NMR spectrum of compound **36**

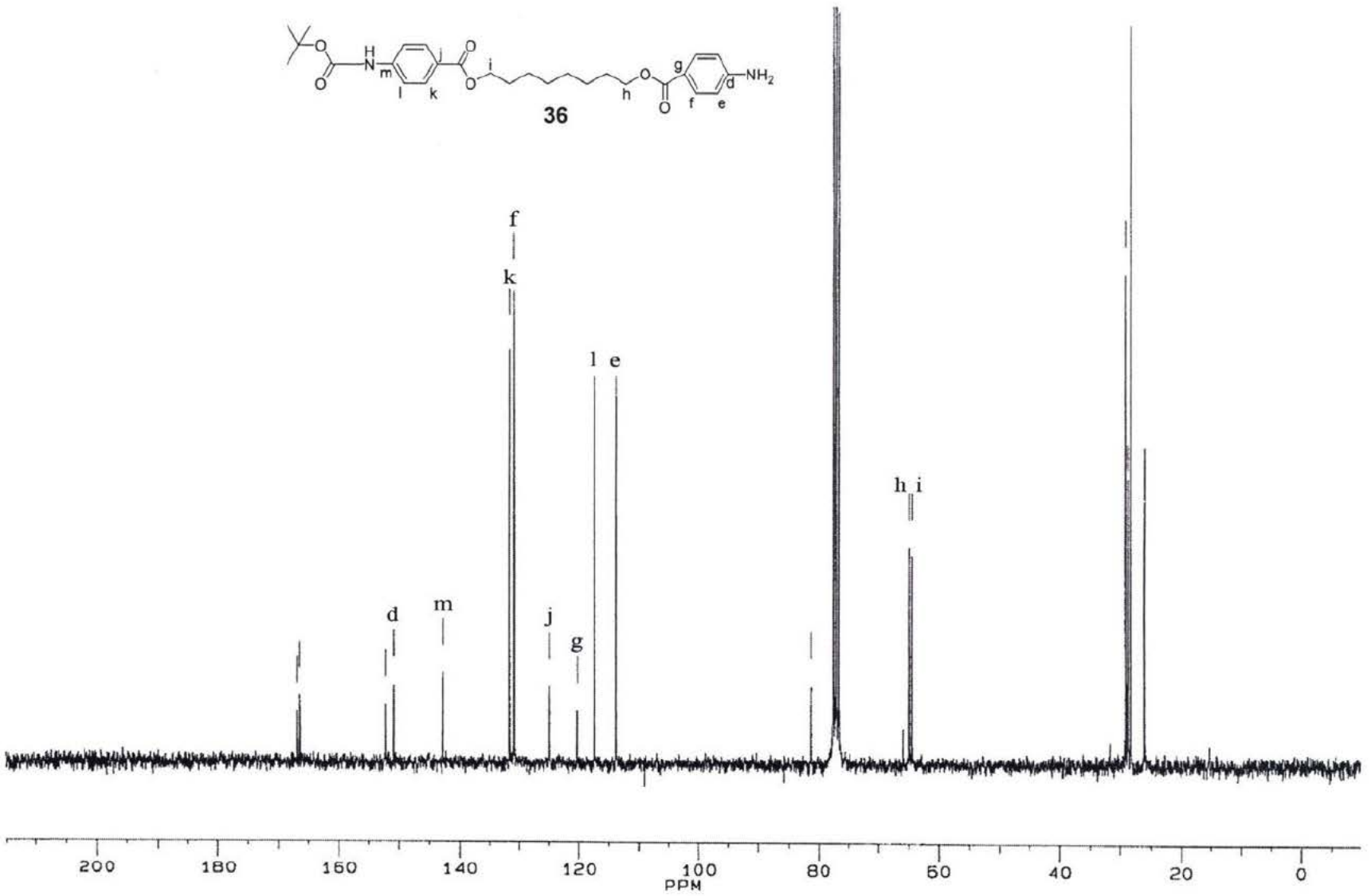

Figure 2.13: Carbon NMR spectrum of compound **36**

Two molecules of **36** were linked via reaction with terephthaloyl dichloride to form **37** and the mixture was purified by silica chromatography. The integration of the proton NMR spectrum (Figure 2.14) is consistent with a 2:1 ratio of components derived from the two reactive pairs. The proton NMR spectrum of **37** shows the inclusion of terephthalamide with a peak at 8.13 ppm **(a)**. Similarly the carbon NMR spectrum of **37** (Figure 2.15) shows two of the three expected peaks from terephthalamide at 137.3(**b**) and 127.9 ppm (**a**). The third expected linker peak (**c**) should have showed up around 165 ppm, however, it probably overlapped one of the other two peaks in that area. The NMR solvent was changed from chloroform in **36** to DMSO in **37** due to solubility problems. This creates an inconsistency when comparing the two proton NMR spectra. However, the changes in chemical shifts of the **b** and **c** protons between **36** and **37** were still consistent with a decrease in electron donating capability of an aromatic primary amine changing to a secondary amide. Upon reaction the **b** protons underwent a downfield shift from 6.61 ppm in **36** to 7.98 ppm in **37**. A smaller downfield shift for the **c** protons from 7.84 to 7.98 ppm, is also observed. The chemical shift of the carbons **d**, **e** and **g** changed: **d** shifted from 150.7 ppm in **36** to 143.4 ppm in **37**, **e** changed from 113.8 ppm in **36** to 119.7 ppm in **37** and **g** changed from 120.2 ppm in **36** to 123.0 ppm in **37**. These shifts are also consistent with a decrease in the electron donating capability of an aromatic primary amine changing to a secondary amide. The quality of the carbon NMR spectrum is low due to solubility problems. All of the respective peaks in both carbon and proton NMR spectrum matched the structural calculation estimates.

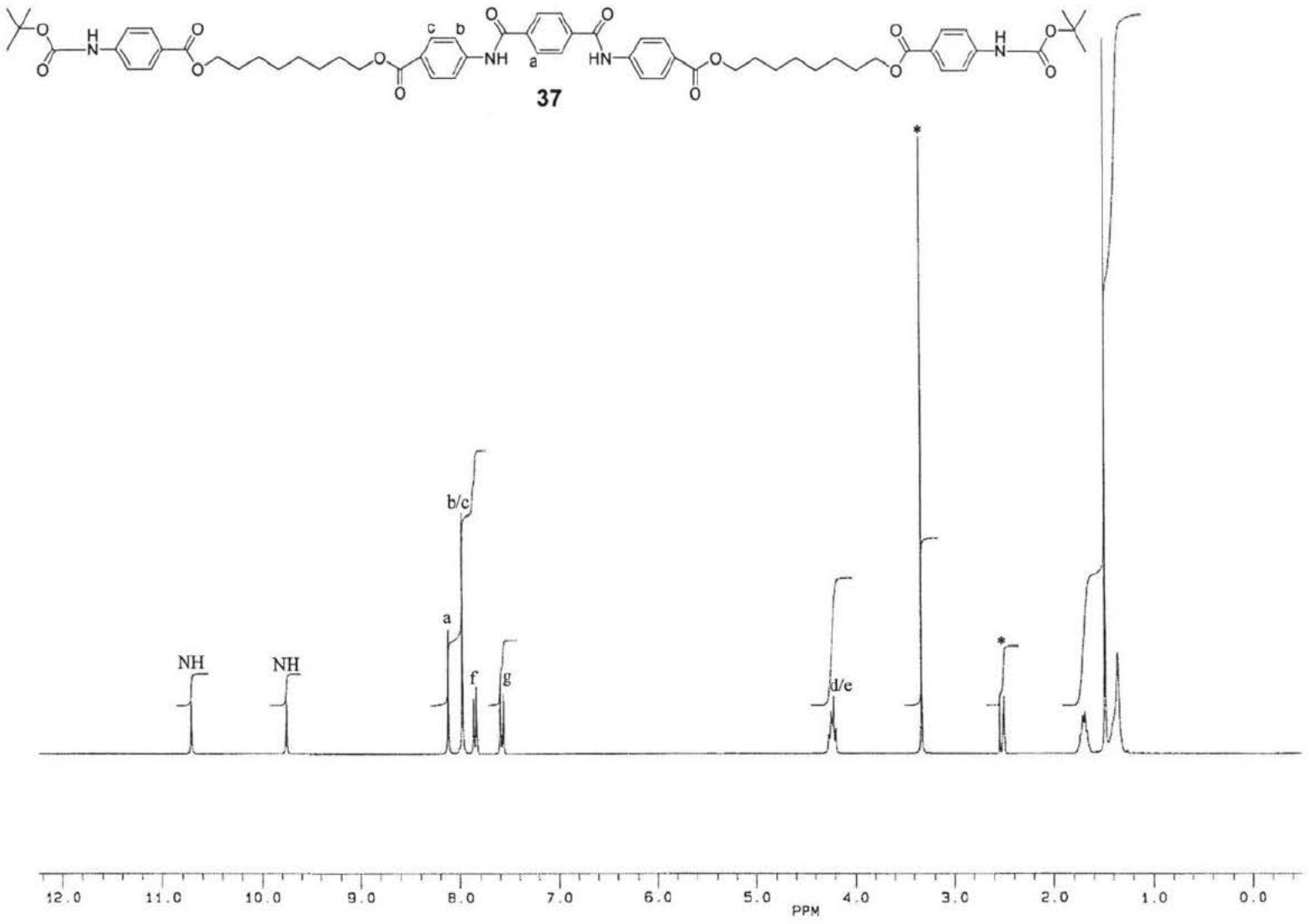

Figure 2.14: Proton NMR spectrum of compound **37**

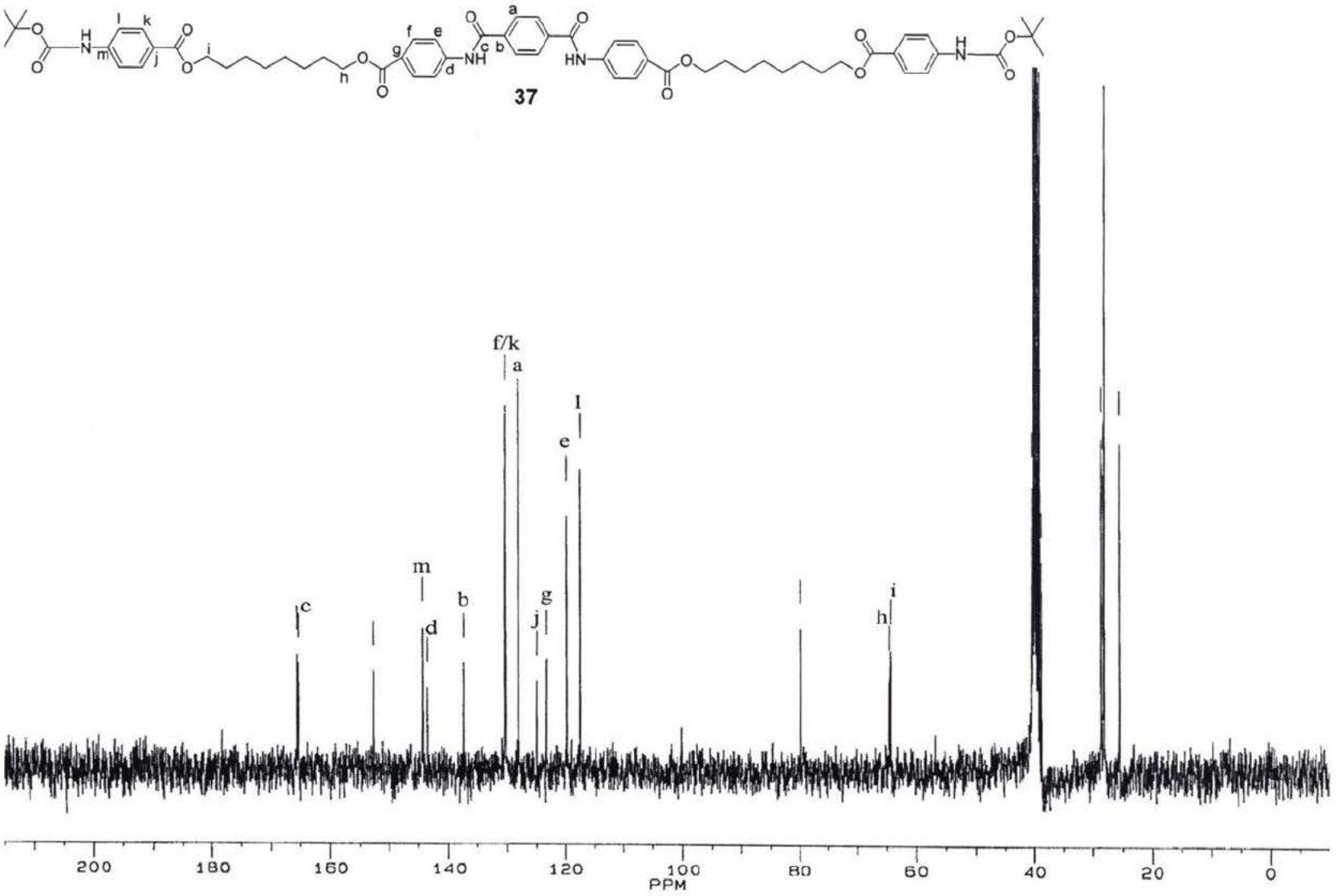

Figure 2.15: Carbon NMR spectrum of compound **37**

The deprotection of **37** forming **20** was done with TFA in dichloromethane and the insoluble product was washed with dichloromethane to eliminate residual TFA and other impurities. There was no evidence of the 1.40 ppm peak of Boc protecting group in the proton NMR spectrum (Figure 2.16) or the 79.7, 28.0 and 152.5 ppm peaks of the Boc protecting group in the carbon NMR spectrum (Figure 2.17). The chemical shift of the amine protons is located at 5.94 ppm in **20** and the respective amide peak of **37** which was at 9.75 ppm in the proton NMR of **37** is not apparent in the proton NMR spectrum of **20**. Both the carbon and proton NMR spectra are consistent with an increase in electron donating power of an aromatic secondary amide changing to a primary amine. This is shown by the chemical shift of aromatic protons **g** shifting upfield from 7.88 ppm in **37** to 6.57 ppm in **20** and in the carbon NMR spectra by the chemical shift of carbon **j** shifting from 123.0 to 116.1 ppm, **l** shifting from 117.3 to 112.6 ppm and **m** shifting from 144.1 to 153.4 ppm All of the peaks in the carbon and proton NMR spectrum are consistent with the estimated values of structural calculations.

Compound **20** was a white crystalline and crystallized out of DMSO above 20mM. There was no evidence of TFA in the carbon NMR spectrum or the IR spectrum. Also, **20** was basic compared to pH 5 when dissolved in DMSO.

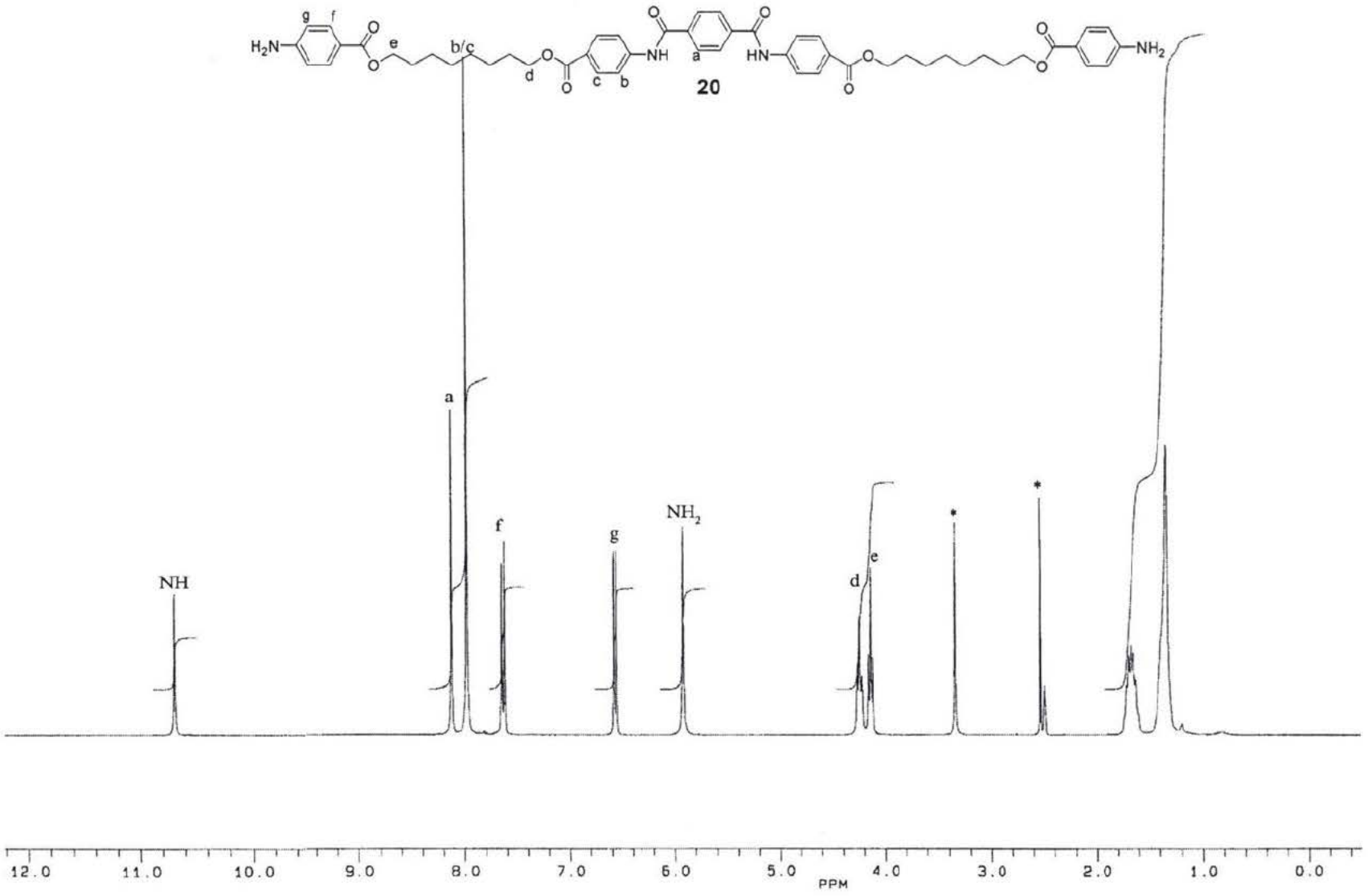

Figure 2.16: Proton NMR spectrum of compound **20**

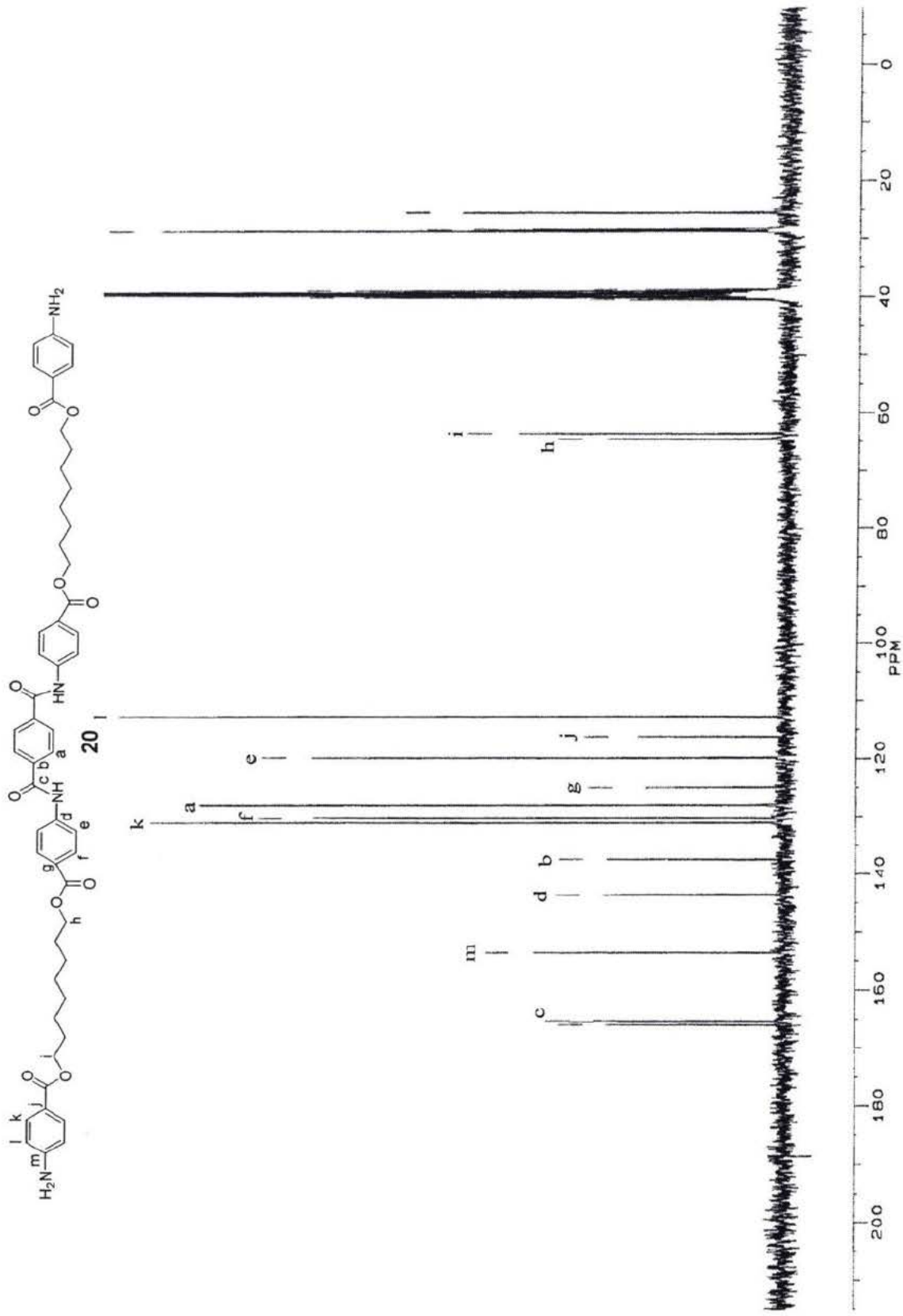

Figure 2.17: Carbon NMR spectrum of compound **20**

2.5 Synthesis of 21:

The synthesis of compound **21** is shown in scheme 5

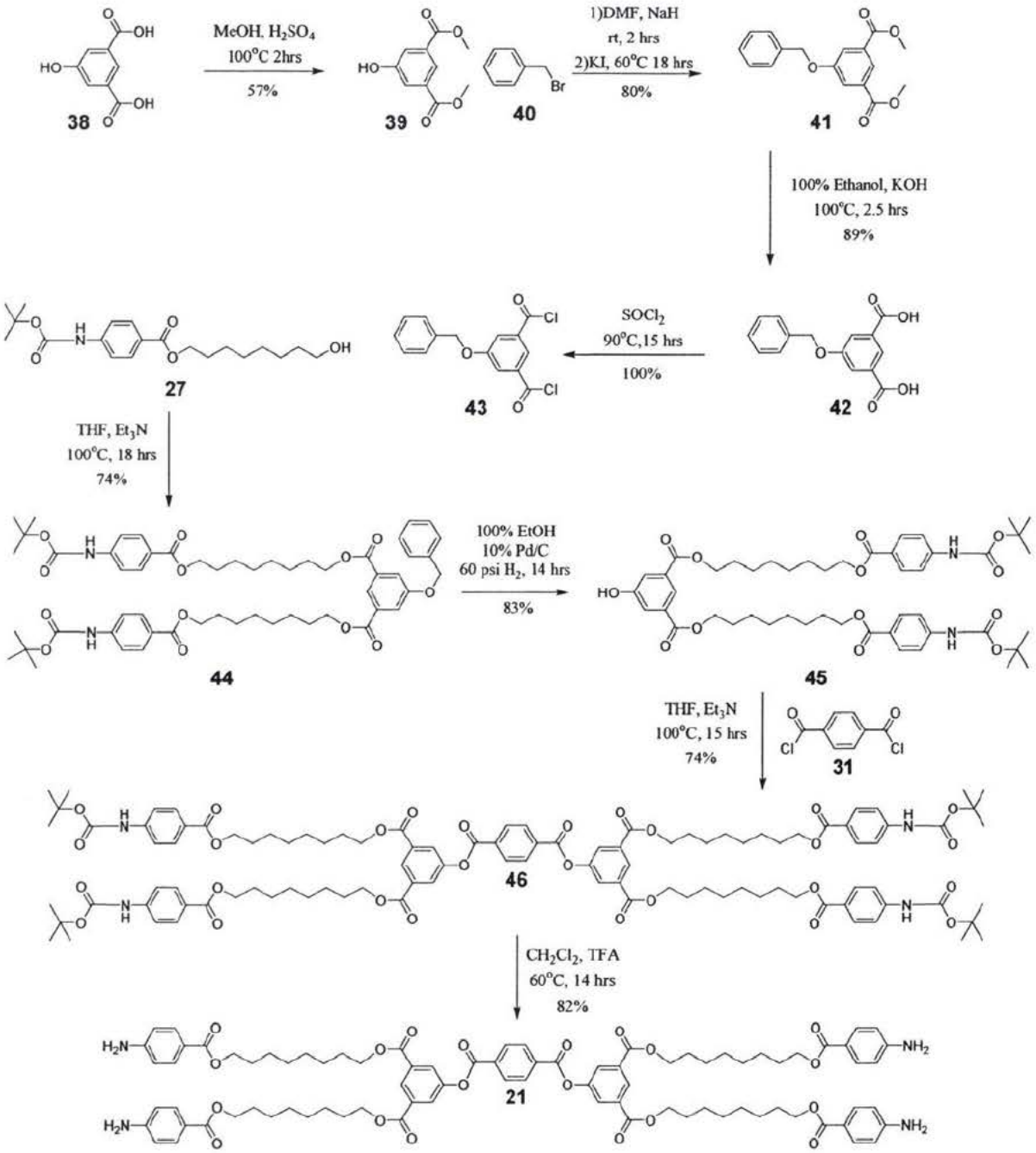

Scheme 5: Synthesis of **21**

The carboxylic acid groups were first protected to prevent side reactions in the next step. Methyl groups were chosen due to ease of deprotection. The carbon and proton NMR spectra of **39** were consistent with literature vaues[44] and structural calculations.

The protection of the alcohol was necessary to prevent side reactions in the following steps. Benzyl ether was chosen due to its robust nature and its reductive removal that would not conflict with the deprotection of carboxylic acids. Mixing **39** with NaH and then adding **40** with a catalytic amount of KI resulted in **41**. The proton NMR spectrum shows the chemical shift of the aromatic protons from the benzyl ether at 7.38 ppm, the chemical shift of the protons from the benzylic group at 5.14 ppm, the chemical shift of the aromatic protons from the protected **39** at 8.28 and 7.83 ppm in a 1:2 ratio and the chemical shift of the methyl groups at 3.92 ppm Both the carbon and proton NMR spectra are consistent with chemical shift calculations of the assigned structure.

The carboxylic acids of **41** were deprotected to form **42**. There was no evidence for the methyl peak at 3.92 ppm in the proton NMR spectrum or at 52.4 ppm in the carbon NMR spectrum. Both the carbon and proton NMR spectra are similar to estimated values given by structural calculations.

Mixing **42** with $SOCl_2$ made the acid chloride **43**. In the carbon NMR spectrum (Figure 2.19) the chemical shift of the benzylic carbon remained constant at 71 (**n**), as expected. The chemical shifts of the carbons that did shift from **42** to **43** were **d** from 159.9 to 159.3 ppm, **e** from 120.8 to 123.2 ppm, **f** from 133.2 to 135.1 ppm, **g** from 123.9 to 126.2 ppm and **o** from 166.6 to 167.6 ppm. Both the carbon and proton NMR spectra are consistent with chemical shift calculations of the assigned structure.

The esterification to form **44** was done via an acid chloride reaction with the alcohol **27**, followed by purification by silica chromatography. The proton NMR

spectrum of the product (Figure 2.20) is consistent with the structure of **44.** Notably, the signal for the **d** protons appears at 4.25 ppm in **44,** downfield from 3.50 ppm for the same methylene group in **27**. Similarly the carbon NMR spectrum (Figure 2.21) shows the **h** carbon at 65.5 ppm in **29** compared to at 62.4 ppm in **27**. The integration of the proton NMR is consistent with a 2:1 ratio of components derived from the two reactive pairs (protons **d**, **e**, **f** or **g** : protons **b)**. The proton NMR spectrum showed an upfield shift in the chemical shift of the aromatic protons, excluding the protecting group, of **43** from 7.98 and 8.46 ppm to 7.81 and 8.29 ppm for **b** and **c** respectively in **44**. All of the compound peaks in both the proton NMR spectrum and carbon NMR spectrum were consistent with chemical shift calculations of the assigned structure.

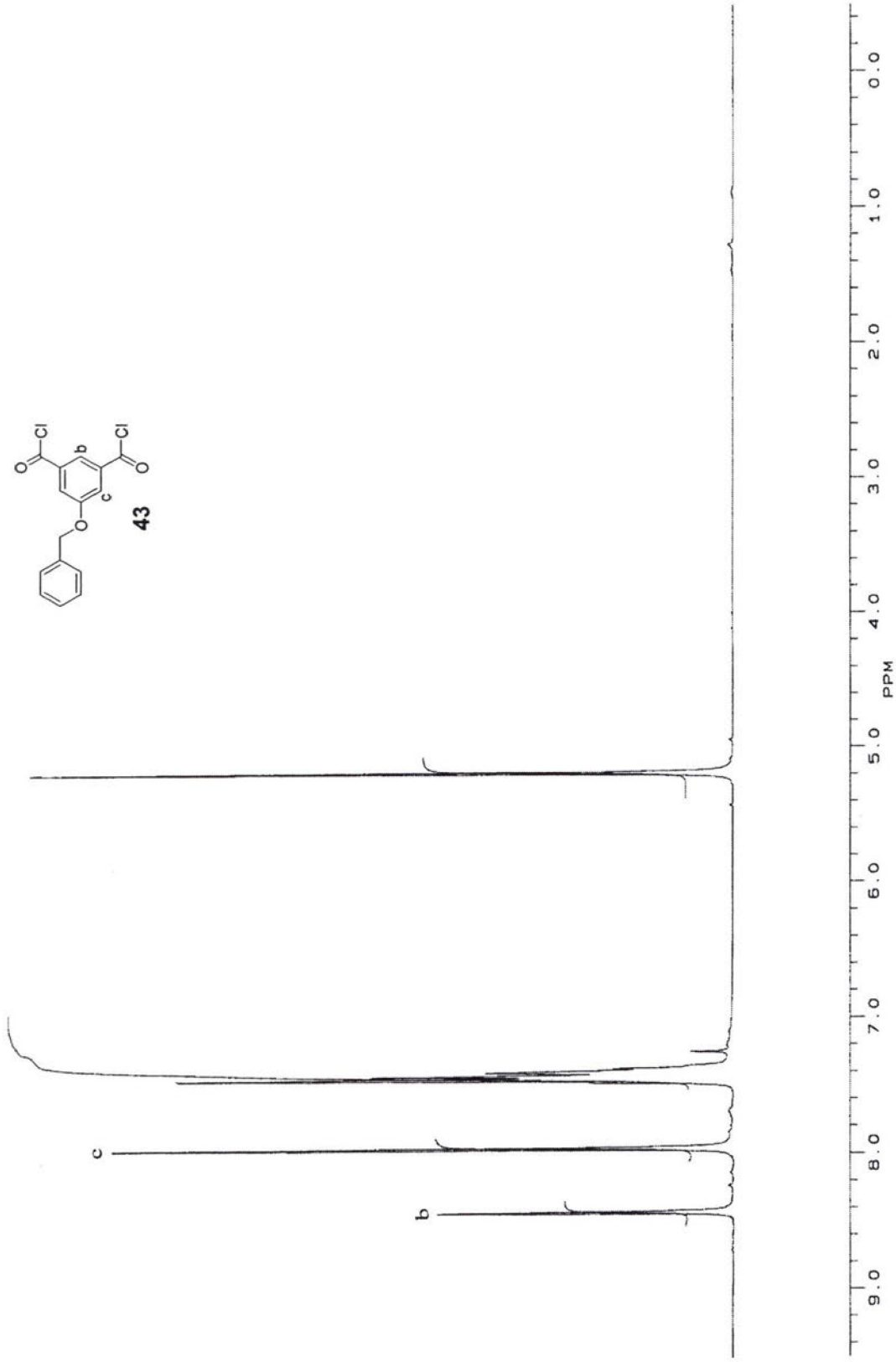

Figure 2.18: Proton NMR spectrum of compound **43**

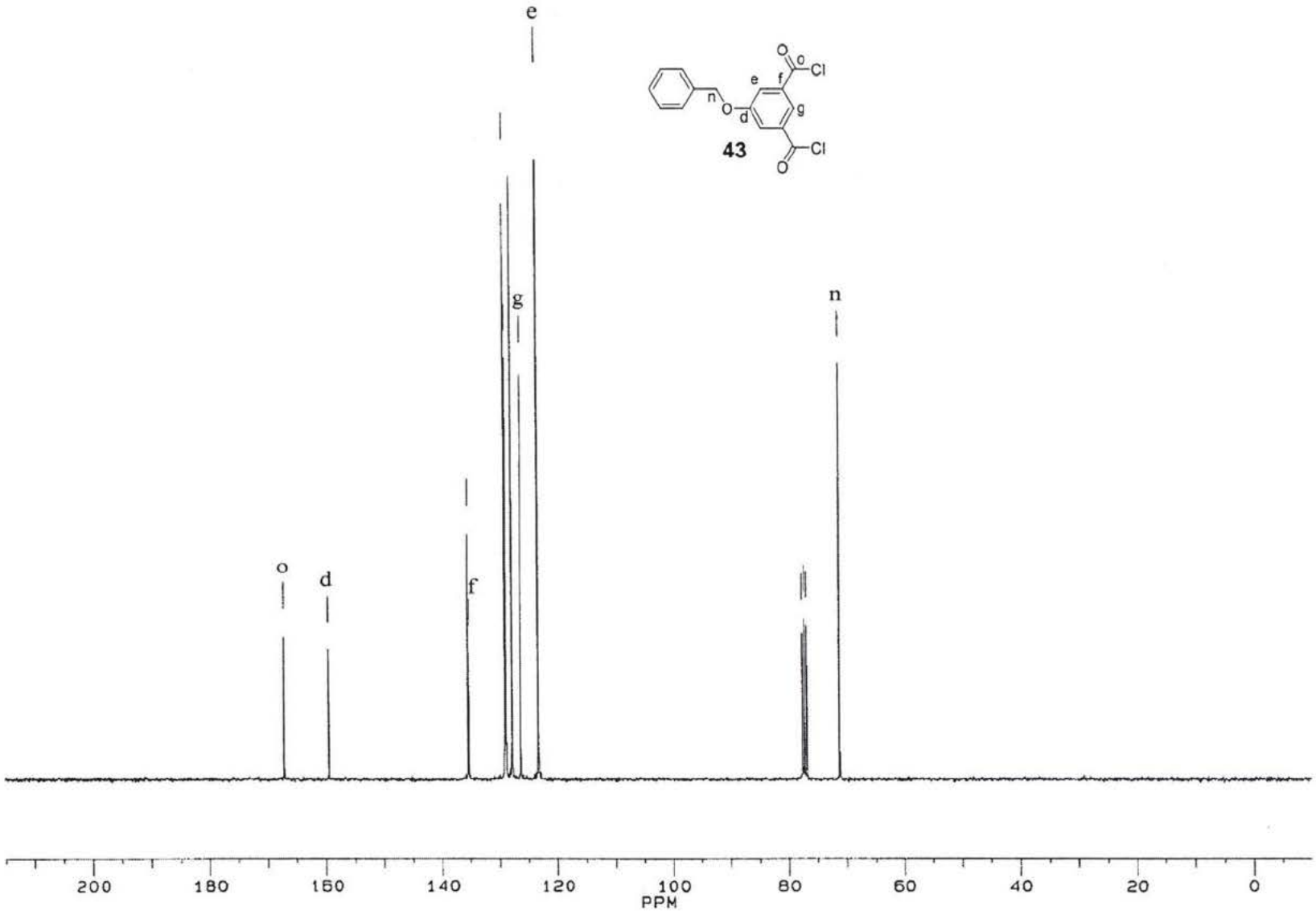

Figure 2.19: Carbon NMR spectrum of compound **43**

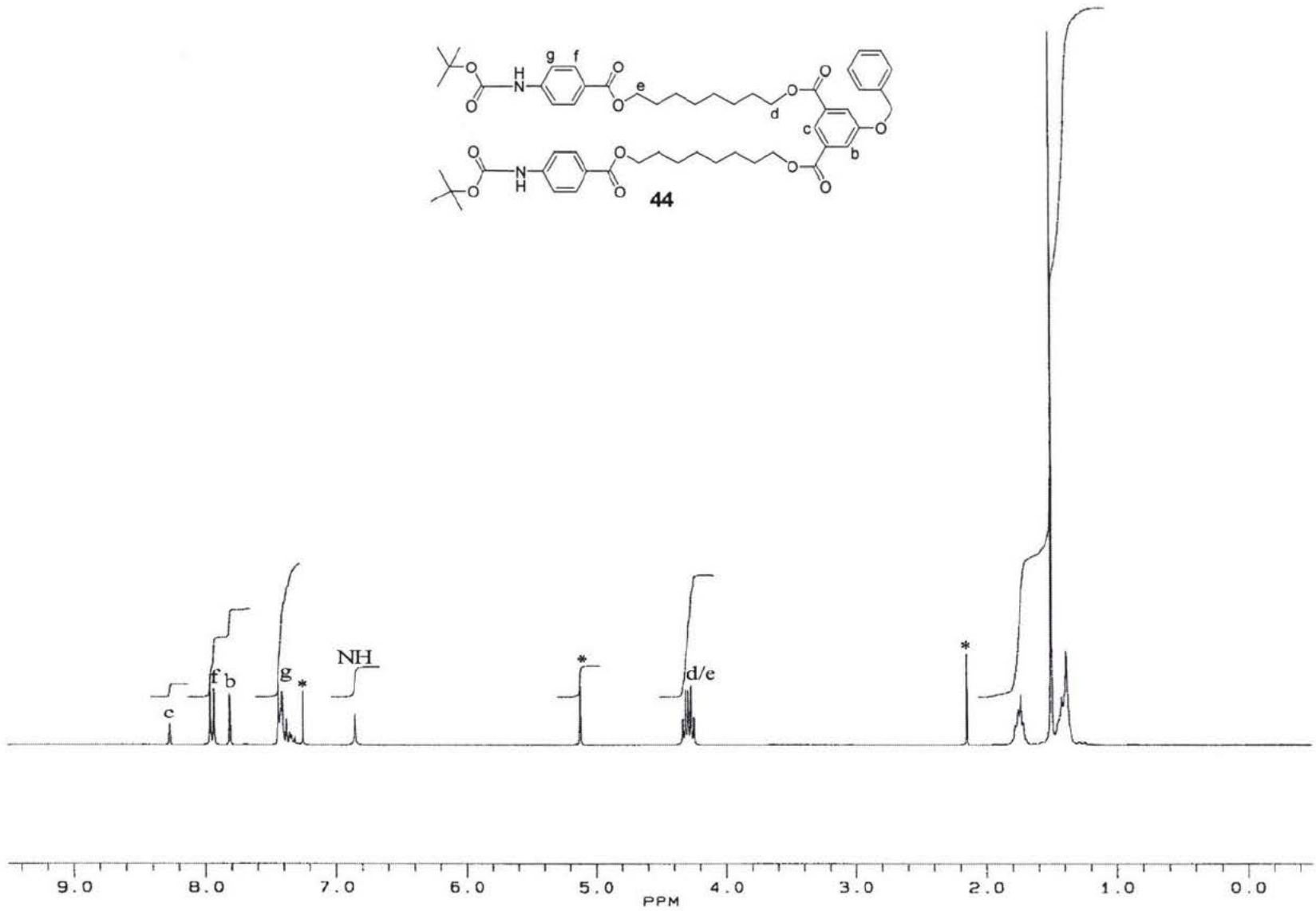

Figure 2.20: Proton NMR spectrum of compound **44**

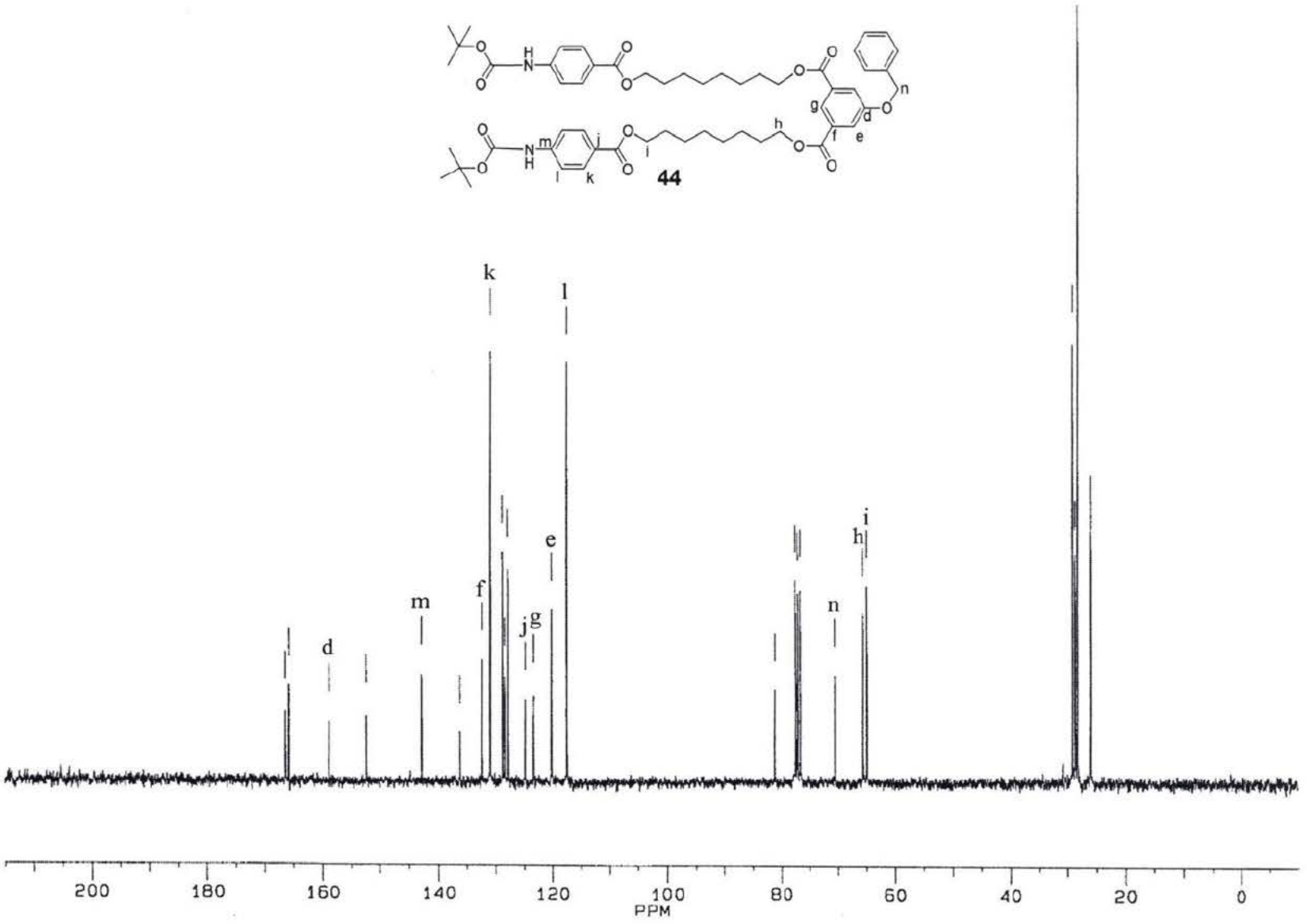

Figure 2.21: Carbon NMR spectrum of compound **44**

The benzyl ether protecting group was removed from **44** to form **45** by reduction with H_2 under pressure. The catalyst used was 10% Pd/C. The purification was done by silica chromatography. There was no evidence for the benzyl ether peaks in either the proton NMR spectrum (Figure 2.22) or the carbon NMR spectrum (Figure 2.23). The benzyl ether peaks included the 7.30 ppm multiplet and the 5.14 ppm singlet in the proton NMR spectrum and the 136.1, 128.7, 128.3, 127.6 and 70.5 ppm peaks in the carbon NMR spectrum. All of the peaks in the carbon and proton NMR spectra were consistent with chemical shift calculations of the assigned structure.

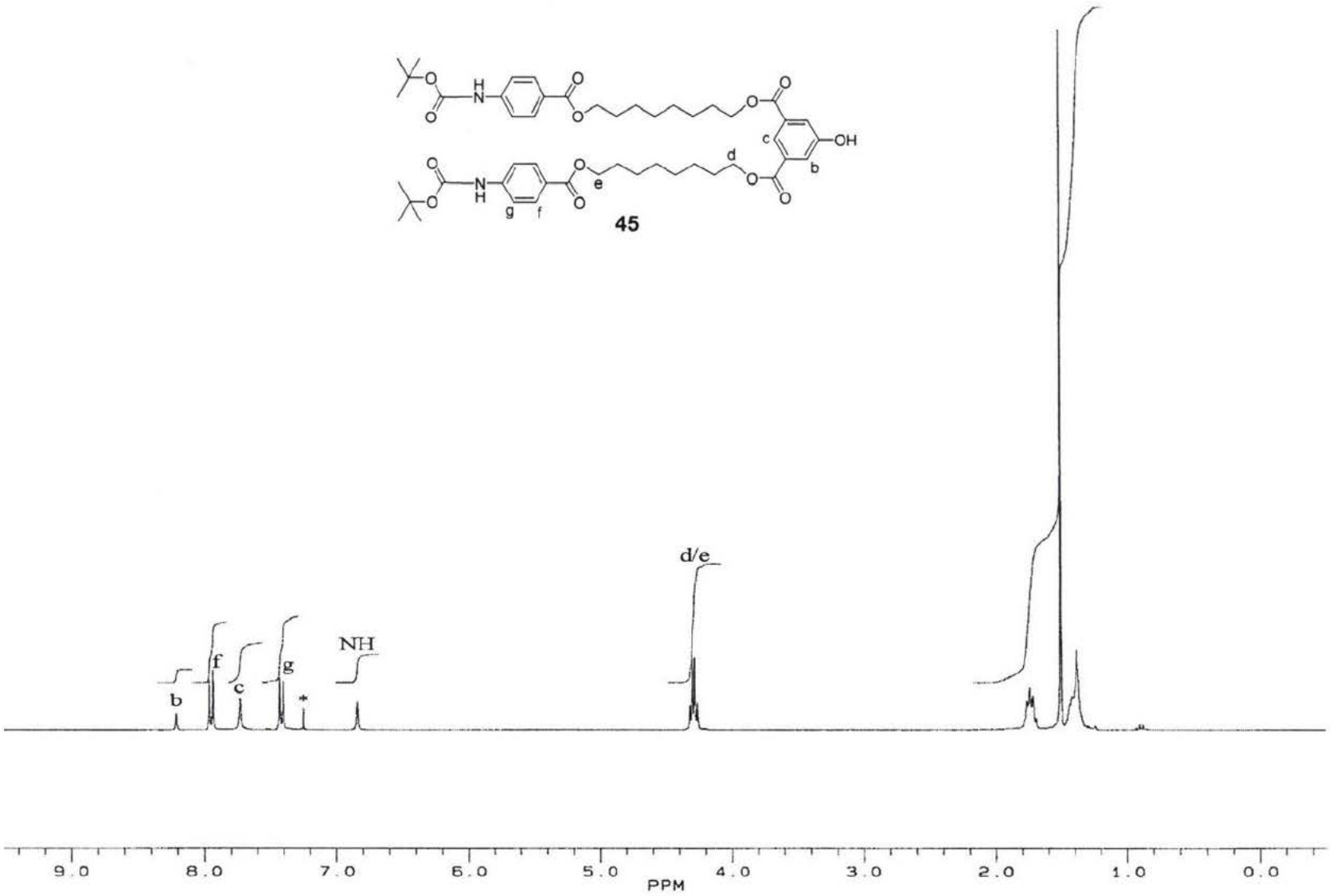

Figure 2.22: Proton NMR spectrum of compound **45**

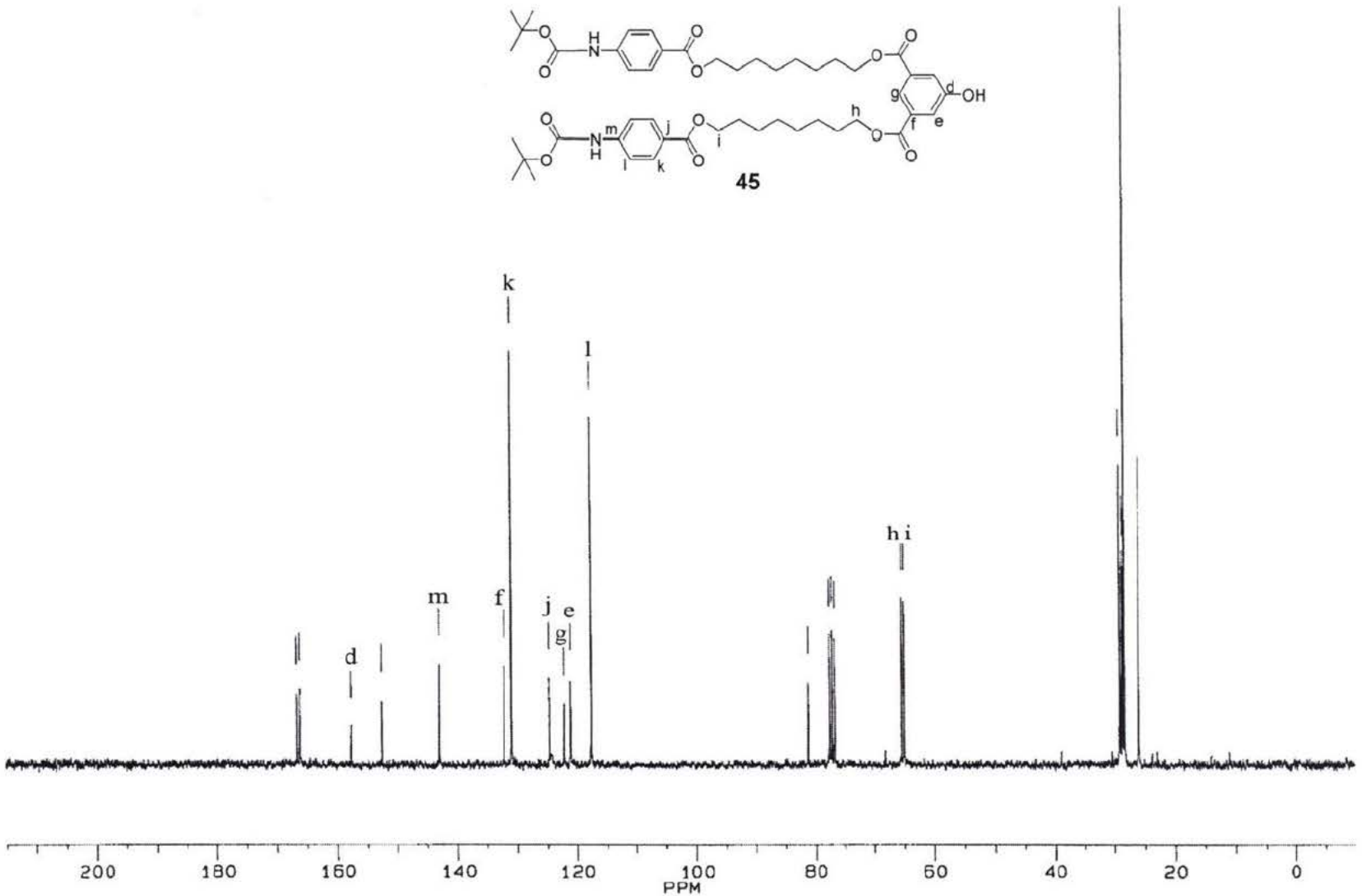

Figure 2.23: Carbon NMR spectrum of compound **45**

Two molecules of **45** were linked via reaction with terephthaloyl dichloride to form **46** and the mixture was purified by silica chromatography. The integration of the proton NMR spectrum (Figure 2.24) is consistent with a 2:1 ratio of components derived from the two reactive pairs. The proton NMR spectrum of **46** shows the inclusion of terephthalamide with the peak 8.34 ppm (**a**). Similarly the carbon NMR spectrum of **46** (Figure 2.25) shows the three expected peaks from terephthalamide at 164.9(**c**), 133.5(**b**) and 132.6 ppm (**a**). The changes in chemical shifts of the **b** and **c** protons between **45** and **46** were consistent with a decrease in electron donating capability of an aromatic alcohol changing to an ester. Upon reaction the **b** protons underwent a downfield shift from 7.73 ppm in **45** to 8.04 ppm in **46.** A smaller downfield shift for the **c** protons from 8.22 to 8.58 ppm, is also observed. The chemical shift of the carbons **d**, **e** and **g** changed: **d** shifted from 157.4 ppm in **45** to 150.6 ppm in **46**, **e** changed from 120.9 ppm in **45** to 127.0 ppm in **46** and **g** changed from 122.0 ppm in **45** to 128.3 ppm in **46**. These shifts are also consistent with an aromatic alcohol changing to an ester. All of the respective peaks in both carbon and proton NMR spectrum matched the structural calculation estimates.

An exact mass measurement of the parent ion of **21** was not possible. The mass spectrometer cleaved the Boc protecting groups as found for **36**. The progression of the masses as the Boc groups are removed is 1883, 1783, 1683, 1583 and 1483 Da with all Bocs protecting groups removed. As shown by Figure 2.26, all of those peaks were present, with the peak representing complete cleavage of the Boc protecting group as the dominant peak.

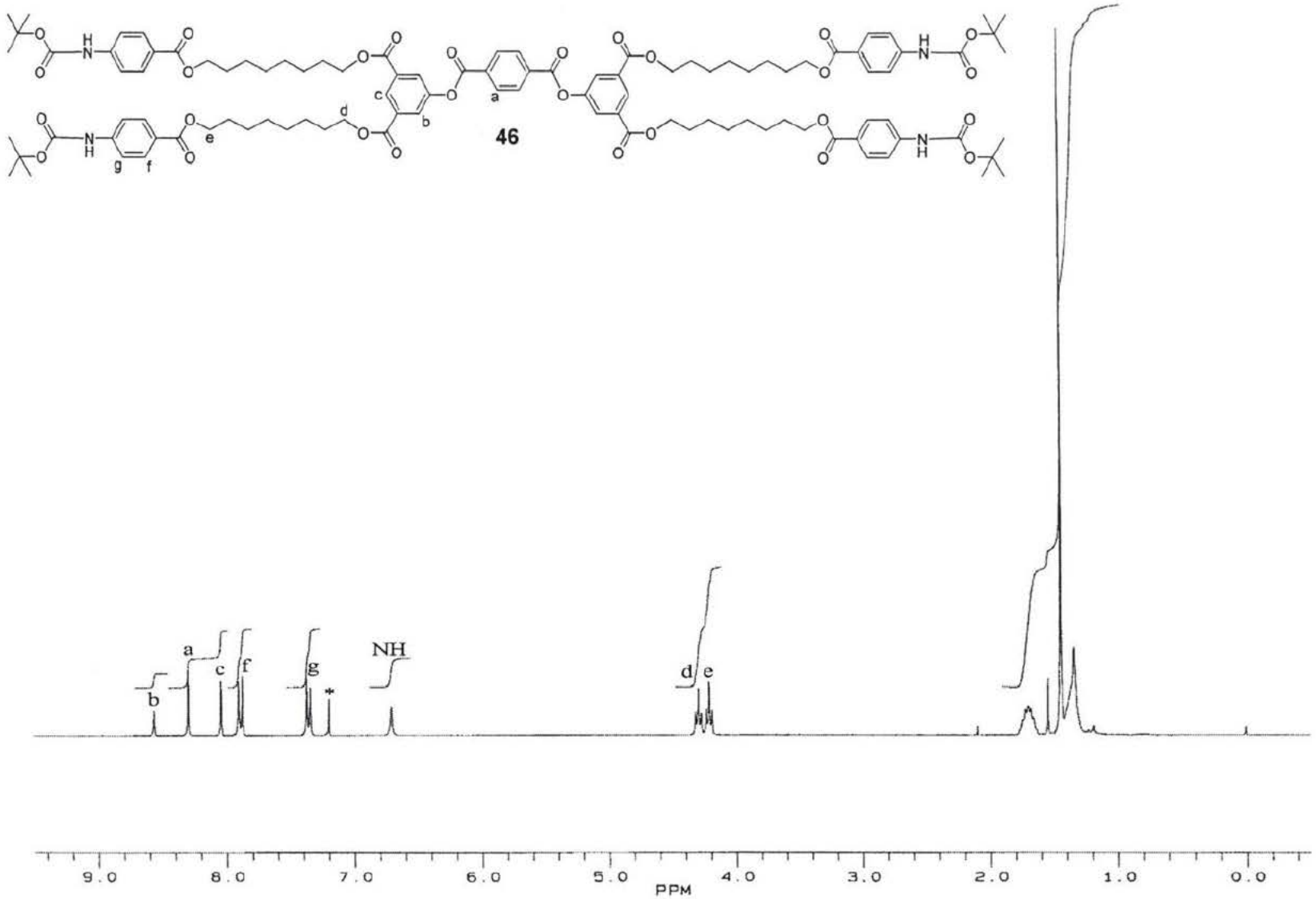

Figure 2.24: Proton NMR spectrum of compound **46**

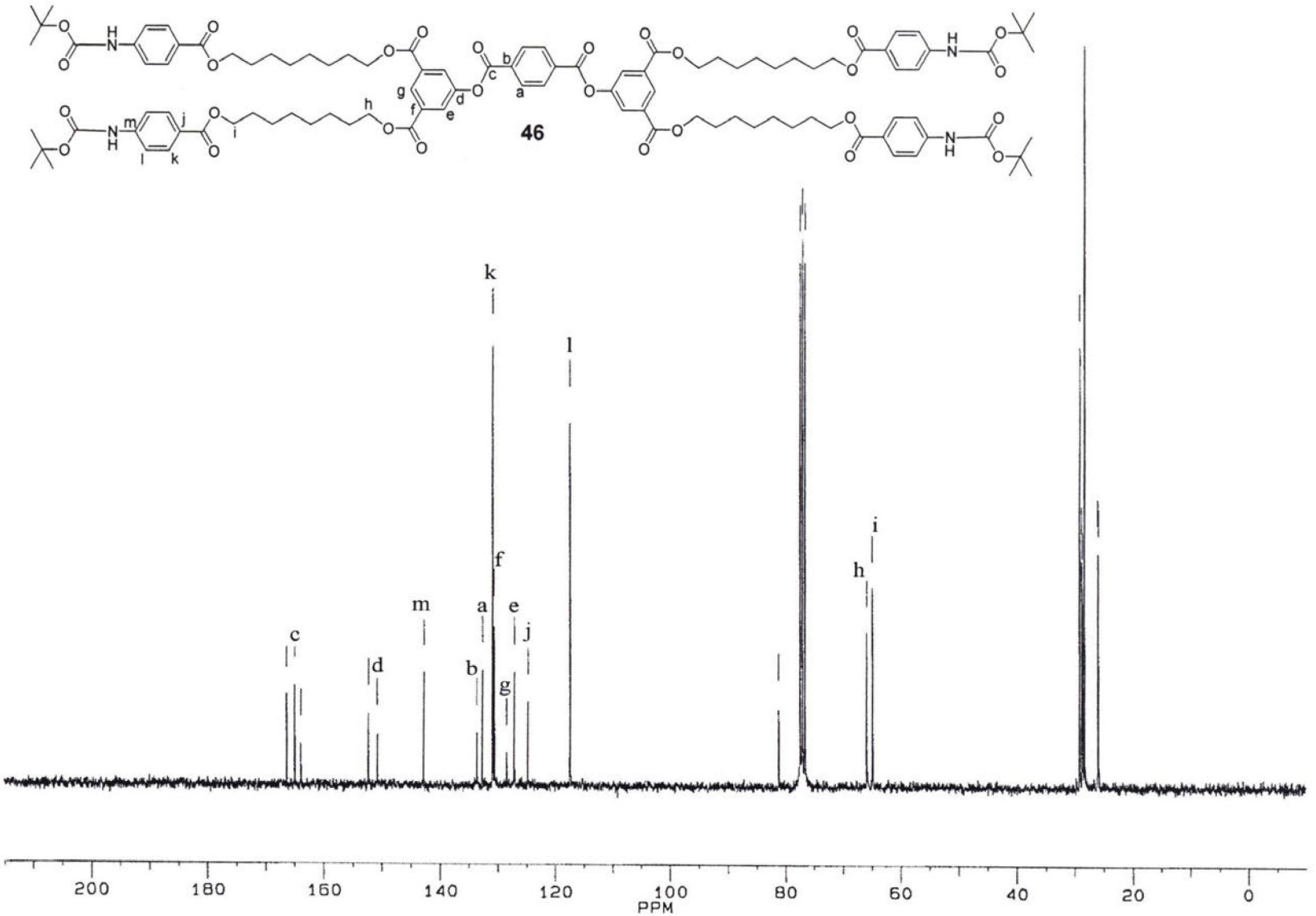

Figure 2.25: Carbon NMR spectrum of compound **46**

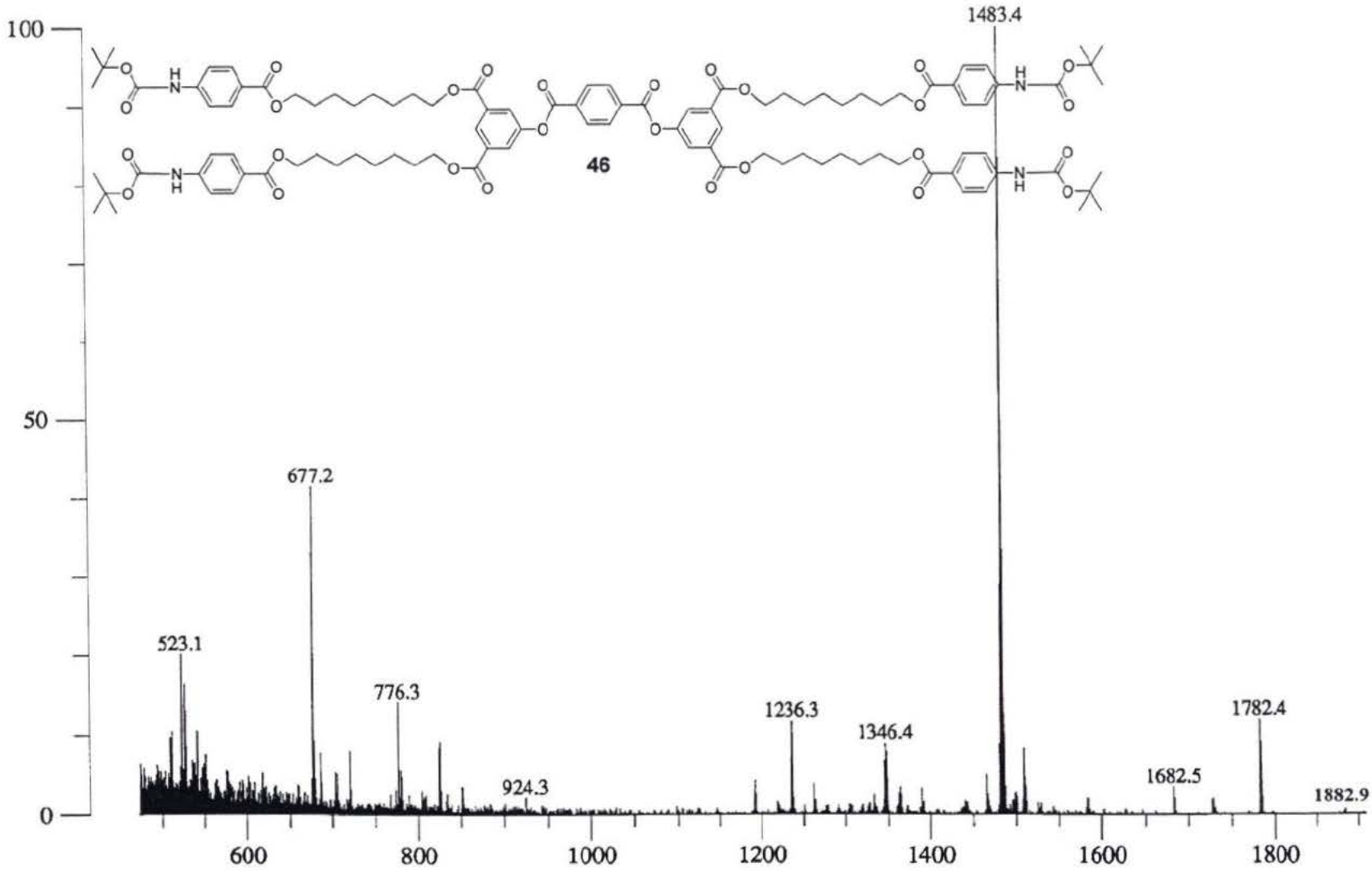

Figure 2.26: Low resolution mass spectrum of compound **46**

The deprotection of **46** forming **21** was done with TFA in dichloromethane and was purified by size exclusion chromatography on Bio Beads SX-3. There was no evidence of the 1.40 ppm peak of Boc protecting group in the proton NMR spectrum (Figure 2.27) or the 81.1, 28.3 and 152.2 ppm peaks of the Boc protecting group in the carbon NMR spectrum (Figure 2.28). The chemical shift of the newly formed amine protons varied depending on the solution of **21** Both the carbon and proton NMR spectra are consistent with the removal of a Boc protecting group from an aniline aromatic system. This is shown by the chemical shift of aromatic protons **f** and **g** shifting up field from 7.91 and 7.38 ppm in **46** to 7.81 and 6.60 ppm in **21** respectively. Also, this was shown in the carbon NMR spectra by the chemical shift of carbon **m** shifted from 142.6 to 150.3 ppm, **l** shifted from 117.3 to 113.8 ppm and **j** shifted from 124.7 to 117.0 ppm. All these shifts are consistent with chemical shift calculations of the assigned structure.

Compound **21** was a clear glass that dissolved in chloroform. There was no evidence of TFA in the carbon NMR spectrum or the low resolution mass spectrum. Also, when dissolved in DMSO, **21** was basic compared to pH 5.

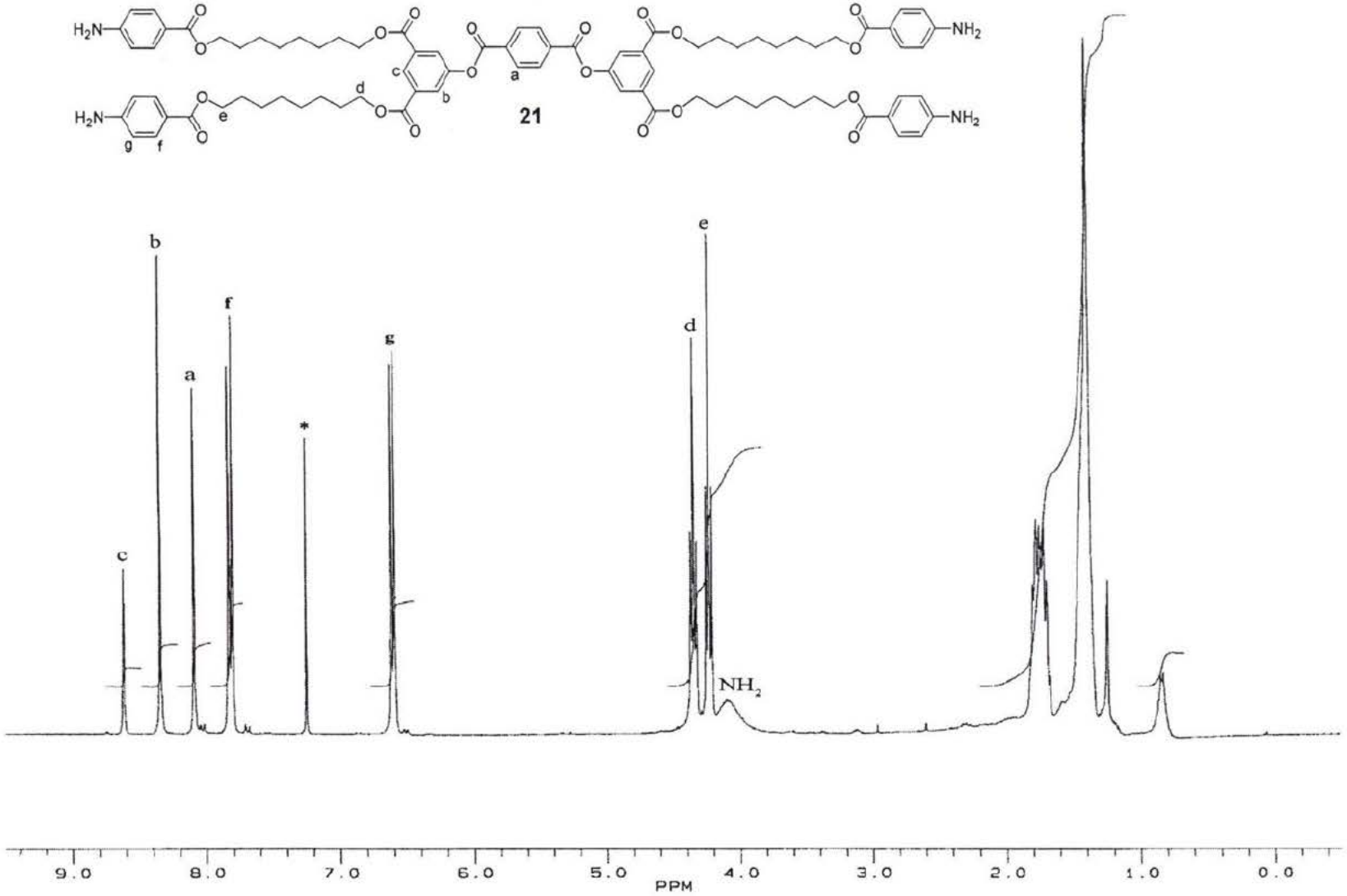

Figure 2.27: Proton NMR spectrum of compound **21**

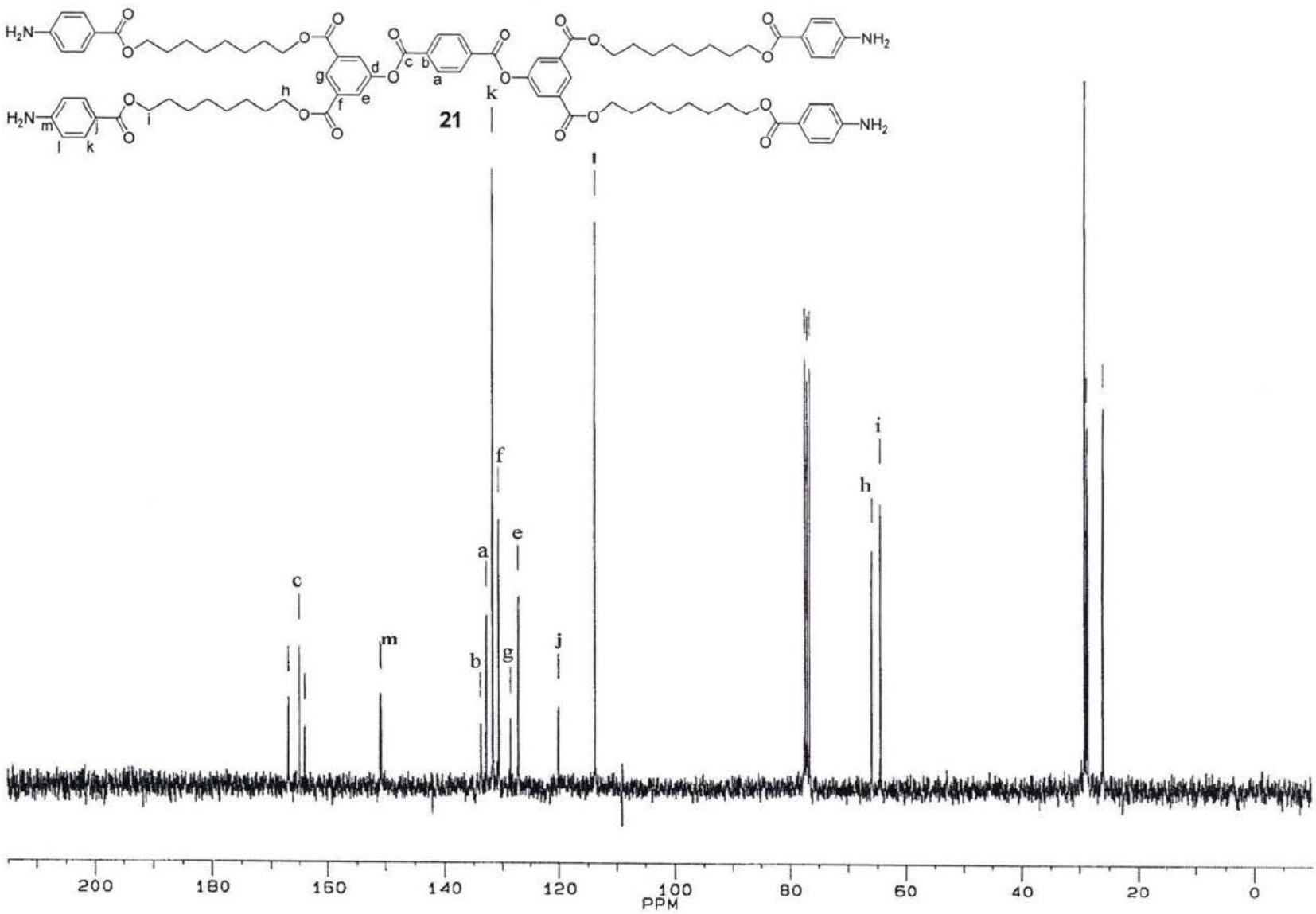

Figure 2.28: Carbon NMR spectrum of compound **21**

2.6 Summary:

The overall yield for these syntheses from 1,8-octanediol, excluding the production of the acid chloride **L** linkers, was 13% for **19**, 10% for **20** and 11% for **21**. If the synthesis of the acid chloride **L** linker is included into the overall synthetic yield, then the overall yield for **21** decreases to 4%. These synthetic yields do not portray optimized reactions. The reactions were only done enough times to establish the basic chemistry and to achieve the necessary amount of product to finish the synthesis.

Assuming that more than one reaction can be run at a time and one column can be run per day, then the minimum time to synthesize **19** or **20** is 14 days and the minimum time is 9 days for compound **21**. With optimization for time, these reaction times could be significantly reduced. All of these times are significantly shorter than required to produce **16**.

Chapter 3: Transport Data Analysis

3.1 Introduction:

In this section the transport activities of compounds **19**, **20**, and **21** will be surveyed. Previous studies by former group members have used pH-stat titration of vesicles. The pH-stat titration examines the bulk properties of transporters. The procedure used was developed by Kaye and showed reproducibility within a 15% error margin[45]. The system also offers a rapid survey of compounds and varying metal salts. Other experiments, such as ^{23}Na NMR and fluorescent vesicle experiments, are limited to certain metal salts[46]. The planer bilayer clamp experiment examines single channel behavior. This experiment is the most sensitive measure of ion activity to date. Both the pH-stat titration and the plainer bilayer clamp experiment are proven, powerful tools to analyze ion channel activity[13,14,34,44].

3.2 Preparation of vesicles:

A mixture of egg phosphatidylcholine (PC), egg phosphatidic acid (PA) and cholesterol in an 8:1:1 ratio was used. This lipid mixture was used to increase the lipid packing density thereby increasing vesicle stability and decreasing the proton leakage[42]. The mixture was dissolved in diethyl ether and an internal buffer with a pH of 3.3 was added. A high dispersion of the aqueous phase into small droplets was then achieved by using a high powered sonicator. The solution was then taken down to a viscous fluid by rotoevaporation and an unbuffered external solution (refer to chapter 5.2) was added. The complete removal of ether from the water-oil-water emulsion forms vesicles. The vesicles

were sized through a 0.4 μm Nucleopore membrane filter and the small vesicles were removed by size exclusion chromatography. The size of vesicles was established by dynamic light scattering[47]. After 3.5 hours of data collection, the typical vesicle solution contained predominantly 200nm diameter vesicles with some smaller vesicles around 50 and 10 nm in diameter and some larger diameter vesicles around 900 nm in diameter. It was found that the fraction of larger vesicles increased in proportion over time, indicating some instability in the preparation.

3.3 pH-stat titration:

The principle of the pH-stat experiment is shown in Figure 3.1. It is based on proton release via a cation – proton exchange mediated by a transporter. Vesicles are prepared in a buffer with a pH of 3.3 and a purified unbuffered electrolyte solution. After the external pH of the vesicle solution was adjusted to pH 5, FCCP (carbonyl cyanide 4-(trifluoromethoxy)phenylhydrazone)[48] and an alkali metal sulfate were added. The FCCP is a known proton carrier and was added to ensure proton release could rapidly occur in response to other cation responses. FCCP combined with the alkali metal sulfates to set up an alkali metal cation gradient and an opposing pH gradient. Thus, when a transporter is added, the pH and the cation gradients collapse creating a drop in external pH which was quickly rectified by the automatic titrator.

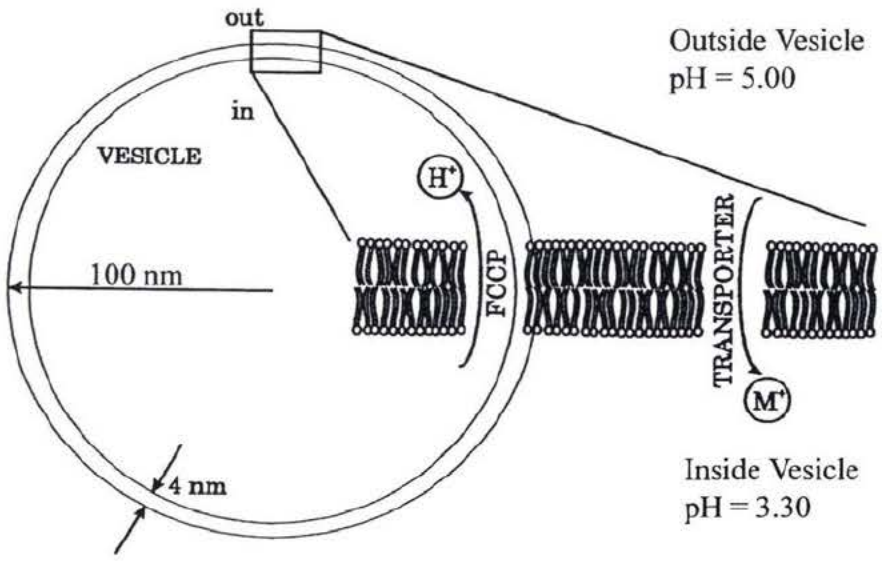

Figure 3.1: Schematic description of transport kinetics

Typical data are shown in Figure 3.2. The volume of choline hydroxide added is recorded as a function of time.

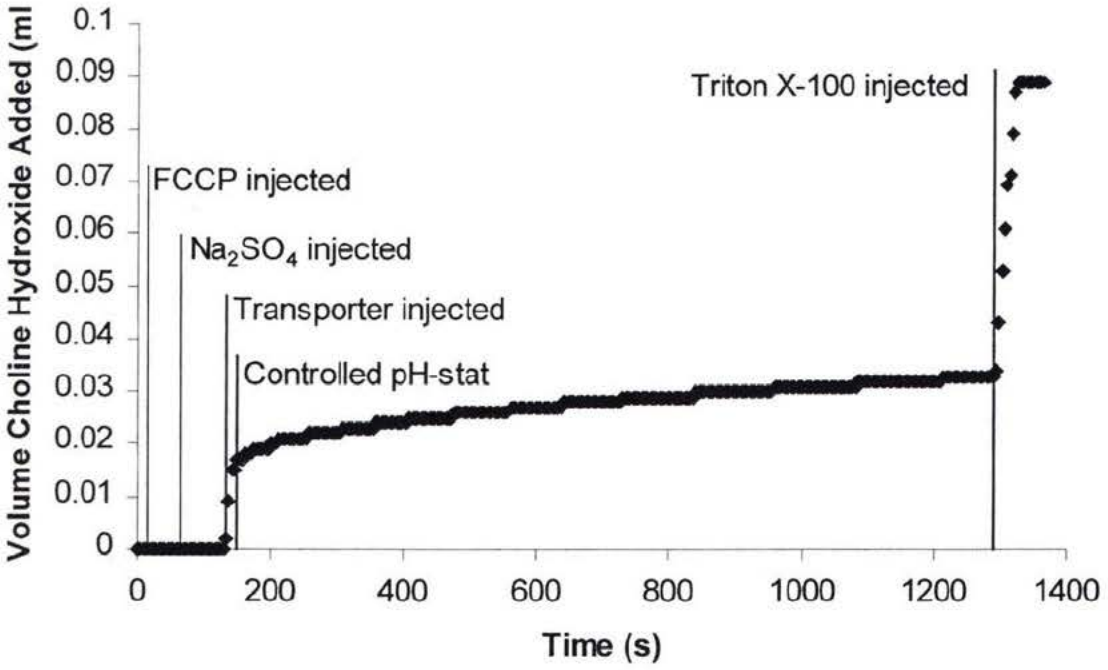

Figure 3.2: pH stat titration experiment, 0.33 nmols of **20** in a 50 μL solution of DMSO

During the initial stage of the curve, where FCCP and the alkali metal sulfate were added, there was an immeasurably small proton leakage. This was followed by a sharp uncontrolled increase after the transporter was added. Once the pH-stat gained control over the pH change there was a slow exponential growth. This was where the rate data was collected. After sufficient data was collected the detergent, triton X-100, was added. This induced lysis in the vesicles producing a sharp increase to a plateau where all the vesicles had been equilibrated.

An automatic titrator capable of adding 0.2 μL aliquots of basic titrant at a time was used. In the typical titration the external electrolyte was added to the system, and the pH was adjusted to 5. Previously, the chosen external pH for vesicle studies was 7.6. In many cases this was to deprotonate the carboxylate groups of the transporters, producing a bolaamphiphile. In this experiment the head groups of the transporters were aromatic amines. At pH 7.6 these head groups would be neutral and this would be expected to give compounds without the polar head groups which are believed necessary to create an amphiphilic structure. Therefore it was necessary to lower the external system pH to 5. This created several problems for analyzing the vesicles and transporters.

In order to determine number of vesicles available to a transporter, it is useful to know the proportion of vesicles bounded by one bilayer (unilamellar vesicles). Normally the mellitin assay determines the proportion of protons entrapped by unilamellar vesicles. At pH 7.6 it is known that mellitin can only enter the outer layer of the vesicles[49]. By adding several sequential injections of mellitin one can estimate the proportion of protons trapped under one layer, two layers and so forth. However, as shown by Figure 3.3, the mellitin assay was altered beyond use by lowering the pH to 5. A single injection of a

small amount of mellitin eventually emptied the vesicles of their proton content. At pH 5 mellitin has at least one more positive charge than pH 7.6. This is evidently enough to break the bilayer selectivity of the peptide. Thus for experiments done at pH 5 the proportion of unilamellar vesicles will be unknown.

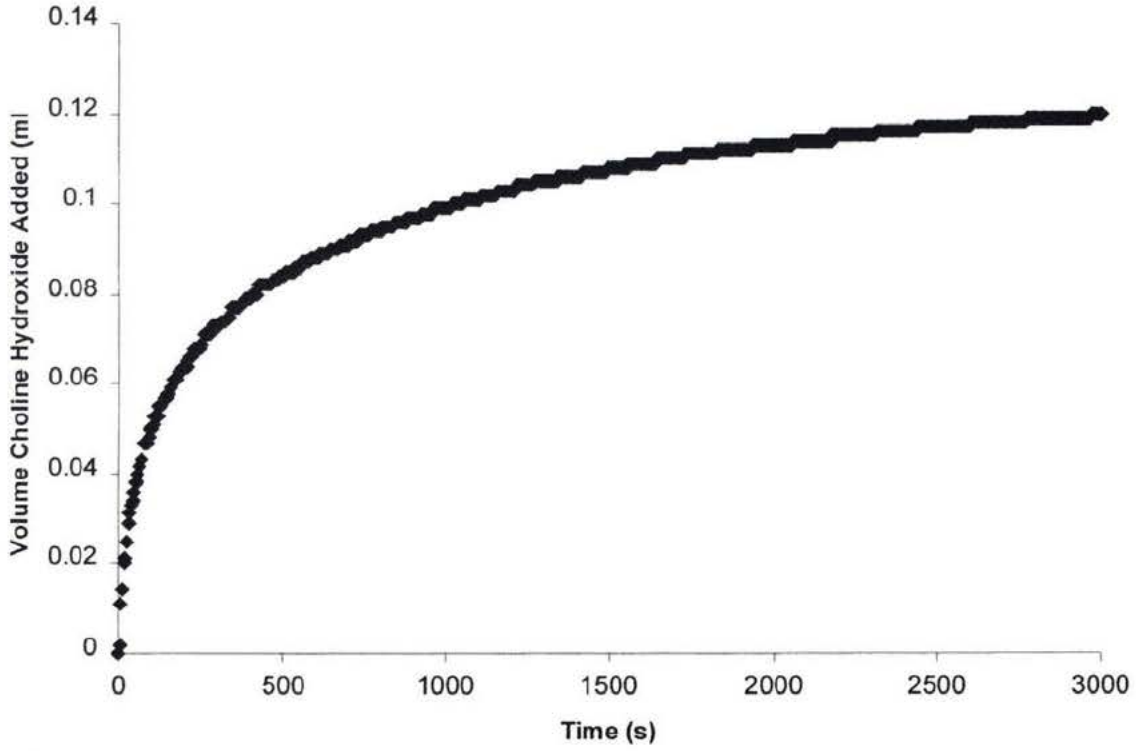

Figure 3.3: pH stat titration of 9 nmols of melitin in 3 μL of methanol

Another useful assay, which is pH dependent, is the carboxyfluorocein assay for large defects[41,50]. In this assay carboxyfluorocein is entrapped at high concentration in the vesicles. Any carboxyfluorocein leakage results in an increase in fluorescence. A calibration will establish the percent release scale. The problem was that carboxyfluorocein fluorescence is highly pH dependent and at pH 5 the fluorescence is below usable levels. Thus at pH 5 it will be impossible to establish if large defects are being created by the compounds.

Gramicidin is typically used as a standard for transport properties in vesicles[51]. It is an active transporter with characteristics that allow day to day reproducibility to be determined. As Figure 3.4 shows, gramicidin has the expected transport properties at an external pH of 5. Thus the vesicles of pH 5 are poorly characterized relative to their pH 7.6 counterparts. However, the transport curves of gramicidin establish that the experimental system could detect an active transporter among the compounds prepared.

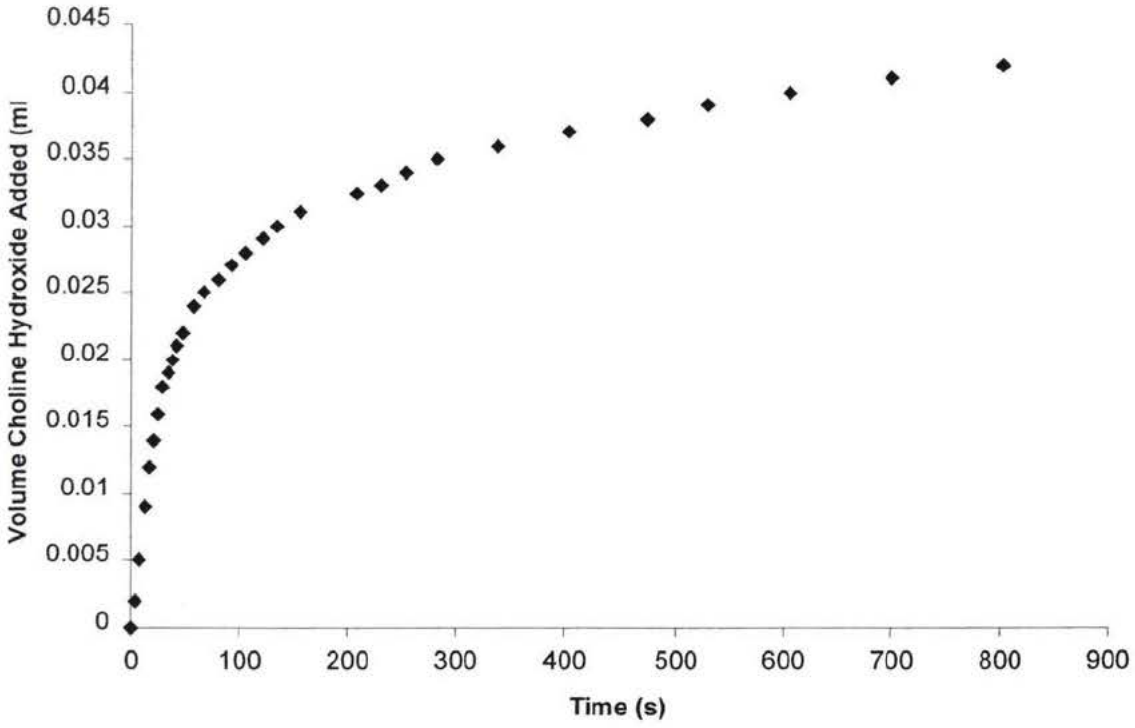

Figure 3.4: pH stat titration of gramicidin with a 1μL injection of 9 nmols in methanol

3.4 pH-stat Analysis:

All three compounds are active by the pH-stat method. All three displayed two main regions in their rate curves, as shown by an expanded plot of Figure 3.2 given as Figure 3.5. This could be explained as a superposition of two rate processes differing by a significant proportion. The faster rate following the initial injection could be explained as the compound moving from the DMSO solution into the vesicles. The second much slower rate could be the rate the compounds move between vesicles. Between the two rates there was a transition region where the observed rate was a composite of the slow and fast rate. The exact position where the data became dominated by the slower rate was unclear.

The following analysis was based on a time window from 80 to 750 seconds for compound **20** and from 250 to 1000 seconds for compounds **19** and **21**. The window was determined by data set size for compound **20** and by the initiation of the exponential curve for compounds **19** and **21**. Due to the digital limitations of the automatic titrator the data came in 1 μL increments (shown by Figure 3.4 as the discrete data points and in Figure 3.5 as dashed grey lines). In order to achieve an exponential fit, each 1 μL volume increment was treated as a single value for an average time increment that spanned the volume increment. This is shown in Figure 3.5 as the discrete data points. The faster rate was too fast for the titrimeter to follow and was reported as a volume "jump" that occurred in the first 40 seconds.

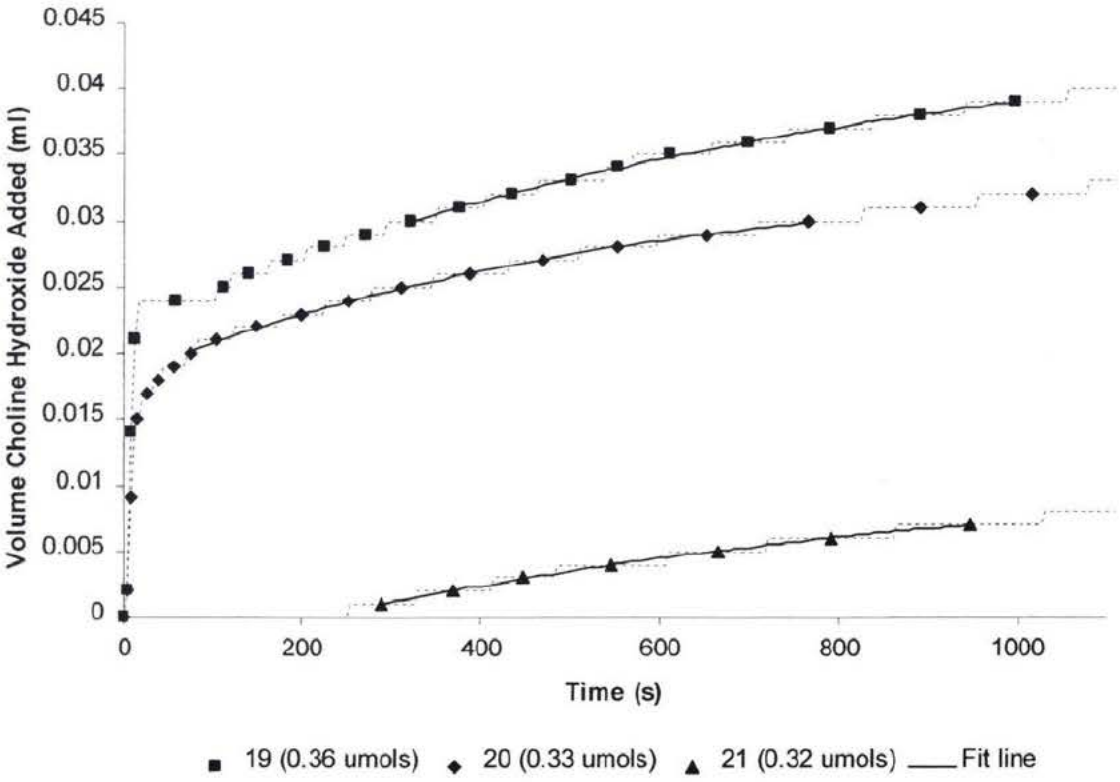

Figure 3.5: A depiction of the time window to collect rate data for each compound. The symbols depict the averaged data, the grey dashed lines depict the actual data and the dark black lines depict the numerical fit

If the compound being tested forms an active ion channel then it will exhibit an "all or nothing transport"[35,37]. This means that quickly after the channel opening the entire contents of the vesicle are equilibrated. Thus the pH-stat will only show the rate at which new channels open in non-equilibrated vesicles. Previous studies have shown this rate follows a pseudo first order processes according to the equation 1.

$$V_i = V_{\inf} + (V_o - V_{\inf})e^{kt} \qquad \textbf{Equation 1}$$

Where V_i is the volume of choline hydroxide added at time t
V_o is the volume of choline hydroxide added at time 0
V_{inf} is the volume of choline hydroxide added at infinite time
k is the rate constant
t is the time at volume V_i

Once the pH-stat gained control of the proton efflux, all of the compounds displayed the pseudo first order processes and thus fit first order exponential growth curves with r^2 between 0.998 and 1.000. Table 3.1 summarizes the rate data obtained for these curves. The expected reproducibility between runs was 15%[14,45].

Table 3.1
Calculated transport rate data from first order exponentials and volume "jump" data from the first 40 s of each run

#	Compound	Amount (umols)	Metal ion	Jump (uL)	V_o-V_{inf} (x100) (μL)	V_{inf} (μL)	-k (x1000) (s^{-1})
1		0.10	Na	6	17	20	1.1
2		0.26	Na	19	17	38	1.4
3	**19**	0.26	K	15	17	29	1.3
4		0.26	Cs	13	20	32	1.2
5		0.36	Na	24	23	45	1.3
6		0.17	Na	6	12	19	1.6
7		0.33	Na	18	16	34	1.8
8	**20**	0.33	K	16	13	29	1.6
9		0.33	Cs	18	14	26	1.6
10		0.46	Na	23	12	36	2.0
11		0.66	Na	40	21	63	2.0
12		0.32	Na	0	15	11	1.3
13		0.45	Na	0	20	15	1.2
14	**21**	0.90	Na	0	23	18	1.4
15		0.90	K	0	19	18	1.4
16		0.90	Cs	0	21	18	1.3
17		2.3	Na	0	31	30	1.3
18	Gram[1] 80-750	0.090	Na	61	21	82	2.0
19	250-1000	0.090	Na	61	25	89	1.1

1: Gramicidin

The initial jump was dependent on the amount of transporter injected, as shown Table 3.1. For example entries 1, 2 and 5 of **19** and entries 6, 7, 10 and 11 of **20** show clear dose dependence. Compound **21** is not shown as having an initial jump. However, the initial jump can be inferred to exist through a smaller volume of choline hydroxide required after the addition of Triton X-100. Triton X-100 promotes lysis in vesicles, giving the total amount of protons trapped in the vesicles. Thus, if the total amount of protons was less with transporter added than without, it can be assumed that the protons were neutralized by a source other than the pH-stat. Since the only difference between the two runs was the transporter, the difference in the total amount of protons suggests that the compound was basic compared to pH 5. However, there is a 15% error between runs. Therefore the Triton X-100 data should only be used to suggest that the initial jumps were larger than displayed in the tables. By the same criterion **19** and **20** also appeared to be basic compared to pH 5.

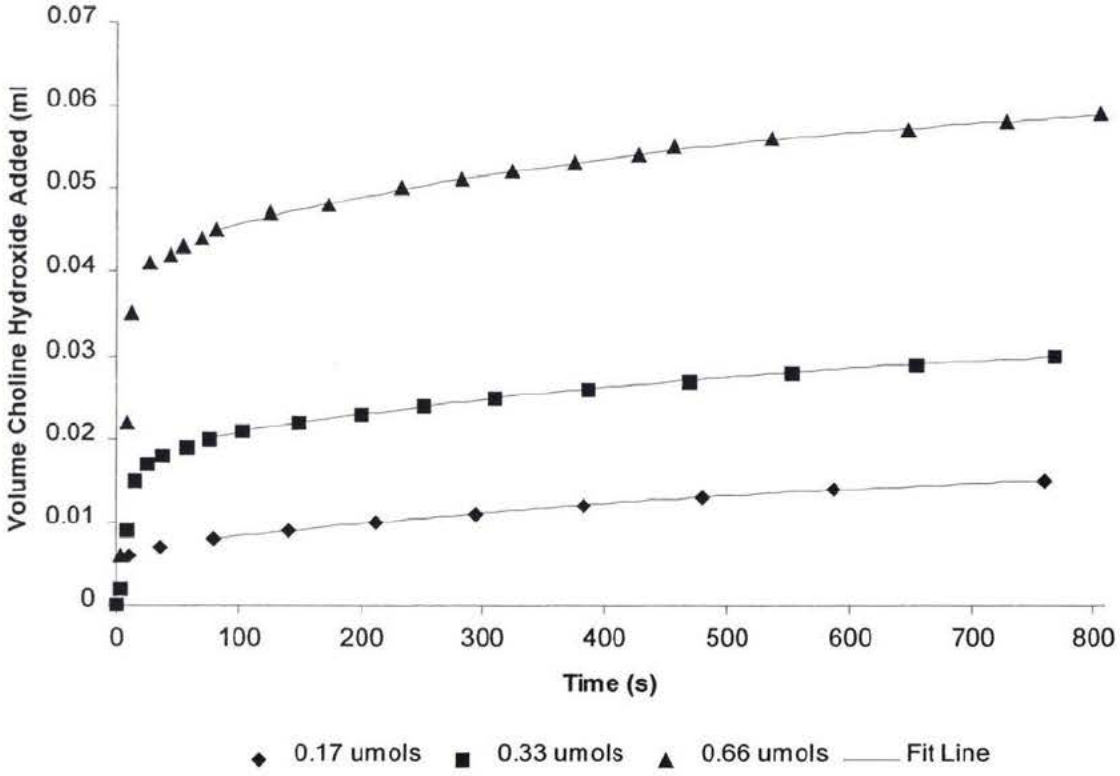

Figure 3.6: Volume of base added as a function of time for three concentrations of **20**

As shown by both Table 3.1 and Figure 3.6, after the initial jump the rates were apparently independent of the amount of transporter injected. It also appears that these rates are compound independent as well. When gramicidin and the three compounds were compared over identical data windows, the rates were the same within the expected errors. This suggests that an aspect of the solution and not the transporter controls the slower rate process. However, when 50 μL of DMSO was injected into a vesicle solution, there was no measurable proton leakage for 40 minutes. This implies that the efflux of protons was due to the transporter, but the rate the compound transfers between vesicles was solely dependent on the vesicles in the solution. This would be consistent with the possibility that the compounds do not transfer from the vesicles into the solution, but instead must be transferred by collision between vesicles. Another aspect which points

toward a vesicle to vesicle collision rate was the calculated extent of transport (V_{inf}). As shown in Table 3.1 and Figure 3.6, the calculated V_{inf} was not only significantly below the total amount of protons included in the vesicles, but it also varied with the amount of transporter added. This is a characteristic displayed by compounds which do not transfer between vesicles and solution efficiently[45].

Table 3.2
Exponential fits of pH-stat rate data for 0.36 nmols of **19** at three different time periods of the same run, showing the dependence of the slow rate with time

#	Time period (s)	-k (s^{-1} x 1000)
20	100-600	1.3±0.2
21	600-1100	0.83±0.03
22	1100-1600	0.44±0.11

Another interesting facet of the slower rate was that it appears to be decreasing with time. This was demonstrated by fitting three sequential 500 second time periods of a single run. Table 3.2 shows this data. The interdependence of this effect between compounds was shown by two different rate fits for gramicidin (Table 3.1). Even though **20** was fit to a different time window than **19** and **21**, when gramicidin was fit to the same time window it came to the same rate as **20**. This suggests that the slow rate was decreasing with time. As described previously, the size of the vesicles appeared to increase with time. This would slow the average diffusion speed of the vesicles and decrease the collision rate between vesicles.

An experiment that was done to test the ability of the compounds to transfer from vesicle to solution to vesicle provided some confounding insights. Two vesicle batches

were made up, and the first batch was injected with **20.** The pH-stat data was recorded for a while and then the second vesicle batch was added.

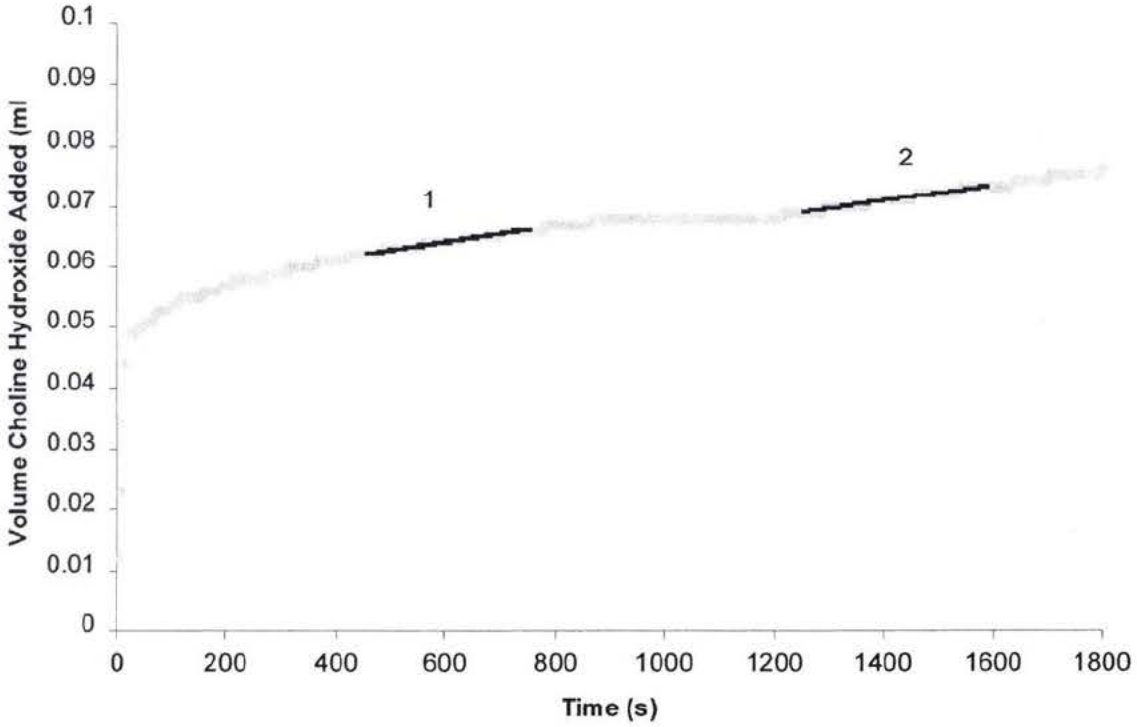

Figure 3.7: Volume of base added as a function of time for sequential addition of vesicle solutions

Table 3.3
First order exponential fit data for Figure 3.7

Regression #	V_{inf} (μL)	V_o-V_{inf} (μL)	-k (s^{-1}) (x10000)
1	144±49	89±48	0.17±0.10
2	102±9	53±7	0.39±0.11

As shown by Table 3.3 and Figure 3.7, the rate calculated for regression #2 was higher than the rate calculated for regression #1. This change is consistent with a decrease in the average vesicle size. An increase in the rate constant would also suggest an increased availability of vesicles to the transporter. However, if that was the case then

the total protons available to the vesicles (V_{inf}) would be independent of the amount of transporter. As shown in Table 3.1 and Figure 3.6 V_{inf} was highly dependent on the amount of transporter added. Also, if this increase in rate was due to an increased availability of unilamellar vesicles, an initial jump should be observed. As clearly displayed in Figure 3.7 this was not the case.

3.5 pH-stat Summary:

All three of the compounds were active; **19** and **20** showed the highest level of activity and compound **21** showed significantly lower levels. Once inserted into the bilayer all three compounds displayed a tendency to stay inserted. The size order of the alkali metal cations is $Na^+ < K^+ < Cs^+$. The alkali metal selectivity observed for compound **19** was the opposite of the size order with $Na^+ > K^+ > Cs^+$. Assuming a 15% error between runs, the data was very close to that error, thus the selectivity was modest at best. Table 3.1 also shows a small variation with alkali metal sulfate for **20**. However, this variation is well within the 15% reproducibility. Finally, this series of compounds was designed to probe if hydrogen bonding in the centre of a channel-forming compound affects ion channel activity. Replacing the amide group in **19** with an ester in **21** tests this question. As shown by Figure 3.5 and Table 3.1, compound **21** had significantly less activity than **19**. This qualitative analysis ignores the complications described previously. However, the anticipated errors would tend to obscure real differences in activity between compounds **19** and **20**.

3.6 Bilayer Clamp Experiment:

As stated previously, the bilayer clamp method is able to detect single channels. The principle of the technique works by applying a bias across a bilayer formed on a small hole in a hydrophobic support separating two cells. The bilayer clamp set up is shown in Figure 3.8. If a channel is formed in the bilayer, a current will flow. Thus, if the time dependence of the current is recorded, when a channel forms in the bilayer, the initiation, the time span, as well as the current flowing through the channel can be measured. In the presence of an active channel, step changes indicate the on and off states. As shown in Figure 3.8, there tends to be more than one step in current flow. This is due to more than one channel opening at one time. The current flowing through one channel can be seen as the average of the unit step sizes. The specific conductance of the channel can be found from the slope of the current-voltage line drawn from the average step heights at different voltages[46,52].

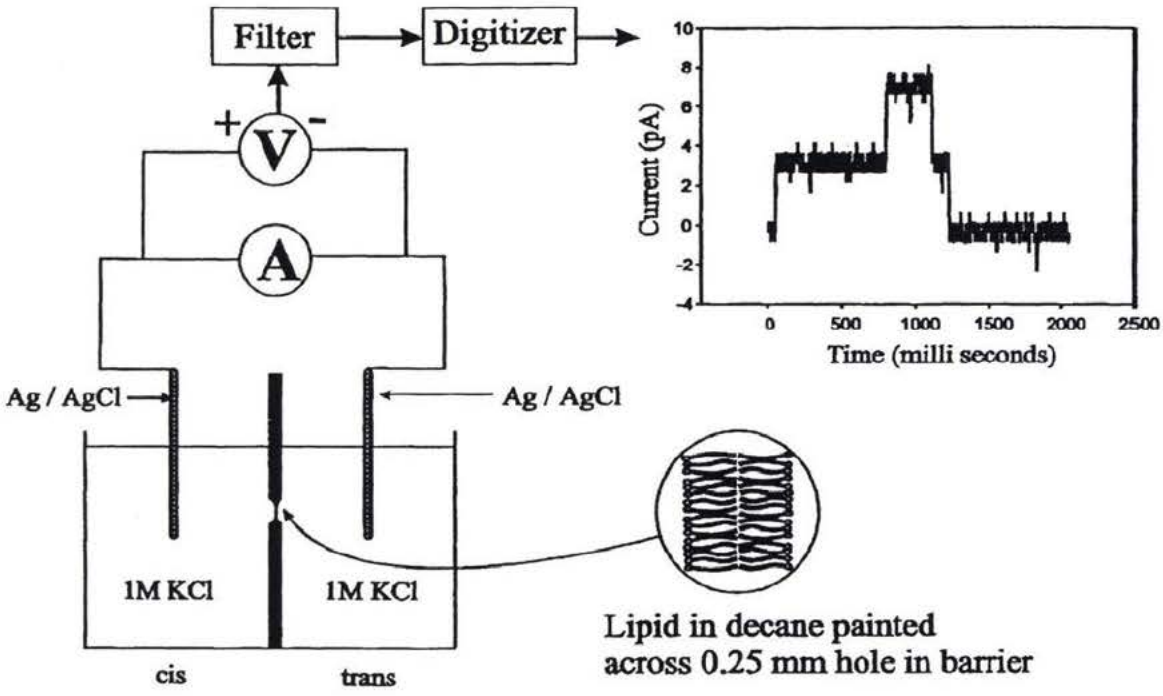

Figure 3.8: Schematic of the bilayer clamp experiment

Todd Sutherland has begun to explore the bilayer activity in compounds **19**, **20** and **21** with the bilayer clamp experiment. As shown by Figure 3.9 compounds **19**, **20** and **21** all display the characteristic step conductance changes of channels. The step height in the illustrated cases appears to be approximately the same for all three compounds. The time that the channels were open was longest for **20**, with a maximum period around 45 s (not shown), followed by **19** and, with significantly shorter opening periods, **21**. What is not well illustrated in Figure 3.9 is the period between openings that appears to be significantly longer for compound **20**, than for compounds **19** and **21.** That is: compound **20** forms long lived channels infrequently, **19** forms shorter lived channels frequently and **21** forms short lived channels frequently.

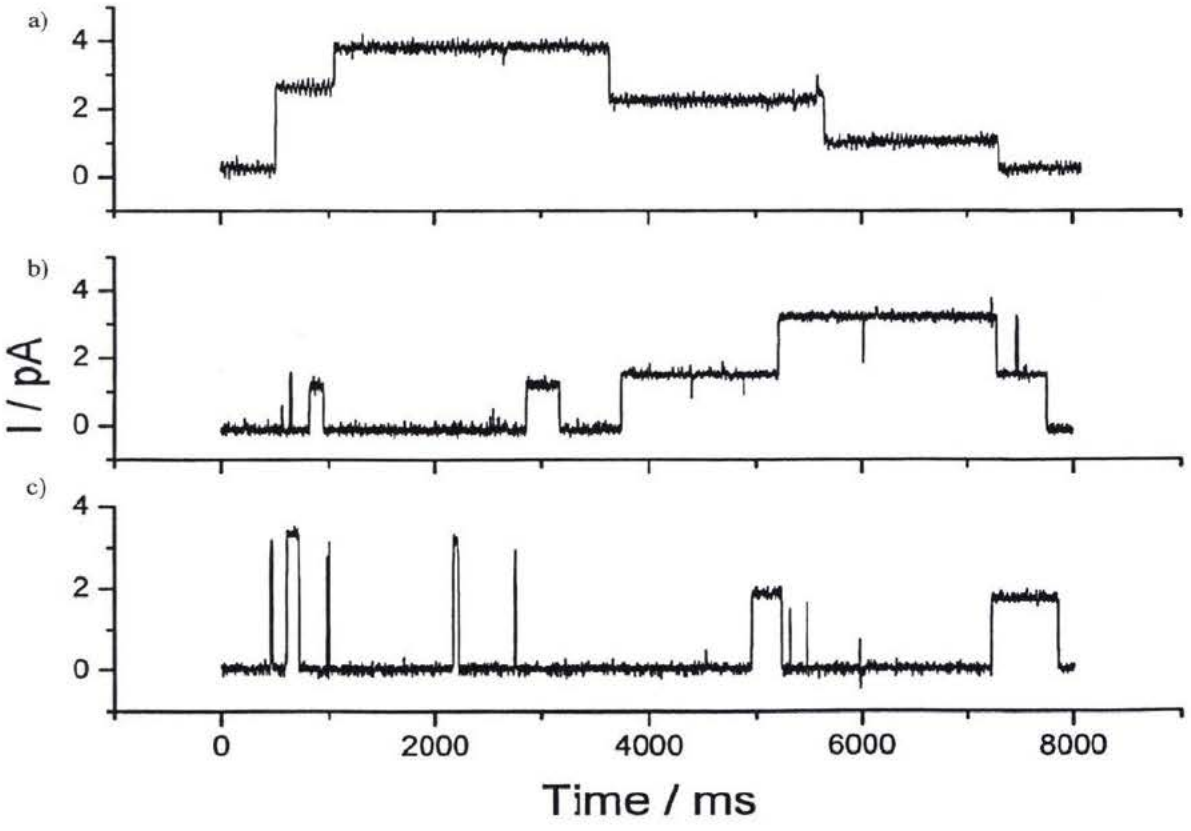

Figure 3.9: Bilayer clamp run with 1M CsCl at +80mV for a) **20**, b) **19** and c) **21**

As described earlier, the step conductance changes shown in Figure 3.9 are characteristic of channels opening and closing. Therefore, all three compounds can form ion channels.

The step height at a certain voltage is not necessarily an indication of the compounds ability to conduct ions. The property of an ion channel to conduct ions is usually described as the specific conductance, which as described earlier is calculated from a current-voltage curve over several different voltages. It was found that compound **19** had a specific conductance of about 40 pS, compound **20** had a specific conductance of about 60 pS and compound **21** had a specific conductance of about 20 pS with CsCl as the electrolyte. These specific conductivities are significantly higher than the majority of synthetic channels to date, as well as higher than gramicidin.

The span of time a channel remains open is an indication of the stability of the channels formed. Therefore, at 45 second openings, compound **20** forms extremely stable channels. Even compound **19** forms channels that have a higher degree of stability than gramicidin. Compound **21** on the other hand forms channels that are about on par with gramicidin.

The time span between openings for compound **20** is probably a solubility issue. When the compounds are introduced to the bilayer in the bilayer clamp experiment, they must first traverse a distance of water to reach the bilayer. When compound **20** was introduced, some of it precipitated out of solution before reaching the bilayer. This would lower the concentration of the compound in the bilayer, which would reduce the number of collisions between compounds and thus the number of channels formed per unit time.

This could also be an indication of how many molecules must collide and aggregate to form a channel.

The full details of the channel behavior for **19**, **20** and **21** are still being determined. These preliminary results simply establish the significant channel activity of all three compounds.

Chapter 4: Structural and Mechanistic Discussion

The most apparent finding from this series of compounds was that macrocycles were not necessary to achieve activity. In fact, the activities of all the acyclic bola-amphiphiles in this thesis were significantly higher than any of the macrocyclic channels tested previously.

As shown by both pH-stat and the bilayer clamp experiment, compound **20** indisputably had the highest level of activity. This would suggest that the increased volume of the macrocycle in **16** and the extra tails of **19** inhibited ion channel activity.

As for the question of the role hydrogen bonding plays, both the pH-stat and the bilayer clamp experiment agree quite vigorously. The pH stat experiment showed that there was no initial jump displayed by compound **21** and it took significantly more of the compound to display a significant response. On the other hand, compound **19** displayed a significant response on injection. However, as described in the pH-stat section, the method had some drawbacks, thus drawing inferences between compounds was troublesome. The bilayer clamp experiment did not suffer from those problems and the differences between compounds were clearly visible. Compound **19** displayed significantly higher activity than **21** in both stability and specific conductance. This indicates that although the lipid will initially organize the molecule into a channel, hydrogen bonding plays a significant role in enhancing the stability of the channels once formed. The role of hydrogen bonding in this series of compounds was further illustrated by the solubilities of compounds **19**, **20** and **21**; **20** crystallized out of DMSO above 20 mM, it was necessary to heat **19** to dissolve the crystals in DMSO and **21** was soluble in chloroform. This clearly shows that the ability to form crystals/strength of the

intermolecular forces was significantly stronger in **20** than **21** and **19** had significantly stronger intermolecular forces than **20.**

As for the conformation that allowed the high level of activity in **20**. It seems unlikely that a single molecule which, if the length estimate is correct, is the right length to participate in the hydrogen bonding between lipids could produce an activity significantly higher than any synthetic channel made. It also seems unlikely that with the wall unit volume decreased by one half, that the specific conductance of a dimer would increase five fold. It has not been previously shown that a simplistic dimer could support ion transport at this level of activity and it seems even less likely with an opening of 0.28 nm (possible hydrogen bond length in the linker) that this activity could stem from a dimer. On top of this, all previous macrocyclic channels have been dimers or higher order aggregates. Thus the increase in activity is probably due to the increase in the intermolecular hydrogen bonding ability of **20** and **20** probably formed aggregates of three or more molecules. A possible hexameric aggregate of **20** is shown in Figure 4.1.

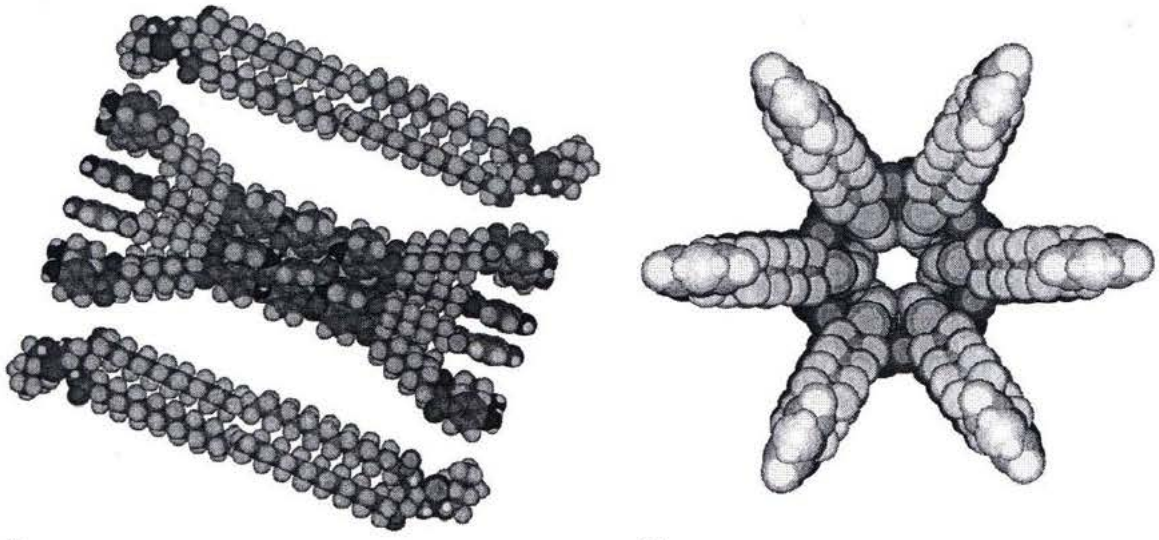

a) b)

Figure 4.1: 3D view of a possible barrel stave of **20**

As shown in Figure 4.1a, the fully extended tails of **20** place the carbonyl groups approximately even with the ester carbonyl groups of the phospholipids. The separation of the carbonyls at the ends of the tails is 4.04 nm for **20** as compared to 4.06 nm for the bilayers' lipids. As described in the introduction, the head group solvation as well as apparent structural similarity to the bilayer would give the aggregates structural stability. In the sketch, the carbonyl groups are directed towards the center of the channel providing a hydrophilic center. The distance between individual molecules was set from the carbonyl–amide hydrogen bond distance of 0.28 nm. It should also be noted that the membrane is a fluid, thus by having the flexible alkyl arms the compound can presumably adjust to bilayer motions.

Similar arguments for the extent of aggregation of **20** can be used for **19**. There are several ways to explain the lower activity of compound **19** though. One is the possibility that **19** would act as an aggregate with a similar conformation to the aggregate of **20** shown. The decreased stability would be caused by extra unfavorable interactions due to the tails of **19**. If the tails of **19** adopted a Y conformation in a similar aggregate to Figure 4.1, the open volume of the aggregate would close. The tails of **20** could also close the channel in this way, however, **19** has two disadvantages over **20**; **19** has two more tails and the tails of **19** are located in the 3,5 positions. However, if the amide-isophalate bond is rotated such that the isophalates are offset to the central linker aromatic, while at the same time allowing the flexible tails to position themselves into the minimum energy states, a stable aggregate might form. The possibility that **19** forms a dimer can not be ruled out. However, there is still a problem with the strong intermolecular forces incorporated into this series of channels.

Compound **21** lacks the hydrogen bond interactions described in **16**, **19** and **20**. Thus, the arguments for higher order aggregates do not apply. However, **21** still displayed activity significantly higher than both gramicidin and previous macrocyclic channels. Since intermolecular forces were not twisting the linker section towards conformation (c) (Figure 1.12 and 1.13), **21** may have adopted conformation (a) (Figure 1.12). This allows the linker carbonyls to point into the hydrophilic center of the channel. Also the flexibility of the four tails should allow them to move into positions that form a cone shaped opening, aligning with the angled hydrophobic lipid tails. Using the hydrophobic lipid tails as a support structure may be an effective method to increase the activity of channel forming compounds.

In terms of the relationship to compound **16**, all three compounds were easier to handle and had significantly higher stability and specific conductances. Compound **16** is shorter than all three compounds and has a rigid bulky structure. This could potentially have made it difficult for **16** optimize itself for aggregation. As shown by the difference between compounds **19** and **20**, bulkiness appears to reduce activity. Also, since compound **16** is less active than **21,** it suggests that either hydrogen bonding was not playing a role or the conformation of **16** was such that it severely restricted the packing behavior reflective of **20**. This could have been due to the rigidity of the structure.

On the synthetic side, **19**, **20** and **21** had overall yields above 10%. Compound **16**'s overall yield was approximately 2%. Thus, by breaking the macrocycle a five-fold increase in synthetic yield and specific conductance was achieved.

The compounds designed and synthesized in this thesis are a new design for active ion channels. It would be interesting to examine how the following features will

compound **20** had a specific conductance which was five time the specific conductance of gramicidin and a channel stability which far exceeded it. If the specific conductance and channel stability is combined, compound **20** is estimated to transfer over 1000 times more charge per unit time than gramicidin.

Chapter 5: Experimental

5.1 Synthetic Experimental:

8-Bromooctan-1-ol (23)

1,8-Octanediol (50.53g, 345.6mmol) was dissolved in toluene and 40 ml of hydrobromic acid was added to the solution. The flask was then completely filled with toluene, attached to a light liquid continuous extraction device and placed in an oil bath at 90°C. The reaction was left for 72 hours with the continuous extraction of the product to the collecting flask. The collecting flask was disconnected from the apparatus and placed in the freezer for 12 hours. The precipitate was collected and the excess toluene was removed by evaporation. The remaining liquid was distilled under vacuum at 3 mmHg. The yield was 33.86g (162.4mmol, 47%)

^{1}H NMR (300 MHz), $CDCl_3$: 3.59 (t,2H), 3.36 (t,2H) 1.9 - 1.0 (m,12H)

^{13}C NMR (75 MHz), $CDCl_3$: 62.7, 34.0, 32.7, 32.6, 29.2, 28.7, 28.1, 25.6

4-tert-Butoxycarbonylamidobenzoic acid (26)

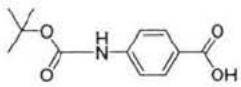

4-Aminobenzoic acid (6.40, 46.7mmol) was dissolved in 60:40 water:methanol mixture saturated with sodium carbonate and heated to 40°C. Di-tert-butylcarbonate (10.24g, 46.9 mmol) was added drop wise. The solution was allowed to stir for 14 hours. The pH was adjusted to 3 with acetic acid and the precipitate was removed by filtration. The yield was 9.74g (41.1mmol, 88%)

^{1}H NMR (300 MHz), C_3D_6O: 8.78 (s,1H), 7.98 (d, 2H), 7.68 (d, 2H), 1.42 (s, 9H)

^{13}C NMR (75 MHz), C_3D_6O: 167.4, 153.4, 145.0, 131.6, 124.9, 118.1, 80.6, obscured by acetone, 28.4

(8-Hydroxyoctyl) 4-tert-butoxycarbonylamidobenzoate (27)

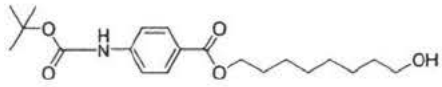

Tetramethylammonium hydroxide (2.84, 15.7mmol) was dissolved in 100 ml of DMSO. Compound **26** (3.28g, 14.6mmol) and sodium iodide (0.23g, 1.5mmol) dissolved in DMSO were added and the solution was heated at 50°C under N_2. Compound **23** (3.28g, 15.7mmol) was added to the solution drop wise. The solution was stirred for 14 hours. Deionised water (900ml) was then added and the precipitate was filtered and dried under vacuum. The crude product was purified by column chromatography on silica using a 3:7 hexane:ether eluent. The yield was 3.74g (10.3mmol, 70%)

^1H NMR (300 MHz), C_3D_6O: 8.78 (s,1H), 7.94 (d, 2H), 7.66 (d, 2H), 4.25 (t, 2H), 3.50 (t, 2H), 1.8 - 1.2 (s, 21H)

^{13}C NMR (75 MHz), C_3D_6O: 166.4, 153.4, 145.0, 131.2, 124.9, 118.1, 80.6, 65.2, 62.4, 33.7, obscured by acetone, 28.4, 26.7, 26.6

MS (EI) exact mass calculated for $(C_{20}H_{31}NO_5)^+$ 365.2202; found 365.2193

5-Nitroisophthaloyl dichloride (28)

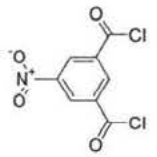

5-Nitro-isophthalic acid (1.06g, 5.02 mmol) and phosphorous pentachloride (3.26g, 15.6 mmol) were mixed. The mixture was then refluxed at 140°C for 6 hours. The product was the placed under vacuum for 8 hours to remove $POCl_3$ and PCl_5.

^{1}H NMR (300 MHz), $CDCl_3$: 9.21 (s,2H), 9.11 (s, 1H)

^{13}C NMR (75 MHz), $CDCl_3$: 165.6, 148.0, 137.4, 136.0, 130.9

bis-[8-(4-tert-Butoxycarbonylamidobenzoyl)octyl] 5-nitroisophthalate (29)

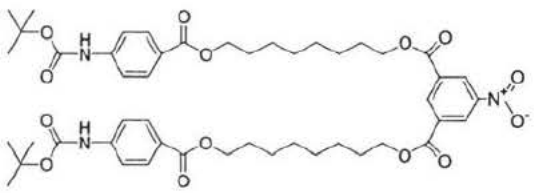

Compound **28** (1.25, 5.04mmol) and triethyamine (2.04g, 20.2mmol) were dissolved in 50ml of dry THF. Compound **27** (3.68g, 10.1mmol) dissolved in 100ml dry THF was added and the mixture heated to reflux at 90°C for 14 hours. The crude product was purified by column chromatography on silica using 3:7 hexane:ether eluant. The yield was 3.24g (3.57mmol, 71%).

^{1}H NMR (300 MHz), $CDCl_3$: 8.99 (s, 2H), 8.93 (s, 1H), 7.94 (d, 4H), 7.42 (d, 4H), 6.81 (s, 2H), 4.38 (t, 4H), 4.29 (t, 4H), 1.8 - 1.2 (m, 42H)

^{13}C NMR (75 MHz), $CDCl_3$: 166.3, 163.8, 152.3, 148.4, 142.8, 135.8, 132.8, 130.9, 128.0, 124.5, 117.3, 81.1, 66.4, 64.8, 29.1, 28.7, 28.5, 28.3, 25.9, 25.8

MS (EI) exact mass calculated for $(C_{48}H_{64}N_3O_{14})^+$ 905.4310; found 905.4321

bis-[8-(4-tert-Butoxycarbonylamidobenzoyl)octyl] 5-aminoisophthalate (30)

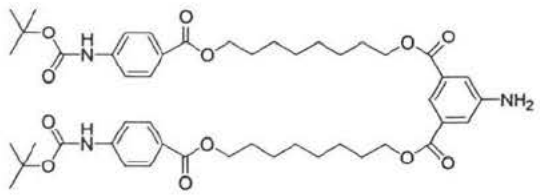

Compound **29** (1.2g, 1.32mmol) was dissolved in 100ml of 95% ethanol and 1.8g of 1% Pt/C was added. The solution was placed under 50 psi of hydrogen and shaked for 144 hours. The catalyst was removed by filtration, the solvent removed by evaporation and the crude product was purified by column chromatography on silica using an 80:20:1 toluene:ethyl acetate:pyridine eluant. The yield was 1.03g (1.17mmol, 89%)

^{1}H NMR (300 MHz), $CDCl_3$: 8.01 (s, 1H), 7.94 (d, 4H), 7.47 (s, 2H), 7.42 (d, 4H), 7.18 (s, 2H), 4.25 (m, 8H), 4.02 (s, 2H), 1.8 to1.0 (m, 42H)

^{13}C NMR (75 MHz), $CDCl_3$: 166.4, 166.1, 152.3, 146.8, 142.8, 131.8, 130.8, 124.6, 120.5, 119.6, 117.4, 81.0, 65.3, 64.8, 29.1, 28.7, 28.6, 28.3, 25.9, 25.9

N, N'-bis(3, 5-bis-[8-(4-tert-Butoxycarbonylamidobenzoyl)octyl]carboxyphenyl) terephthalamide (32)

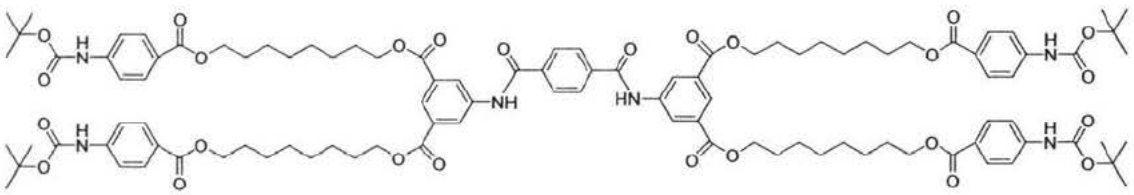

Terephthaloyl dichloride (0.023g, 0.113mmol) was dissolved in 10ml of dry THF and triethylamine (0.20g, 1.98mmol) was added. Compound **30** (0.20g, 0.23mmol) dissolved in 25ml dry THF was added and the solution stirred at 90°C for 12 hours. The crude

product was purified by column chromatography on silica using a 20:80:1 ethyl acetate:toluene:acetic acid eluant. The yield was 0.18g (0.096mmol, 84%).

^{1}H NMR (300 MHz), $CDCl_3$: 9.09 (s, 2H), 8.57 (s, 4H), 8.42 (s, 2H), 7.90 (m, 12H), 7.41 (d, 8H), 7.02 (s, 4H) 4.25 (m, 16H), 1.8 - 1.2 (m, 84H)

^{13}C NMR (75 MHz), $CDCl_3$: 166.5, 165.6, 165.4, 152.4, 142.9, 138.6, 137.5, 131.7, 130.7, 127.7, 126.6, 125.6, 124.5, 117.4, 81.0, 65.7, 64.9, 29.1, 28.6, 28.5, 28.2, 25.9

MS (EI) exact mass calculated for $(C_{104}H_{132}N_6O_{26})^+$ 1880.9191; found 1481.7164

N, N'-bis(3, 5-bis-[8-(4-amidobenzoyl)octyl]carboxyphenyl) terephthalamide (19)

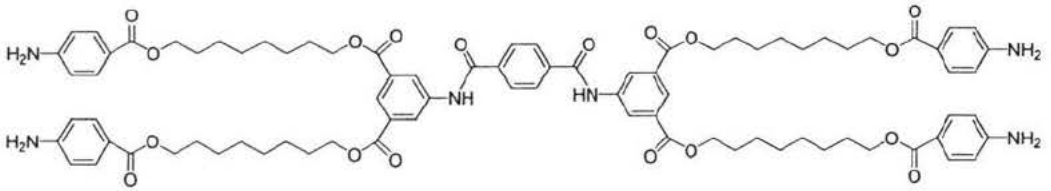

Compound **32** (0.10g, 53μmol) was dissolved in 25ml of dry dichloromethane and trifluoroacetic acid (0.26g, 0.20mmol) was added. The mixture was stirred at 60°C for 14 hours. The solution was decanted and the solid was washed with chloroform and dried under vacuum. The yield was 0.062g (42μmol, 79% yield).

^{1}H NMR (300 MHz), DMSO-d6: 10.88 (s, 2H), 8.75 (s, 4H), 8.23 (s, 2H), 8.16 (s, 4H), 7.72 (d, 8H), 6.79 (d, 8H), 4.70 (s, broad), 4.35 (t, 8H) 4.18 (t, 8H), 1.8 - 1.2 (m, 48H)

^{13}C NMR (75 MHz), DMSO-d6: 165.9, 165.2, 164.8, 153.4, 140.0, 137.1, 131.0, 130.9, 127.9, 124.7, 116.0, 112.6, 65.2, 63.5, 28.6, 28.6, 28.3, 28.1, 25.5

MS exact mass calculated for $(C_{84}H_{101}N_6O_{18})^+$ 1481.7172; found 1481.7181

8-(4-tert-butoxycarbonylaminobenzoyl)octyl 4-nitrobenzoate (35)

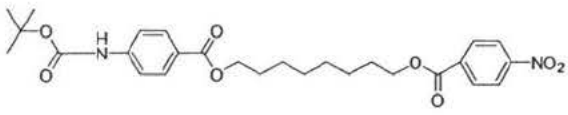

4-Nitrobenzoyl chloride (1.5, 8.08mmol) and triethyamine (3.32g, 32.8mmol) were dissolved in 100ml of dry THF. Compound **27** (3.00g, 8.21mmol) dissolved in 100ml dry THF was added and the mixture heated to reflux at 90°C for 14 hours. The crude product was purified by column chromatography on silica using 3:4:3 chloroform:ether:hexane eluant. The yield was 2.20g (4.28mmol, 53%).

^{1}H NMR (300 MHz), $CDCl_3$: 8.23 (d, 2H), 8.18 (d, 2H), 7.94 (d, 2H), 7.38 (d, 2H), 6.92 (s, 1H), 4.32 (t, 2H), 4.25 (t, 2H), 1.8 - 1.2 (m, 21H)

^{13}C NMR (75 MHz), $CDCl_3$: 166.3, 164.7, 152.3, 150.5, 142.8, 135.9, 130.8, 130.6, 124.6, 123.5, 117.4, 81.0, 66.0, 64.8, 29.4, 28.7, 28.6, 28.2, 25.9, 25.9

MS (EI) exact mass calculated for $(C_{27}H_{34}N_2O_8)^+$ 514.2314; found 514.2315

8-(4-tert-butoxycarbonylaminobenzoyl)octyl 4-aminobenzoate (36)

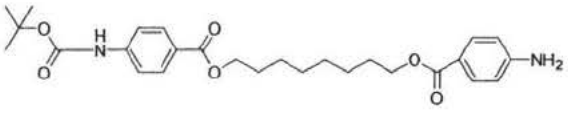

Compound **35** (2.1g, 4.08mmol) was dissolved in 100ml of 95% ethanol and 0.5g of 5% Pt/C was added. The solution was stirred under 50 psi of hydrogen for 144 hours. The catalyst was removed by filtration, the solvent removed by evaporation and the crude product was purified by column chromatography on silica using an 5:4:1 chloroform:ether:hexane eluant. The yield was 1.74g (3.59mmol, 88%).

^{1}H NMR (300 MHz), $CDCl_3$: 7.94 (d, 2H), 7.84 (d, 2H), 7.42 (d, 2H), 6.67 (s, 1H), 6.61 (d, 2H), 4.25 (m, 4H), 4.03 (s, 2H), 1.8 - 1.2 (m, 21H)

^{13}C NMR (75 MHz), $CDCl_3$: 166.7, 166.3, 152.7, 150.7, 142.6, 131.5, 130.8, 124.8, 120.2, 117.3, 113.8, 81.2, 64.9, 64.4, 29.2, 28.8, 28.7, 28.3, 26.0, 25.9

MS (EI) exact mass calculated for $(C_{27}H_{36}N_2O_6)^+$ 484.2573; found 484.2575

N, N'-bis(4-([8-(4-tert-butoxycarbonylaminobenzoyl)octyl]carboxyphenyl) terephthalamide (37)

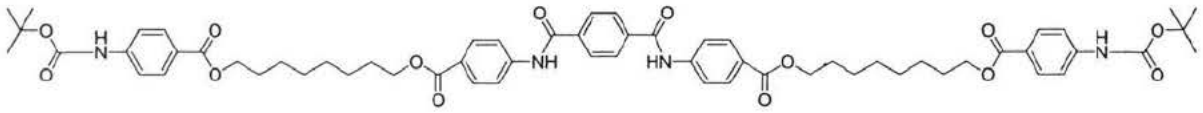

Terephthaloyl dichloride (0.1502g, 0.7398mmol) was dissolved in 10ml of dry THF and triethylamine (0.62g, 6.1mmol) was added. Compound **36** (0.712g, 1.46 mmol) dissolved in 25ml dry THF was added and the solution was stirred at 90°C for 14 hours. The crude product was purified by column chromatography on silica using a 20:80:1 ethyl acetate:toluene:acetic acid eluant. The yield was 0.73g (0.67mmol, 90%).

^{1}H NMR (300 MHz), DMSO-d6: 10.70 (s, 2H), 9.75 (s, 2H), 8.11 (s, 4H), 7.98 (s, 8H), 7.88 (d, 4H), 7.61 (d, 4H), 4.25 (m, 8H), 1.8 - 1.2 (m, 42H)

^{13}C NMR (75 MHz), DMSO-d6: 165.4, 165.2, 152.5, 144.1, 143.4, 137.3, 130.2, 130.1, 127.9, 124.8, 123.0, 119.7, 117.3, 79.7, 64.5, 64.2, 28.6, 28.2, 28.0, 25.4

MS exact mass calculated for $(C_{62}H_{75}N_4O_{14})^+$ 1099.5280; found 1099.5274

N, N'-bis(4-[8-(4-amido-benzoyl)octyl]carboxyphenyl)terephthalamide (20)

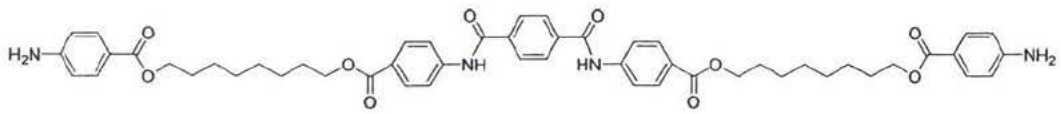

Compound **37** (0.70g, 0.64mmol) was dissolved in 25ml of dry dichloromethane and trifluoroacetic acid (0.66g, 5.8mmol) was added. The mixture was stirred at 60°C for 14 hours. The solution was decanted and the solid was washed with chloroform. The yield was 0.46 (0.51mmol, 80% yield)

^{1}H NMR (300 MHz), DMSO-d6: 10.71 (s, 2H), 8.13 (s, 4H), 8.00 (s, 8H), 7.63 (d, 4H), 6.57 (d, 4H), 5.94 (d, 4H), 4.25 (t, 4H), 4.17 (t, 4H), 1.8 - 1.2 (m, 24H)

^{13}C NMR (75 MHz), DMSO-d6: 165.9, 165.4, 165.2, 153.4, 143.4, 137.3, 131.0, 130.1, 127.9, 124.9, 119.7, 116.1, 112.6, 64.4, 63.5, 28.6, 28.4, 28.2, 25.5

MS exact mass calculated for $(C_{52}H_{59}N_4O_{10})^+$ 899.4231; found 899.4178

Dimethyl 5-Hydroxyisophthalate (39)

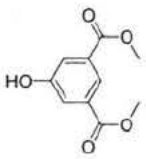

5-Hydroxyisophthalic acid (15.03g, 82.52mmol) was dissolved in methanol (400ml). Concentrated sulfuric acid (1ml) was added drop wise. The mixture was refluxed in an oil bath at 100°C for 2 hours. The solvent was removed and the residue was dissolved in ethyl acetate and placed in a separatory funnel. The impurities were then removed by extracting 3x with a 5% w/w solution of sodium bicarbonate. The organic phase was then isolated and dried. The yield was 9.96g (47.4mmol, 57.4%)

^{1}H NMR (300 MHz), C_3D_6O: 9.11 (s,1H), 8.10 (s, 1H), 7.59 (s, 2H), 3.91 (s, 6H)

^{13}C NMR (75 MHz), C_3D_6O: 167.4, 159.4, 134.0, 122.1, 121.0, 51. 6

Dimethyl 5-Benzyloxyisophthalate (41)

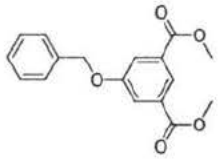

Compound **39** (9.90g, 47.1mmol) was dissolved in 150ml of dry DMF and sodium hydride (60% w/w in oil washed with pentane, 1.70g, 74.6mmol) was added. The solution was stirred at room temperature for 2 hours. Benzyl bromide (8.20g, 47.9mmol) and a catalytic amount of KI was added and the solution was stirred at 60°C for 18 hours. Distilled water was added to the solution until a precipitate stopped forming. The precipitate was separated by filtration and dried. The yield was 11.26g (37.5mmol, 80%)

^1H NMR (300 MHz), $CDCl_3$: 8.28 (s, 1H), 7.83 (s, 2H), 7.38 (m, 5H), 5.14 (s, 2H), 3.92 (s, 6H)

^{13}C NMR (75 MHz), $CDCl_3$: 166.1, 158.8, 136.1, 131.8, 128.7, 128.2, 127.6, 123.2, 120.2, 70.5, 52.4

5-Benzyloxyisophthalic acid (42)

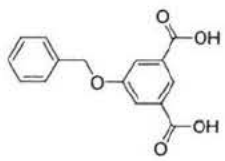

Compound **41** (11.20g, 37.3mmol) was dissolved in 100ml of 100% ethanol and brought to 100°C. Potassium hydroxide (2.09g, 37.3mmol) was added in a 2:1 ethanol:water solution and the reaction was stirred for 40 minutes. The solution was then adjusted to pH

1 with concentrated HCl, the ethanol was removed by evaporation and the product was precipitated in an ice bath. The precipitate was separated by filtration, washed with deionized water and dried. The yield was 9.04g (33.2mmol, 89%).

^{1}H NMR (300 MHz), C_3D_6O: 8.34 (s, 1H), 7.90 (s, 2H), 7.56 (d, 2H), 7.38 (m, 3H), 5.35 (s, 2H)

^{13}C NMR (75 MHz), C_3D_6O: 166.6, 159.9, 137.7, 133.2, 129.3, 128.8, 128.5, 123.9, 120.8, 71.0

MS (EI) exact mass calculated for $(C_{15}H_{12}O_5)^+$ 272.0685; found 272.0689

5-Benzyloxyisophthaloyl dichloride (43)

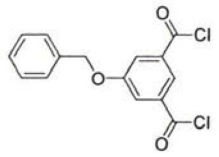

Thionyl chloride (25 ml) was added to compound **42** (0.5g, 1.84mmol) and the mixture was stirred at 90°C for 15 hours. The thionyl chloride was removed by evaporation. The yield was 0.57g (1.84mmol, 100%)

^{1}H NMR (300 MHz), $CDCl_3$: 8.46 (s, 1H), 7.98 (s, 2H), 7.42 (m, 5H), 5.18 (s, 2H)

^{13}C NMR (75 MHz), $CDCl_3$: 167.1, 159.3, 135.4, 135.1, 128.9, 128.7, 127.7, 126.2, 123.2, 71.1

Bis-[8-(4-tert-butoxycarbonylamidobenzoyl)octyl] 5-benzyloxyisophthalate (44)

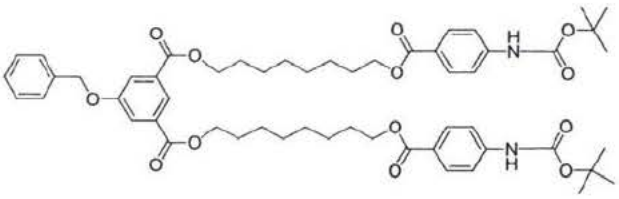

Compound **43** (0.96, 3.1mmol) and triethylamine (2.50g, 24.7mmol) were dissolved in 50ml of dry THF. Compound **27** (2.08g, 5.69mmol) dissolved in 100ml dry THF was added and the mixture was heated to reflux at 90°C for 18 hours. The crude product was filtered, dried and purified by column chromatography on silica using a 3:5:2 chloroform:ether:hexane eluant. The yield was 2.01g (2.08mmol, 67%).

^{1}H NMR (300 MHz), $CDCl_3$: 8.29 (s,1H), 7.97 (d, 4H), 7.81 (s, 2H), 7.30 (m, 9H), 6.85 (s, 2H), 5.14 (s, 2H), 4.25 (m, 8H), 1.8 - 1.2 (m, 42H)

^{13}C NMR (75 MHz), $CDCl_3$: 166.3, 165.7, 158.7, 152.2, 142.7, 136.1, 132.2, 130.8 128.7, 128.3, 127.6, 124.7, 123.2, 120.0, 117.4, 81.1, 70.5, 65.5, 64.8, 29.1, 28.7, 28.6, 28.3, 26.0, 25.9

Bis-[8-(4-tert-butoxycarbonylaminobenzoyl)octyl] 5-hydroxyisophthalate (45)

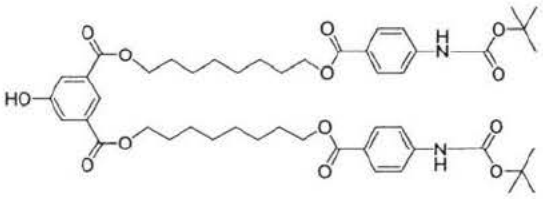

Compound **44** (0.88g, 0.900mmol) was dissolved in 50ml of 100% ethanol and 1.00g of 10% Pd/C was added. The solution was stirred under 60 psi of hydrogen for 14hrs. The catalysist was removed by filtration, the solvent removed by evaporation and the crude

product was purified by column chromatography on silica using an 5:4:1:0.1 chloroform:ether:hexane:pyridine eluant. The yield was 0.66g (0.75mmol, 83%)

^{1}H NMR (300 MHz), $CDCl_3$: 8.22 (s,1H), 7.94 (d, 4H), 7.73 (s, 2H), 7.42 (d, 4H), 6.84 (s, 2H), 4.30 (m, 8H), 1.8 - 1.2 (m, 42H)

^{13}C NMR (75 MHz), $CDCl_3$: 166.5, 166.0, 157.4, 152.4, 142.9, 132.0, 130.8, 124.5, 122.0, 120.9, 117.4, 81.1, 65.3, 34.9, 28.1, 28.7, 28.6, 28.3, 25.9, 25.9

MS exact mass calculated for $(C_{48}H_{65}N_2O_{13})^+$ 877.4487; found 877.4487

bis(3, 5-bis-[8-(4-tert-butoxycarbonylamidobenzoyl)octyl]carboxyphenyl) terephthalate (46)

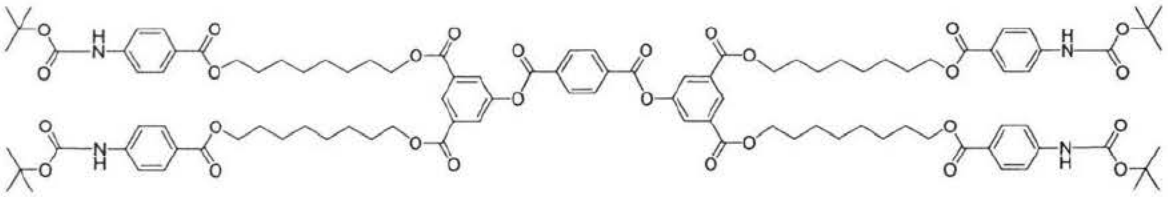

Terephthaloyl dichloride (0.067g, 0.330mmol) was dissolved in 10ml of dry THF and triethylamine (0.30g, 3.0mmol) was added. Compound **45** (0.60g, 0.684mmol) dissolved in 25ml dry THF was added and the solution stirred at 90°C for 12 hours. The crude product was purified by column chromatography on silica using a 5:4:1:0.1 chloroform:ether:hexane:pyridine eluant. The yield was 0.47g (0.23mmol, 75%).

^{1}H NMR (300 MHz), $CDCl_3$: 8.58 (s, 2H), 8.34 (s, 4H), 8.04 (s, 4H), 7.91 (d, 8H), 7.38 (d, 8H), 6.72 (s, 4H), 4.31 (t, 8H), 4.22 (t, 8H), 1.8 - 1.2 (m, 84H)

^{13}C NMR (75 MHz), $CDCl_3$: 166.3, 164.9, 163.8, 152.2, 150.6, 142.6, 133.5, 132.6, 130.8, 130.5, 128.3, 127.0, 124.7, 117.3, 81.1, 65.8, 64.8, 29.1, 28.7, 28.6, 28.3, 25.9

bis(3,5-bis-[8-(4-aminobenzoyl)-octyl]carboxyphenyl) terephthalate (21)

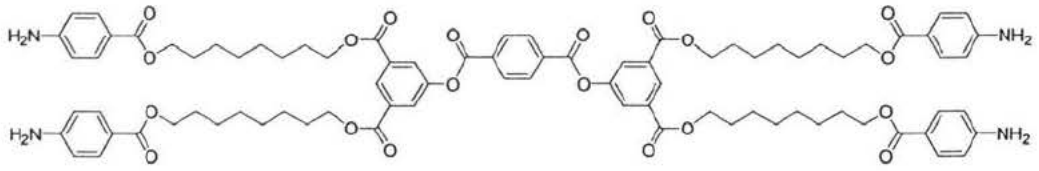

Compound **46** (0.052g, 28μmol) was dissolved in 10ml of dry dichloromethane and trifluoroacetic acid (0.2g, 5.8mmol) was added. The mixture was stirred at 60°C for 14 hours. The mixture was then washed three times with a satureated solution of sodium bicarbonate and purified using bio beads SX-3 using dichloromethane at a flow rate of 3.2 ml/minute. The yield was 0.033 (23μmol, 82% yield)

^{1}H NMR (300 MHz), $CDCl_3$: 8.63 (s, 2H), 8.36 (s, 4H), 8.10 (s, 4H), 7.81 (d, 8H), 6.60 (d, 8H), 4.36 (t, 8H), 4.22 (t, 8H), 4.08 (s, 2H), 1.8 - 1.2 (m, 48H)

^{13}C NMR (75 MHz), $CDCl_3$: 166.7, 164.9, 163.9, 150.8, 150.3, 133.5, 132.6, 131.5, 130.5, 128.4, 127.0, 117.0, 113.8, 65.9, 64.4, 29.1, 28.8, 28.6, 26.0, 25.9

MS exact mass calculated for $(C_{84}H_{99}N_4O_{20})^+$ 1483.6853; found 1483.6845

5.2 pH-stat Experimental

The experimental procedures preparation and pH-stat titration followed the Masters thesis of K. C. Kaye with some changes[45].

The titration system consisted of a Metrohm 655 Dosimat burette, a 614 automatic titrimiter, a 632 pH-meter, a HP-85 and a titration cell. The burette was linked to the HP-85, which was linked to an IBM PC, and the automatic titration and data acquisition was programmed as a Windows and DOS based software by David Robertson and Dr. T.M. Fyles. A W385 Ultrasonic sonicator in the Biochemistry and Microbiology Department, University of Victoria, was used for the sonication in the vesicle preparation. A Nicomp model 370 Submicron Particle Sizer was used for the size distribution analysis.

Egg phosphatidyl choline (PC) and egg phosphatidic acid (PA) were obtained from Avanti Polar Lipids (Alabaster, AL). Cholesterol, choline hydroxide (48 – 50% in water), D-manitol were obtained from Sigma and the citric acid was obtained from Aldrich. PD-10 Sephadex G-25 columns were obtained from Pharmica. D^3 (deionized, double distilled) water was used to make up all aqueous solutions.

Gramicidin, mellitin, FCCP, Triton X-100 and the sulphates of sodium, potassium and cesium were obtained from Sigma/Aldrich

Stock Solutions:

Lipid stock solution: A mixture of PC, PA and cholesterol in a 8:1:1 molar ratio was dissolved in chloroform at 34mg/mL. It was stored in the freezer at approximately -15°C.

Choline sulfate: Choline hydroxide (200 mL of 48% - 50% in water) was titrated to pH 6.5 with concentrated sulphuric acid. Activated charcoal was added and the solution was stirred for 10 minutes. The charcoal was then removed by filtration through Celite, and the solution was concentrated by rotary evaporation. 100% Ethanol (300 mL) was added

to dissolve the tarry residue, followed by adding anhydrous ether (250 mL), and the solution started to precipitate. The solution was cooled in a freezer overnight and the precipitate was collected through filtration. The mother liquor was returned to the freezer overnight for another crop of precipitate. The combined batches of choline sulfate precipitate were dried for 24 hours under vacuum.

Internal buffer solution: 0.2 M citric acid and 0.054 M D-mannitol; the pH was adjusted to 3.3 by choline hydroxide. The internal buffer was made in 100 mL batches.

External solution: 0.11 M choline sulfate, 0.093 M D-mannitol; the pH was adjusted to 3.8 by sulfuric acid. The external solution was made in 500 mL batches.

Choline hydroxide titrant: One liter of 5.27 mM choline hydroxide and 0.35 M D-mannitol was quickly dissolved in D^3 water to make a basic titrant. Its concentration was calibrated by titration of standard potassium acid phthalate.

Lipid vesicle preparation:

1 mL of the stock lipid solution was transferred into a round bottom flask (RBF) and evaporated to dryness under vacuum. 3 mL of anhydrous diethyl ether and 1 mL of the internal buffer solution was added to form a two phase solution. The solution was then sonicated for one minute with 1 second pulses to give a transparent homogeneous solution. The ether was evaporated under vacuum until the solution was a viscous liquid and 1.5 mL of the external buffer solution was added. The remaining ether was evaporated under vacuum. The solution was injected into the sizer and forced 19 times through a 1 μm Nucleopore filter. A Sephadex G-25 disposable column was equilibrated with 10 mL of external solution. The vesicle solution was added and the fractions were

collected after a perfect ring formed in the liquid of the collection flask from a drop from the vesicle fraction. The fraction collection was stopped when drops from the column became clear. The vesicle size distribution was monitored by dynamic light scattering.

pH-stat titration:

5 mL of the external solution was added to the titration cell. This was then adjusted to pH 5 via adding choline hydroxide titrant through the automatic titrator. The computer connected to the automatic titration system collected the data and transferred it to an Excel database after the titration was finished. 0.100 mL of the vesicle solution was added to the cell and the pH was once again adjusted to pH 5. FCCP, alkali metal salt and transporter were added to the solution in the respective order with the automatic titrimiter correcting the pH to 5. After each compound had reached a plateau 0.200mL of Triton X-100 was added to the cell to produce lyseis of the remaining vesicles.

The graphs of the curves were done with Microsoft Excel and the exponential fits were generated with Origin 6.0

Appendix

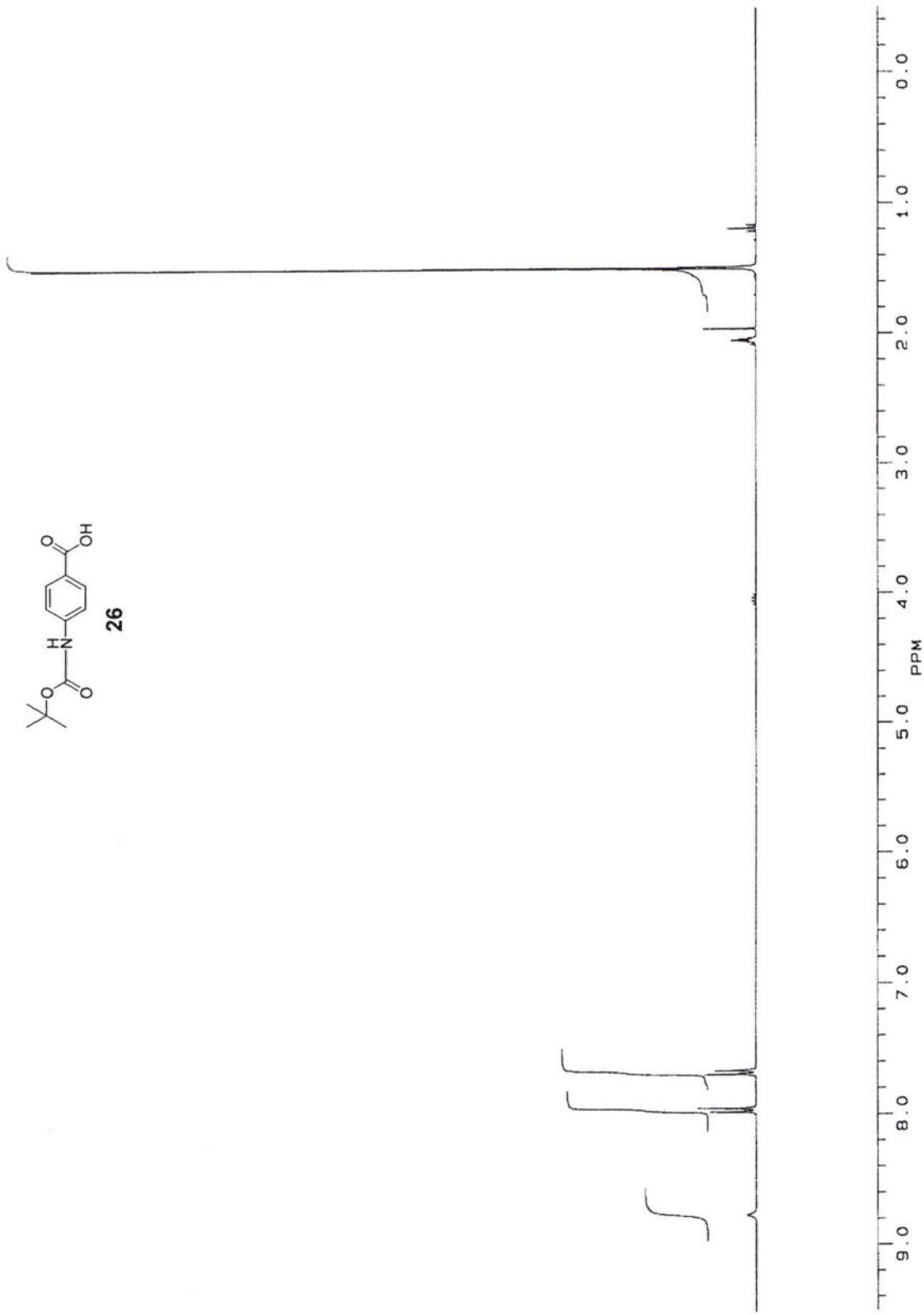

Figure A.1: Proton NMR of compound **26**

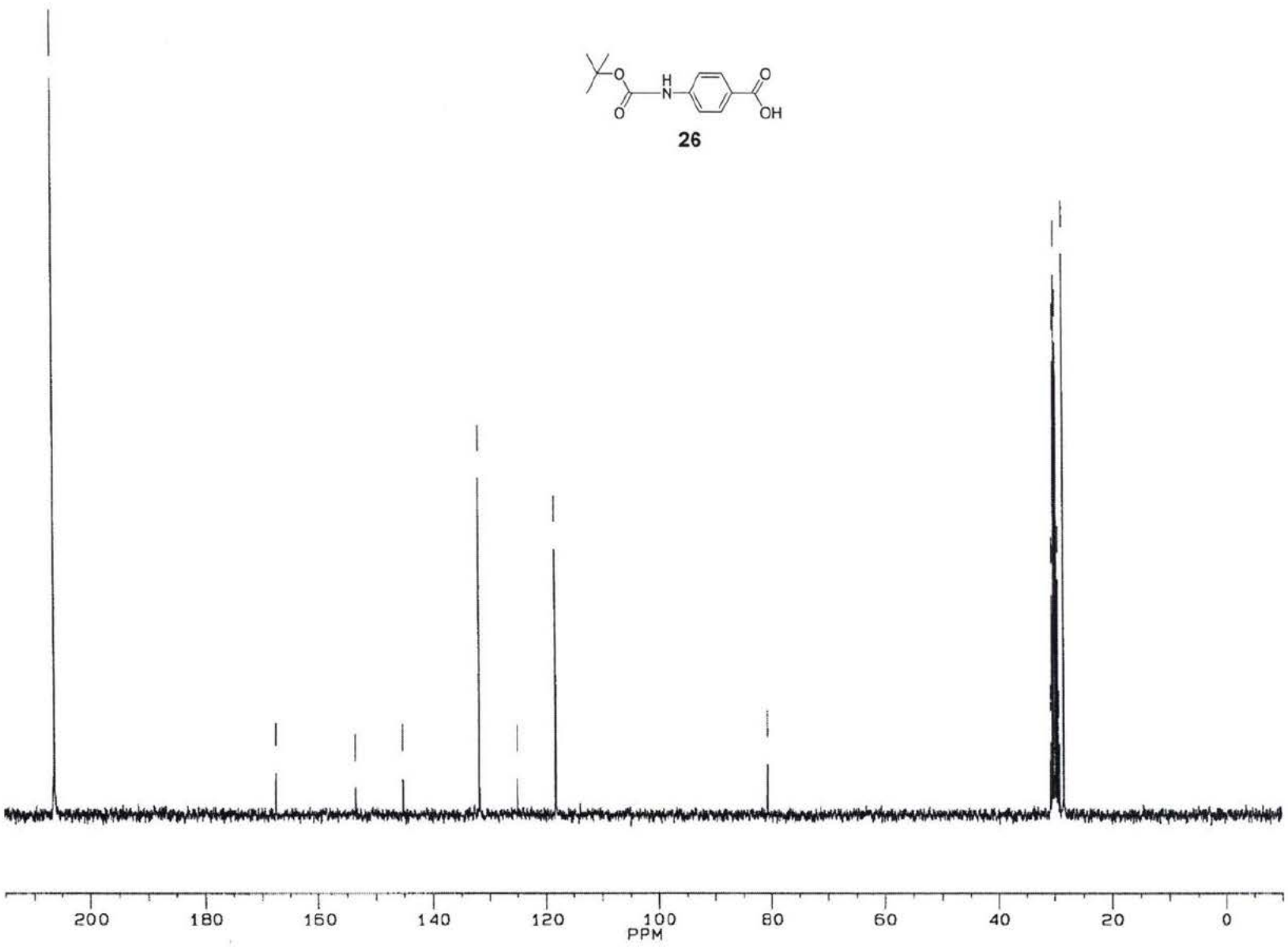

Figure A.2: Carbon NMR of compound **26**

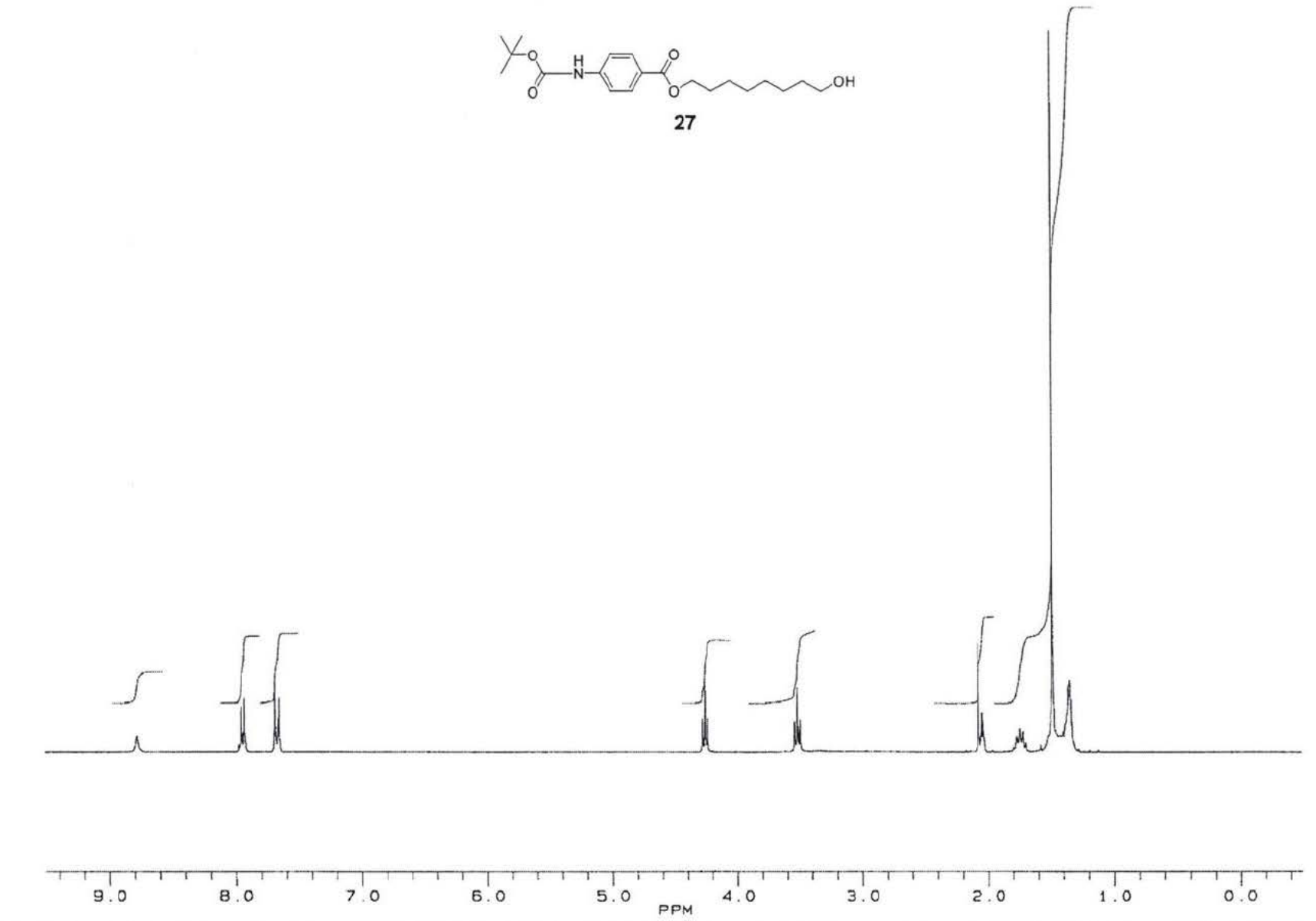

Figure A.3: Proton NMR of compound **27**

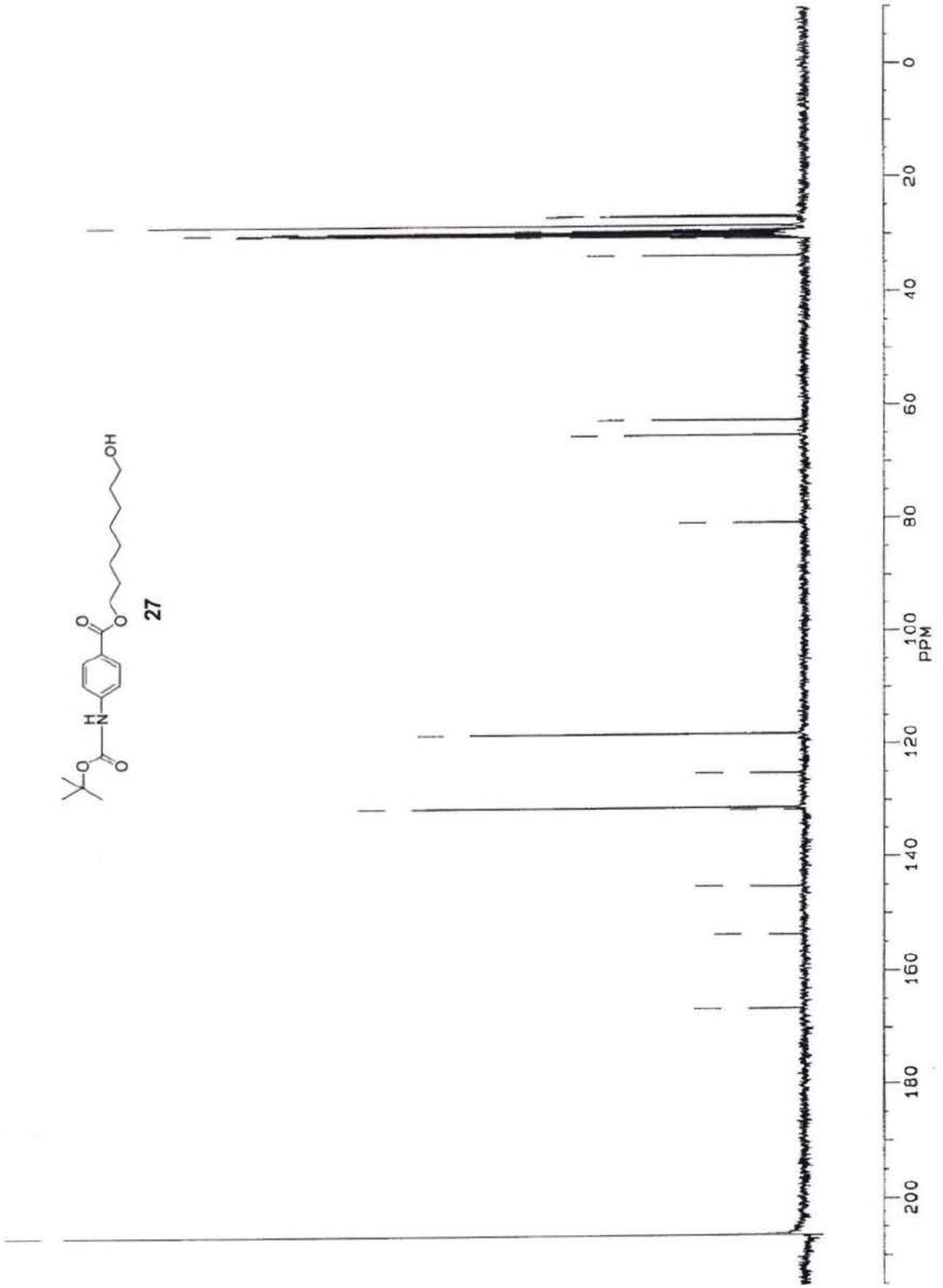

Figure A.4: Carbon NMR of compound **27**

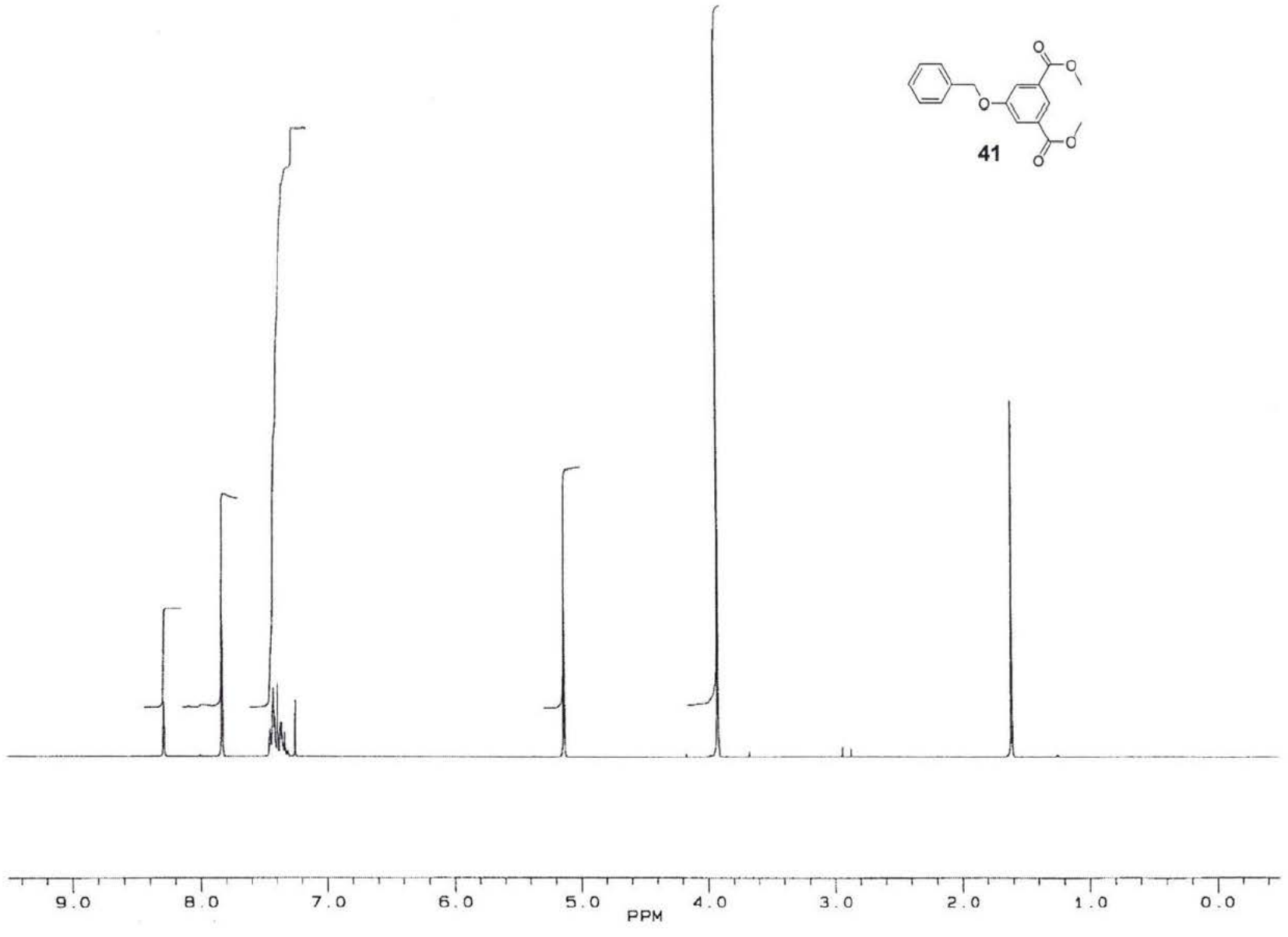

Figure A.5: Proton NMR of compound **41**

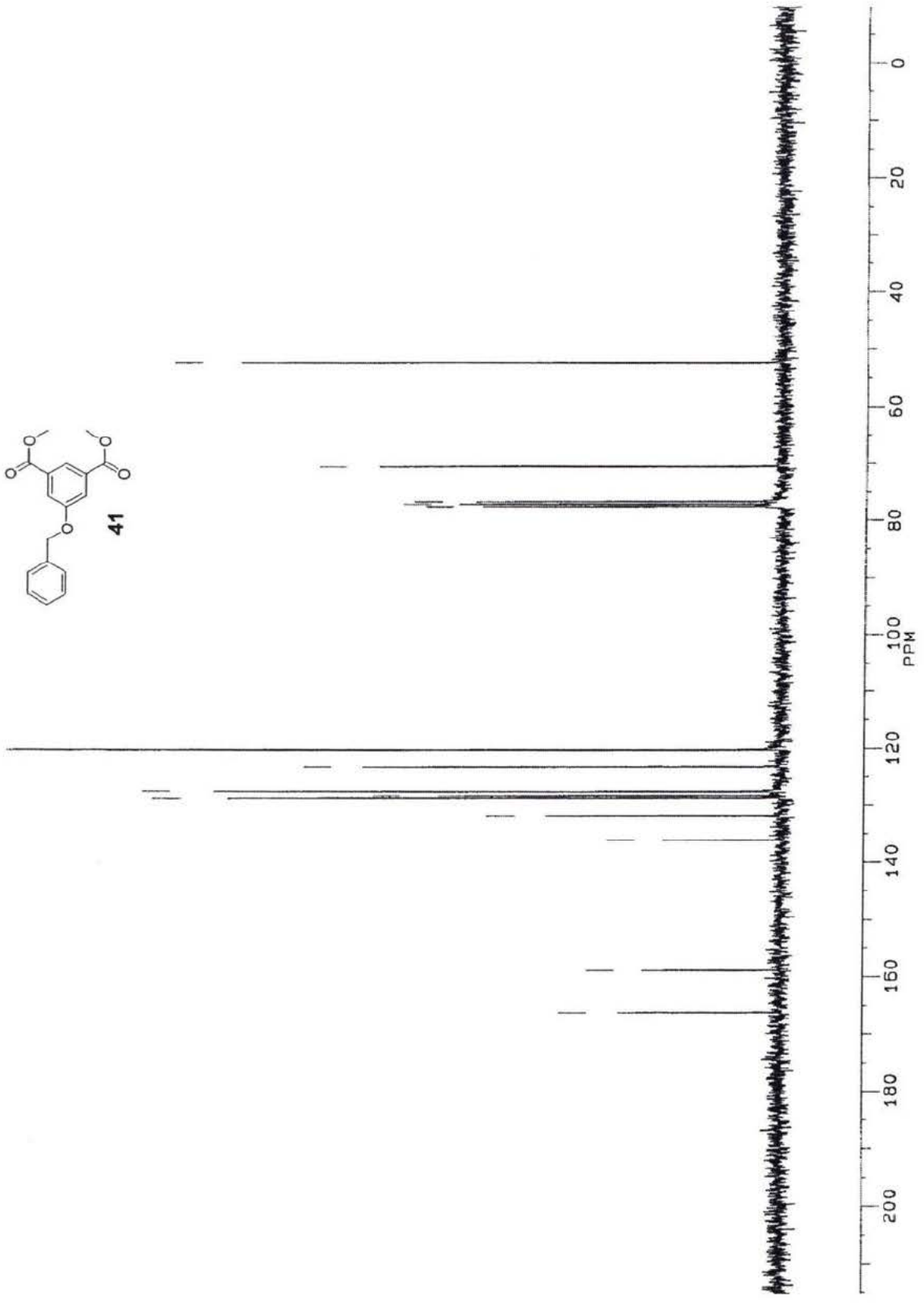

Figure A.6: Carbon NMR of compound **41**

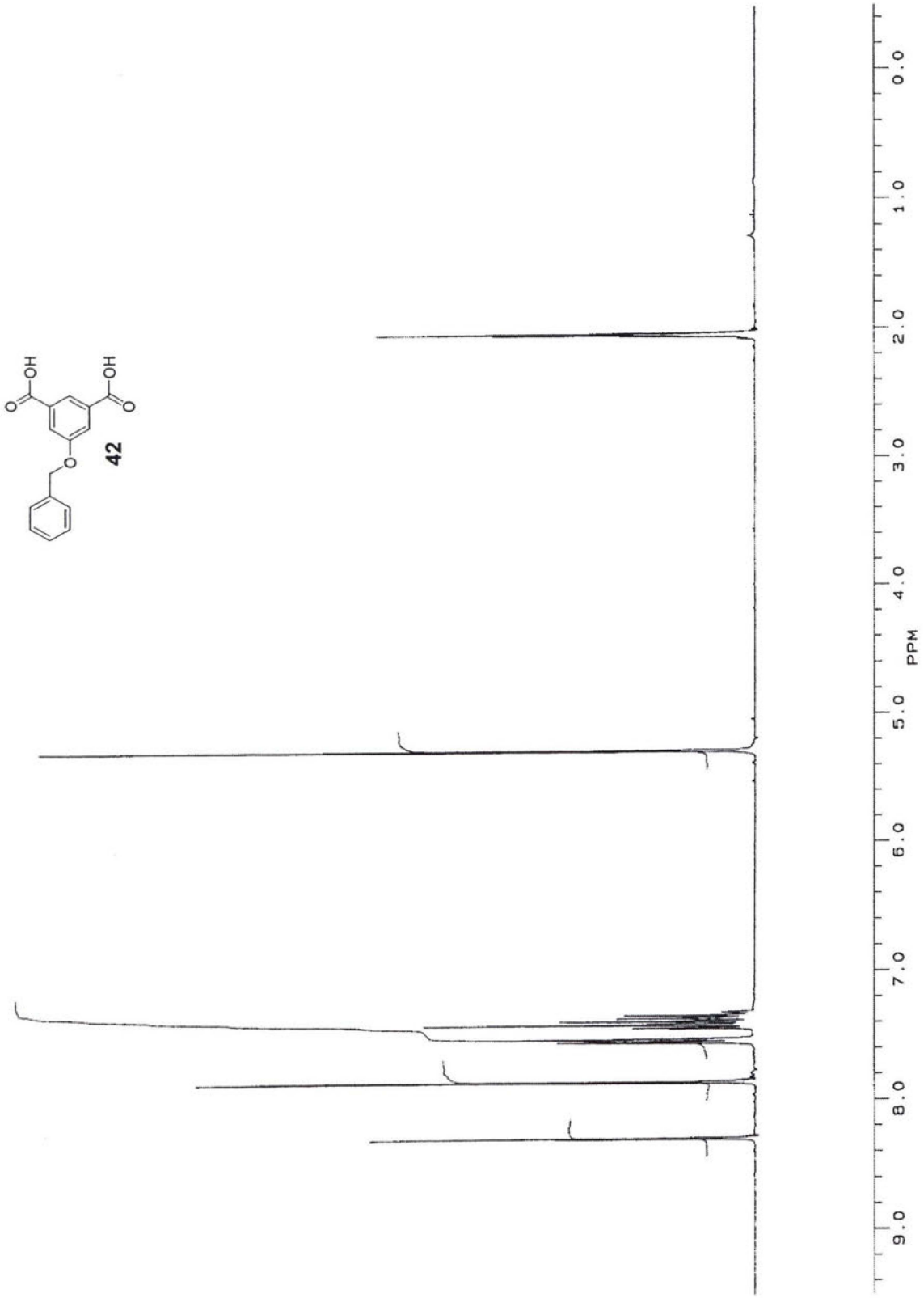

Figure A.7: Proton NMR of compound **42**

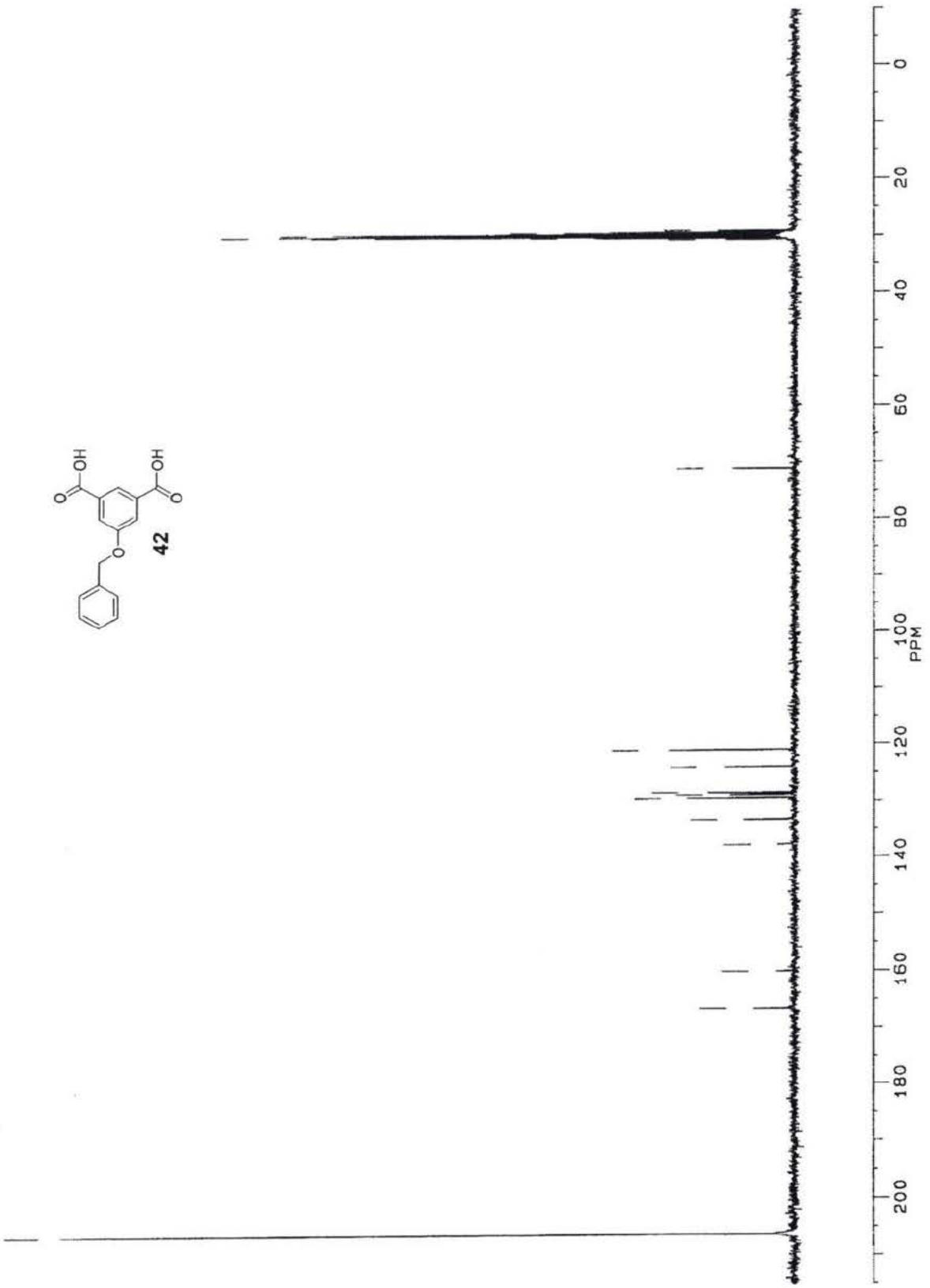

Figure A.8: Carbon NMR of compound **42**

References

1) Kleinsmith, L., J.; Kish, V., M. *Principles of Cell and Molecular Biology,* HarperCollins College Publishers, New York, **1995**, p.155

2) Sargent, P. *An Introduction to Molecular Neurobiology,* Sinauer Associates, Sunderland, **1992**, p.33

3) Doyle, D.; Cabral, J.; Pfuetzner, R.; Kuo, A., Gulbis, J. Cohen, C.; Chait, B. Mackinnon, R. *Science*, **1998**, *280*, 69.

4) Luecke, H.; Richter, H-T.; Lanyi, J. *Science*, **1998**, *280*, 1934.

5) Sarges, R.; Witkop, B. *J. Am. Chem. Soc.,* **1965**, *87*, 2011-2020

6) Woolley, G. A.; Wallace, B. *J. Membrane Biol.*, **1992**, 1*29*, 109-136

7) Myers, V., B..; Haydon, D. *Biochem. Biophys. Acta*, **1972**, *274*, 313-322.

8) Bamberg, E.; Lauger, P. *J. Membrane Biol.*, **1977**, *35*, 351-375.

9) Holz, R., W. *Ann. N.Y. Acad. Sci.,* **1974**, *235*, 469.

10) Andreoli, T. *Ann. N.Y. Acad. Sci.,* **1974**, *234*, 448.

11) Hartsel, S., C; Hatch, C. Ayenew, W.; *J. of Liposome Res.,* **1993**, *3*, 337-408.

12) Fyles, T. *Bioorganic Chemistry Frontiers,* **1980**, p. *71-113*.

13) Cameron, L. *Doctoral Thesis,* University of Victoria, Victoria, B.C., Canada, **1998**

14) Zhou, X. *Doctoral Thesis,* University of Victoria, Victoria, B.C., Canada, **1997**

15) Cross, G.; Fyles, T.; James, Y. D; Zojaji, M. *Synlet,* **1993**, 449-460

16) Gokel, G. *J. Chem. Soc., Chem Commun.,* **2000**, 1-9; Hartgerink, J. D.; Clark, T. D. *Chem. Eur. J.,* **1998**, *4*, 1367-1372.

17) Sakai, N.; Brennan, K.; Weiss, L.; Matile, S. *J. Am. Chem. Soc.*, **1997**, *119*, 8726-8727

18) Tabushi, I.; Kuroda, Y.; Yokota, K. *Tetrahedron Lett.*, **1982**, *23, 44*, 4601

19) Tanaka, Y.; Kobube, Y., Sokabe, M. *Angew. Chem. Int. Ed. Engl.*, **1995**, *34, 6*, 693

20) Jullien, L.; Lehn, J., M. *Tetrahedron Lett.*, **1988**, *29*, 31, 3803

21) Canceill, J.; Jullien, L.; Lacombe, L.; Lehn, J. *Chim. Acta.*, **1992**, *75*, 791

22) Pregel, M., J.; Jullien, L.; Canceill, J.; Lacombe, L.; Lehn, J. *J. Chem. Soc. Perkin Trans., 2*, **1995**, *3*, 417

23) Pregel, M., J.; Jullien, L.; Lehn, J. *Angew. Chem. Int. Ed. Engl.*, **1992**, *31*, 12, 1637

24) Abel, E.; Maguire, G.; Meadows, E.; Murillo, O.; Jin, T.; Gokel, G. *J. Am. Chem. Soc.*, **1997**, *119*, 9061

25) Murray, C.; Gokel, G. *J. Chem. Soc., Chem. Commun.*, **1998**, 2477

26) Maguire, G.; Meadows, E.; Murray, C.; Gokel, G. *Tetrahedron Lett.*, **1997**, *38, 6*, 6339

27) Nolte, R.; Van Beijnen, A.; Neevel, J.; Zwickker, J.; Verkley, A.; Drenth, W. *Isr. J. Chem.*, **1984**, *24*, 297

28) Kragten, U.; Roks, M.; Nolte, R. *J. Chem. Soc., Chem. Commun.*, **1985**, 1275

29) Meillon, J.; Voyer, N. *Angew. Chem. Int. Ed. Engl.*, **1997**, *36*, 9, 967

30) Clark, T.; Buehler, K.; Ghadiri, M. *J. Am. Chem. Soc.*, **1998**, *120*, 651

31) Fernadez-Lopez, S.; Kim, H-S.; Choi, E.; Delgado, M.; Granja, J.; Khasanov, A.; Kraehenbuehl, K.; Long, G.; Weinberger, D.; Wilcoxen, K.; Ghadiri, M. *Nature*, **2001**, *412*, 452

32) Fuhrhop, J-H.; David, H-h.; Mathieu, J.; Liman, U.; Winter, H-J.; Boeclema, E. *J. Am. Chem. Soc.*, **1986**, *108*, 1795

33) Fuhrhop, J-H.; Liman, U., *J. Am. Chem. Soc.*, **1984**, *106*, 4643

34) James, T., *Doctoral Thesis,* University of Victoria, Victoria, B.C., Canada, **1991**

35) Fyles, T.; James, T.; Pryhitka, A.; Zojaji, M., *J. Org. Chem.*, **1993**, *58*, 7456

36) Fyles, T.; James, T.; Kaye, K. *J. Am. Chem. Soc.*, **1993**, *115*, 12315

37) Fyles, T.; Kaye, K.; Pryhitka, A.; Tweddell, J.; Zojaji, M., *Supermolecular Chem.*, **1994**, *3*, 197

38) Fyles, T.; Loock, D.; Zhou, X., *Can. J. Chem.*, **1998**, *76*, 1015

39) Fyles, T.; Loock, D.; van Straaten-Nijenhuis, W.; Zhou, X., *J. Org. Chem.*, **1996**, *61*, 8866

40) Cameron, L.; Fyles, T. M.; Hu, C.; Submitted manuscript

41) Fyles, T. M.; Hu, C.; Knoy, R. *Org. Lett.* **2001**, 1335-1337

42) Fendler, J.; *Membrane Mimetic Chemistry,* John Weiley & Sons, New York, **1982**

43) Leonard, L.; Neeland, E.; Onsworth, J.; Sims, R.; Tishler, S.; Weiler, L.; *Can. J. Chem.*, **1992**, *70*, 1427

44) Knoy. R., *Masters Thesis,* University of Victoria, Victoria, B.C., Canada, **2000**

45) Kaye, K., *Masters Thesis,* University of Victoria, Victoria, B.C., Canada, **1991**

46) Yudilevich, D.; Deves, R.; Peran, S.; Cabantchik, Z. *Cell Membrane Transport: Experimental Approaches and Methodologies,* Plenum Press, New York, **1991**, p.257

47) New, R. et al. *Liposomes,* 1st ed., Oxford University Press, New York, **1990**, p.154

48) Herve, M.; Cybulska, B.; Gary-Bobo. C., *Eur. Biophys. J.,* **1985**, *12,* 121

49) Bhakoo, M.; Birkbeck, T.; Freer, J., *Can. J. Biochem. Cell Biol.* **1985**, *63,* 1

50) Jayasuriya, N.; Bosak, S.; Regen, S., *J. Am. Chem. Soc.* **1990**, *112,* 5844

51) Murray, C.; Meadows, E.; Murillo, O.; Gokel, G., *J. Am. Chem. Soc.,* **1997**, *119,* 7887

52) Hille, B.; *Ionic Channels of Excitable Membranes,* Sinauer Associates Inc., Massachusetts, **1985**

Vita

Surname: Eggers Given Names: Paul Kahu

Place of Birth: Lower Hutt, New Zealand

Educational Institutions Attended:

University of Victoria	2000 to 2001
Okanagan University College	1996 to 2000

Degrees Awarded:

B.Sc.	Okanagan University College	2000

Partial Copyright License

I hereby grant the right the lend my thesis to users of the University of Victoria Library, and to make single copies only for such users or in response to a request from the Library of any other university or similar institution, on its behalf or for one of its users. I further agree that permission for extensive copying of this thesis for scholarly purposes may be granted by me or a member of the University designated by me. It is understood that copying or publication of this thesis for financial gain by the University of Victoria shall not be allowed without my written permission.

Title of Thesis: Design, Synthesis And Characterization Of Acyclic Bola-Amphiphiles That Form Ion Channels

Author [redacted]
Paul Kahu Eggers

18/12/01
Date